Freie Universität Berlin

Polycationic functionalization and characterization of graphene oxide for bacterial adsorption and removal

DISSERTATION

to obtain an academic degree
Doctor rerum naturalium (Dr. rer. nat.)
submitted to the Department of Biology, Chemistry, Pharmacy
of the Freie Universität Berlin

by
Rameez Ahmed
from Sargodha, Pakistan

November 2023

Declaration of honesty

Hereby, I declare and confirm the authenticity of this doctoral thesis. It is the result of my research work. Collaborations with other research groups are specified in the respective projects. Any other sources than those cited have not been used. I also declare that I have not submitted the dissertation in this or any other form to any other institution as a dissertation.

_____

Rameez Ahmed
November (2023).

I dedicate this work to my father, Akhlaq, who always valued education above anything, and to my loving mother, Nasrin, who supported me in more ways than I can count.

"Scientific thought... is the common and shared heritage of mankind."
Dr. Abdus Salam, Nobel Lecture December 1979

This doctoral thesis was performed within the research groups of Prof. Dr. Rainer Haag from April 2018 to November 2023 at the Institute of Chemistry and Biochemistry of the Freie Universität Berlin. This study was funded by the Helmholtz MacroBio graduate school and the Dahlem Research School (DRS).

1. Reviewer: Prof. Dr. Rainer Haag, Freie Universität Berlin

2. Reviewer: Prof. Dr. Mohsen Adeli, Freie Universität Berlin

Location of Defense: Altensteinstr. 23a, 14195 Berlin
Date of Defense: 18.12.2023

Acknowledgments

I sincerely thank Prof. Dr. Rainer Haag for providing me with this opportunity to do doctoral thesis in his group. He supervised me for the last five years during the extraordinary times of the pandemic. His guidance and support were a huge help during the research and writing of this thesis. I would also like to thank Prof. Dr. Mohsen Adeli as the second supervisor of this thesis. I am grateful for his valuable remarks on this work.

I want to express my most profound appreciation for Dr. Olaf Wagner, who gave me a chance to work with him as an intern when I was a master's student. He always took time to listen and guide me through all these years. His suggestions and advice will always be a part of me. I take this opportunity to thank Dr. Luis Cuellar for providing me with AFM training and helping me analyze samples. I want to thank Dr. Ievgen S. Donskyi for performing XPS and NEXAFS measurements on the samples and, most importantly, guiding me with his experiences during this journey.

I want to acknowledge Dr. Ankita Vaishampayan and Prof. Dr. Elisbeth Grohmann from Beuth Hochschule für Technik and Dr. Katharina Achazi and Elisa Quas for collaboration with biological studies. I also acknowledge Dr. Darren J. Wight Freie Universität Berlin, Institute of Virology, for the confocal experiments, Dr. Wolfgang Unger from Bundesanstalt für Materialforschung und -prüfung for XPS characterization, and Cathleen Schlesener for GPC measurements for my samples.

I want to thank my lab mates, Dr. Guy Guday, Dr. Philip Nickl, and M.Sc. Obida Bawadkji for their helpful input with scientific discussions and support. I would also like to acknowledge all present and former group members of the groups of Prof. Dr. Haag for support in daily work and advice regarding research. I thank the Helmholtz MacroBio graduate school and Dahlem Research School (DRS) for funding my doctoral research.

Finally, I express my very profound gratitude to my parents for providing me with unfailing support and continuous encouragement throughout my life and through the process of researching and writing this thesis.

Rameez Ahmed
Berlin, Germany
November 2023

Contents

1. Introduction

Bacterial pathogens continue to pose significant research and biological danger to the world. The emergence of resistance in pathogens against antibiotics is among the most significant concerns nowadays that affect the healthcare system. Multidrug-resistant (MDR) bacterial infections are becoming more widespread and present a severe public health risk, which means fewer antimicrobial medicines are available to treat infections caused by such pathogens.[1] It is estimated that it will be challenging to manage infectious diseases if no effective antibiotics can be designed or identified until 2050.[2] There is a dire need to develop new, effective strategies to minimize the global burden of infectious diseases.

Nanotechnology provides new ways and strategies for creating unique surfaces with precise and strictly controlled surface nanotextures in this regard. Nanoparticles can be employed instead of antibiotics to treat bacterial infections caused by MDR bacteria.[3] Different carbon-based nanostructures such as carbon nanotubes, fullerene, and composite carbon materials receive nowadays attention due to their broad applications and use in antibacterial strategies.[4]

Approximately 2 billion people have a scarcity of safely managed water at the point of consumption.[5] Membrane filtration, working on the principle of size exclusion, is considered the most viable solution for today's water problem. It can remove most of the harmful substances during the process.[6] However, its limitations such as biofouling and clogging have a high impact on the filtration parameters.[7] Regular maintenance and replacement are necessary to run smooth operations, which makes it unsustainable for present future needs.[8]

A unique surface property that all bacteria share is their over negative surface charge.[9] Due to this, bacteria can bind to the positively charged materials because of electrostatic attraction.[10] This work focuses on developing two-dimensional (2D) polycationic material that can effectively bind and remove bacteria from water. Graphene oxide (GO) is functionalized with 2-dimethylamino-ethylmethacrylate polymer, which was quaternized to produce flexible 2D polycationic sheets called GOX. Studies showed that GOX can bind and wrap bacteria cells, which inhibits their proliferation. GOX is further immobilized on cellulose fibers to investigate its bacteria reduction performance. GOX cellulose fibers exhibit high bacterial reduction at a five times higher flow rate than commercial membrane filters without clogging. GOX-functionalized filters could be installed on public water sources to ensure drinking water quality.

1.1 Bacteria

Bacteria are one of the planet's smallest and most abundant living organisms. They are typically in micrometer size range with different morphologies. Virtually all forms of life depend on bacteria for their survival.[11] However, there are several species of bacteria that are pathogenic and can cause severe illnesses.[12] *Mycobacterium tuberculosis* bacteria is one of the deadliest pathogenic bacteria that kills half of the infected hosts.[13] Bacteria exist in humans in localized body areas, performing several key functions like producing nutrition, resisting pathogens, and increasing immunity.[14] [15] The internal tissues are primarily sterile, but bacteria have developed several mechanisms to overcome host barriers and colonize inside the human organs. They can establish an intracellular lifestyle, which gets them internalized and replicated inside host cells. Bacteria can overcome the mucosal barrier and infect and colonize deeper tissues that can provide access to the bloodstream, which is a gateway to potentially all host organs.[16]

Water-borne pathogens are one of the most significant sources of pathogenic infection globally. The ingestion of contaminated water by the host is the leading cause of these infections. After entering the host's body, these bacteria reproduce and start releasing toxins, which cause diseases. Approximately 500,000 people die annually due to diarrhea caused by *Campylobacter, Escherichia coli (E. coli), Salmonella,* and *Shigella* pathogenic bacteria.[17] Cholera (an acute form of diarrhea), caused by curved rod-shaped Gram-negative *Vibrio* bacteria, is responsible for 7 pandemics worldwide.[18]

1.1.1 Classification of bacteria

Bacteria can be classified in many ways[19], but the two most essential classifications for the basis of this thesis are their morphology and Gram staining. According to shape, bacteria are generally divided into five different types. They can be in the form of spherical-shaped cells (cocci), Rod-shaped cells (bacilli), Spiral-shaped cells (spirilla), Comma-shaped cells (vibrio), and corkscrew (spirochaetes). (Figure. 1)

Figure 1: Types of bacteria based on morphology. Modified reprint with the permission from ref.[20]

The cell wall of the bacteria plays many significant roles. It gives bacteria their morphology while protecting them from the surroundings.[21] It regulates the transport of materials between the cell and the environment.[22] It guards bacteria against toxic chemicals and biologically active materials.[23] The Gram staining method classified bacteria into two general types based on their cell wall structure: Gram-positive and Gram-negative.[24] Gram-positive bacteria have a thick layer of peptidoglycans as a cell wall and a thin inner plasma membrane composed of the phospholipid bilayer.[25] Gram-negative bacteria have an outer membrane of lipopolysaccharides and proteins and a thin peptidoglycan layer, jointly forming the bacterial cell wall.[26] (Figure. 2)

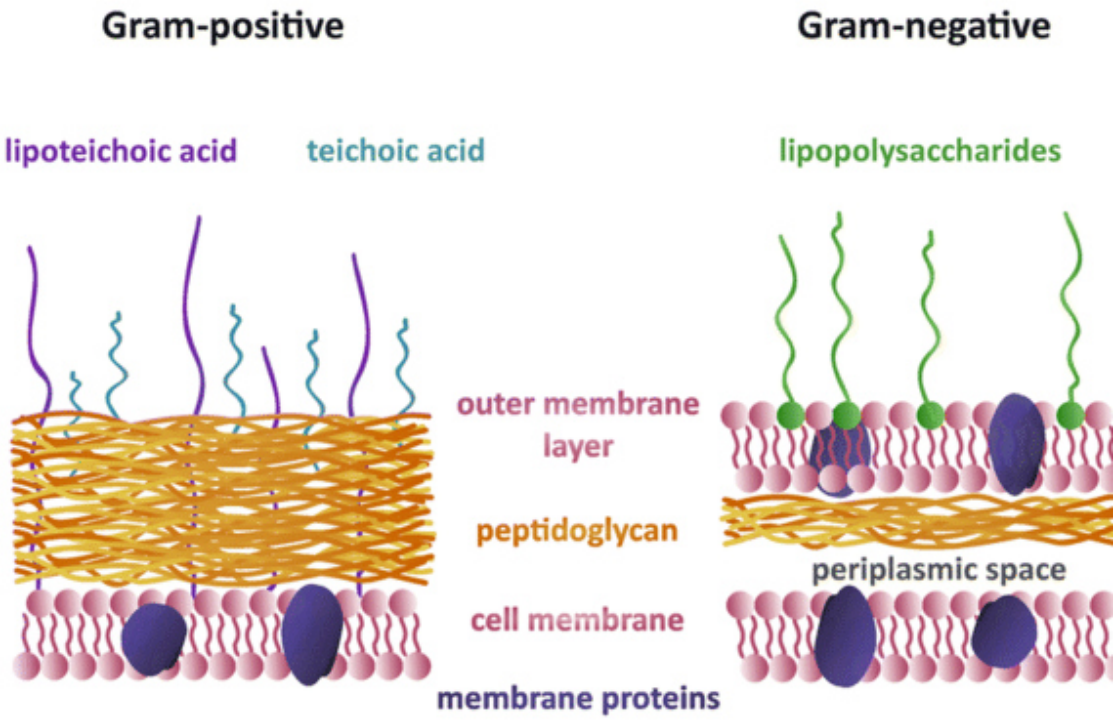

Figure 2: Difference in the cell wall structures of Gram-positive and Gram-negative bacteria. Modified reprint with the permission from ref [27]

Gram-positive and Gram-negative bacteria are known to have an overall negative charge on the surface, but the basis of the charge is different. Teichoic acid in the peptidoglycan layer containing phosphodiester bonds is responsible for the negative charge on the surface of Gram-positive bacteria.[28] Whereas phosphate groups attached to the lipopolysaccharides cause the negative charge of Gram-negative bacteria. It is reported that the surface charge density of *E. coli,* as an example of Gram-negative bacteria, is of the order of 5×10^{14} cm^{-2}.[29]

1.1.2 Multidrug resistance.

Since the discovery of Penicillin in 1928, many commercial antibiotics were developed and produced to combat infectious diseases. High use of these antibiotics to treat humans and animals resulted in emerging strains of bacteria that developed resistance to these antibiotics.[30] E.g., methicillin-resistant *Staphylococcus aureus* (MRSA) is a MDR bacteria that has developed resistance against most commonly known antibiotics.[31] MDR can be developed in microorganisms because of different innate and assimilated mechanisms. Innate resistance appears because of the absence or the presence of low-affinity targets due to gene mutation,[32] enzymatic inactivation of the drug,[33] low cell permeability or efflux mechanism that will remove the drugs from the cells.[34] Assimilated or acquired resistance is due to the mutations in target genes,[32] transfer of resistance genes via plasmid transfer, bacteriophages, and transposons to drug-susceptible cells.[35] Chemotherapeutic drugs, appropriately used, can only delay the inevitability of antibiotic resistance. Therefore, appropriate, long-term solutions are needed to deal with the challenges of multi-drug resistance.

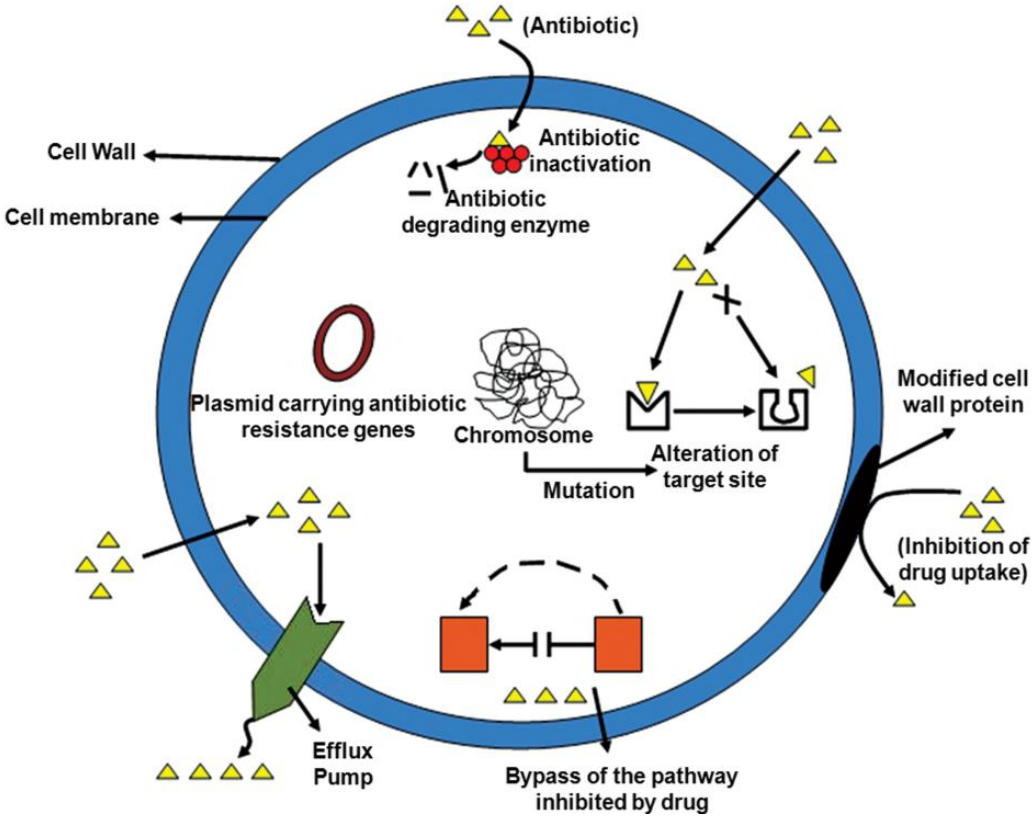

Figure 3: Mechanism of multi-drug resistance. Reprint with the permission from ref [36]

1.2 Nanotechnology for antibacterial applications

Nanotechnology provides a new class of materials that can be engineered to fight against pathogens.[37] Nanomaterials with varying physicochemical characteristics are diverse tools that can interact with bacterial cells through multiple pathways.[38] The physical and chemical properties of materials change drastically at the nanoscale (1-100 nm). These changes are attributed to shape, size, and high surface area-to-volume ratios.[39] Properties like photocatalytic, photothermal activity, and magnetism also vary from the bulk materials. The plasmonic properties of nanomaterials can be augmented by adjusting the shape of these materials.[40] With recent advances in synthesis techniques, varied selections of nanomaterials such as nanoparticles,[41] nanodots,[42] nanocubes,[43] nanorods,[44] nanoshells,[45] nanocages,[46] nanostars,[47] nanoflowers,[48] nanoeggs,[49] nanopopcorn,[50] and numerous other 2D materials[51] are developed.

1.2.1 Mechanism of antibacterial activity of nanoparticles

Several mechanisms of antibacterial activity of different nanomaterials are proposed in various reports.[52] The antimicrobial activity of nanomaterials is due to their ability to influence multiple biological pathways, which makes it challenging to dissociate individual mechanisms responsible for those interactions.[53]

Physical interactions: Metal nanoparticles (NPs), typically positively charged, can interact with negatively charged cell walls via electrostatic interactions.[54] [55] These physical interactions alter the surface charge of the bacterial membrane, which ends in membrane disruption. A leaky membrane results in the loss of fluids from the cytosol, and severe damage causes cell death. Metal NPs bind the cytosolic proteins, inhibiting the respiratory and metabolic mechanisms. Among published reports, silver nanoparticles can trap the enzymes within the respirator DNA chain, which inhibits their growth.[56]

Reactive oxygen species (ROS) production: ROS such as hydrogen peroxide (H_2O_2), superoxide anions ($^{\bullet}O_2^-$), or singlet oxygen ($^1O_2$) can disrupt membranes, denature proteins, and degrade genetic material of bacteria.[57] ROS are produced in lower concentrations inside the cells because of different biological processes regulated by ROS-scavenging enzymes.[58] Metal NPs can manipulate ROS-associated enzymes, which can induce a cell response to produce ROS.[59] A higher concentration of ROS instigates oxidative stress that causes cavities in bacterial membranes, causing cell lysis.[56] Furthermore, metal NPs such as silver,[60] zinc oxide[61], and titanium oxide[59] can directly initiate ROS production by reducing oxygen from the environment.[62]

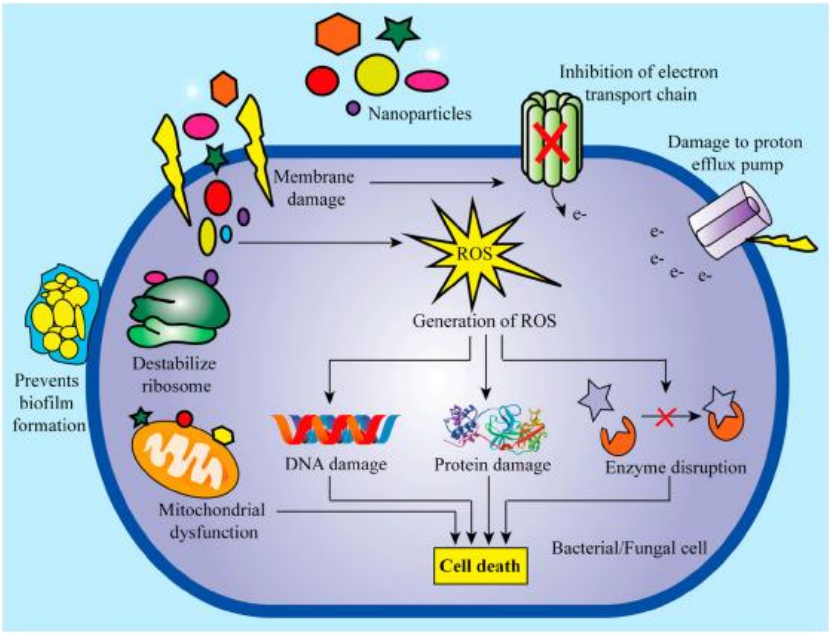

Figure 4: Schematic represents antimicrobial pathways (such as ROS processes, physical membrane damage, cell efflux mechanism disruption and metabolic interruption) of various nanoparticles. Reprint with the permission from ref [63]

Plasmonic photothermal effect: When light of a particular wavelength is shined on metal nanoparticles, the electrons in the conduction band start to oscillate due to the interference with the electromagnetic field.[64] This results in the formation of a rapidly moving electron cloud, which, upon relaxation, can either emit a photon (radiative decay) or electron lattice phonon coupling, which induces vibrations to the lattice, releasing thermal energy (non-radiative decay).[65] plasmonic photothermal effect depend upon the electron density of the nanoparticles; hence, they can be manipulated by their shape, size, and composition.[66] Gold nanoparticles were the first reported to employ the mechanism of photothermal effect in their antibacterial activity. Conjugated gold nanoparticles bound to the cell wall induced high localized temperature and bubble formation upon irradiation that disrupted the cell wall.[67]

Magnetic Effect: In ferromagnetic materials like iron, the electron spin direction in its individual atoms can align under an applied magnetic field, hence magnetizing the material.[68] In terms of antibacterial activity, generally, two different mechanisms of magnetic effect are used. 1)Magnetic hyperthermia works on the principle of localized heat. When magnetic force is applied to a ferromagnetic material until the point of saturation of magnetic flux density, it forms a permanent magnet. Once the force is reversed, ferromagnet starts to demagnetize, which results in loss of energy in the form of heat, also known as hysteresis loss.[69] Iron oxide nanoparticles,[70] Iron oxide-zinc oxide composite nano particles[71] have been reported for

antibacterial activity by the principle of magnetic hyperthermia. 2) The magnetophysical effect utilizes the physical movement of nanoparticles under the actuating magnetic field to remove biofilm and destroy individual cells. Micro rods consisting of gold and iron have been reported to remove to disrupt the biofilm of pathogenic fungi *Aspergillus fumigate* in an early study.[72] Recently, iron oxide nanoparticles have been reported to have dual catalytic-magnetic functionality. These so-called catalytic antimicrobial robots can remove biofilms with accuracy under a controlled magnetic field, simultaneously generating ROS due to its catalytic functionality that kills the individual cells and inhibits the growth of biofilm.[73]

1.3 Carbon-based nanomaterials.

Carbon, which exists in various allotropic forms, is equipped with unique properties that are considered to revolutionize the chemistry and surface interactions.[74] Graphite and diamond are the naturally occurring allotropes due to the hybridization of orbitals in sp^2 and sp^3 configurations, respectively.[75] Sp^2 hybridization allows carbon atoms to form hexagonal structures, which give rise to allotropic forms like nanotubes,[76] fullerenes,[77] and graphene. Due to their highly tunable electrical, mechanical, photoluminescence, and biological properties based on size, shape, structure, and composition, carbon nanomaterials have huge potential from superconductors,[78] energy storage,[79] sensors,[80] drug and gene delivery,[81] tumor therapy,[82] antibacterial and antiviral applications.[83]

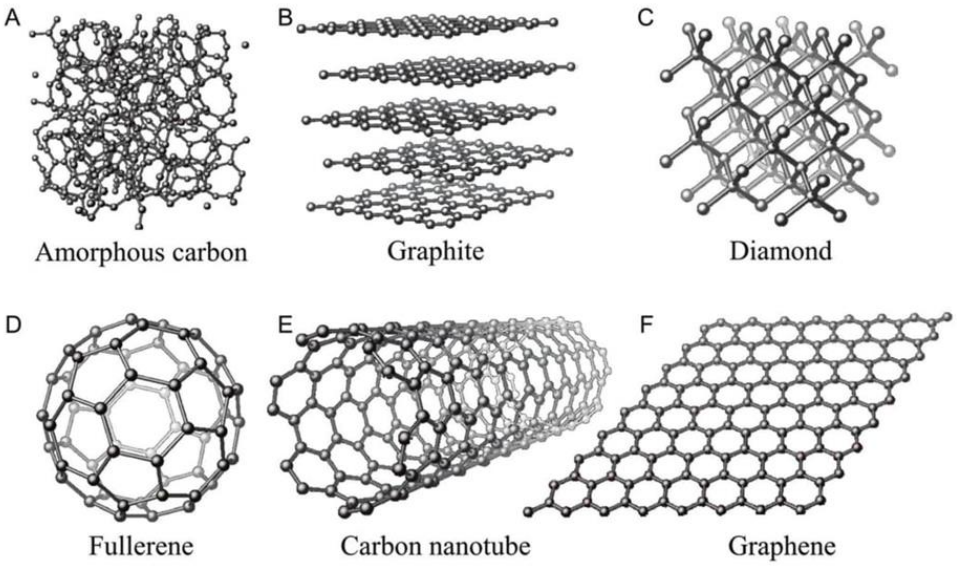

Figure 5. Allotropes of carbon with 3D (A: amorphous carbon, B: graphite, and C: diamond), 2D (F: graphene), 1D (E: carbon nanotube), and 0D structures (D: fullerene). Reprint with the permission from ref [84]

1.4 Graphenic materials

Graphene is a 2D, single atomic layer, crystalline allotrope of carbon, which is widely regarded as the building block of sp^2 hybridized carbon allotropes. This highly flexible, honeycomb-like structure was initially observed in graphite-related experiments and was later isolated and characterized by Andre Geim and Konstantin Novoselov in 2004.[85] Graphene is a sheet of sp^2-hybridized carbon atoms that are connected to three adjacent carbons with the σ-bonds and one π-bond perpendicular to the plane. The π-bonds form a conjugated system that stabilizes the crystalline structure and is responsible for its electronic properties.[86] Since its discovery, graphene has gained interest from all disciplines of science due to its unique set of properties, e.g., enormous surface area (2600 m^2/g), high mechanical strength (Youngs' modulus of 1 TPa), thermal conductivity (5000 W/K*m), and others.[87] This has driven scientists to explore ways to produce graphene materials on larger scales.

The current production methods can be classified into two main approaches: bottom-up and top-down.[88] Chemical vapor deposition (CVD) is a two-step method for producing graphene through a bottom-up approach.[89] Methane/hydrogen precursors are passed through transition metal substrate at high temperature to decompose and dissolve the carbon into the metal. Upon cooling, the dissolved carbon atoms diffuse out from the metal, growing transferable graphene film on the metal surface.[90] High-quality, large-size graphene sheets can be produced from CVD, but the scalability of the process still remains an enormous challenge.[91]

The top-down approach involves the exfoliation of graphene layers from graphite via physical, chemical, and mechanical methods.[92] Graphite is a multilayered carbon material where graphene sheets are stacked together due to weak van der Waals and π–π interactions contributing to high-thermodynamic stability.[93] Mechanical exfoliation methods such as micromechanical cleavage,[94] ball milling, and pressure or mixer-driven fluid dynamics use shear or nominal forces to overcome weak interactions to produce few-layer graphene materials.[95]

Graphene can be exfoliated chemically by oxidation of graphite dispersions with strong acids or oxidizing agents. The reaction produces oxygen-containing functional groups (e.g., hydroxyl, carboxylic, and epoxides) on the structure, which can be exfoliated by sonication into graphene oxide (GO) sheets.[96] Hummer's method is the most common method used today for producing GO by the chemical process.[97] The control over the conditions allows the production of GO with lower defects. Improved method to produce oxographene at low

temperatures allows production of material with low amount of defects.[98] [99]GO sheets can be further thermally or chemically reduced to restore graphene structure.[100] The electrostatic repulsion between the GO layers due to hydroxyl and carboxylic functional groups keeps them dispersed in aqueous medium.[101]

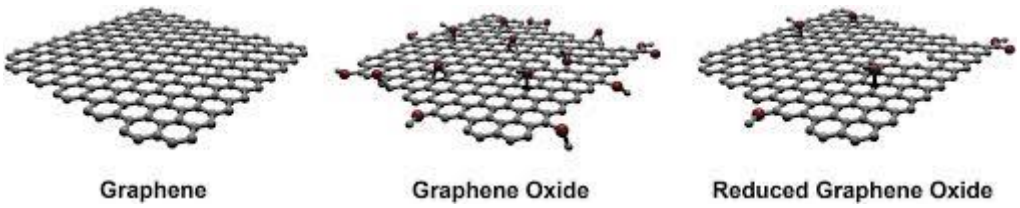

Figure 6: Structure of graphene, GO, and rGO. Reprint with the permission from ref [102]

1.4.1 Antimicrobial mechanisms of Graphenic materials (GMs)

Graphenic materials have been investigated for various bio-medical applications (such as drug delivery, gene delivery, and tumor therapy) due to their unique properties of large surface area, photothermal activity, and photodynamic properties.[103] GMs have been reported for pathogen inhibitions through multiple mechanisms.[104] Insight into those mechanisms is essential to design materials with effective antimicrobial activity for future bio-medical remedies.[105] The mechanism of antibacterial activity of GMs will be discussed in the following section.

Sharp edge cutting

Graphenic materials have extremely sharp edges due to their 2D morphology. Those sharp edges act as knives that can cut through the cell membranes upon interaction with cells.[106] Once the membrane is breached, phospholipid bilayer and peptidoglycan proteins can interact with the GMs due to hydrogen bonding or π-π interaction, further disrupting the cell membrane.[107] Physical damage on the cell wall causes the loss of fluid and intercellular contents and inhibits its duplication, eventually causing cell death. Akhavan and Ghaderi first proposed the mechanism of sharp edge cutting by depositing GO and rGO nanowalls on stainless steel surfaces. rGO nano walls have shown more potent toxicity to both gram-positive and gram-negative bacteria compared to GO nanowalls.[108] This is attributed to the better charge transfer in rGO due to the restoration of the π-conjugated system along with the high density of negatively charged functional groups on the edges of GO causing electrostatic repulsion.

Oxidative stress

The most extensively reported mechanism for graphene material's antibacterial activity is the oxidative stress that interferes with microorganism's cellular functions.[109] Due to their sizeable conductive surface, GMs can activate the O_2 in the solution by donating electrons. The super anion oxide radicals ($^{\bullet}O_2^-$) can further react with the protons in water, generating H_2O_2. ROS can cause the deactivation of membrane proteins, interfere with metabolic functions, and damage the cell membrane.[110] The microbial membrane requires electron transfer from the environment for its respiratory functions.[111] It has been reported that the respiratory proteins in the membrane act as a semiconductor.[112] Upon contact with GMs, the fermi level alignment takes place according to band theory, which transfers electrons from the membrane to GMs.[113] Li et. al. studied the antibacterial effect of larger graphene single sheets on conductive, semiconductive, and insulator substrates. They reported that the direct contact of gram-positive and gram-negative bacteria resulted in membrane damage for the conductive surfaces. In contrast, no such behavior was observed for the graphene on the insulator substrate.[114] Therefore, oxidative stress due to charge imbalance is proposed as the mechanism of loss of membrane integrity.

Cell entrapment and wrapping

Due to their flexibility, 2D and large surface area GMs can entrap individual bacteria cells from the environment. The entrapment of bacteria can cut off the supply of nutrients that inhibit bacterial growth. The effect of entrapment is largely correlated with the size of GMs. Smaller-size GMs require a large number of sheets to entrap a single cell.[115] Due to their smaller size, they have higher edge density, leading to sharp edge cutting, which makes cells lose their morphology. A larger size sheet can wrap around individual bacterial cells, isolating them completely.[116] Wrapping further applies oxidative stress that damages the cells.

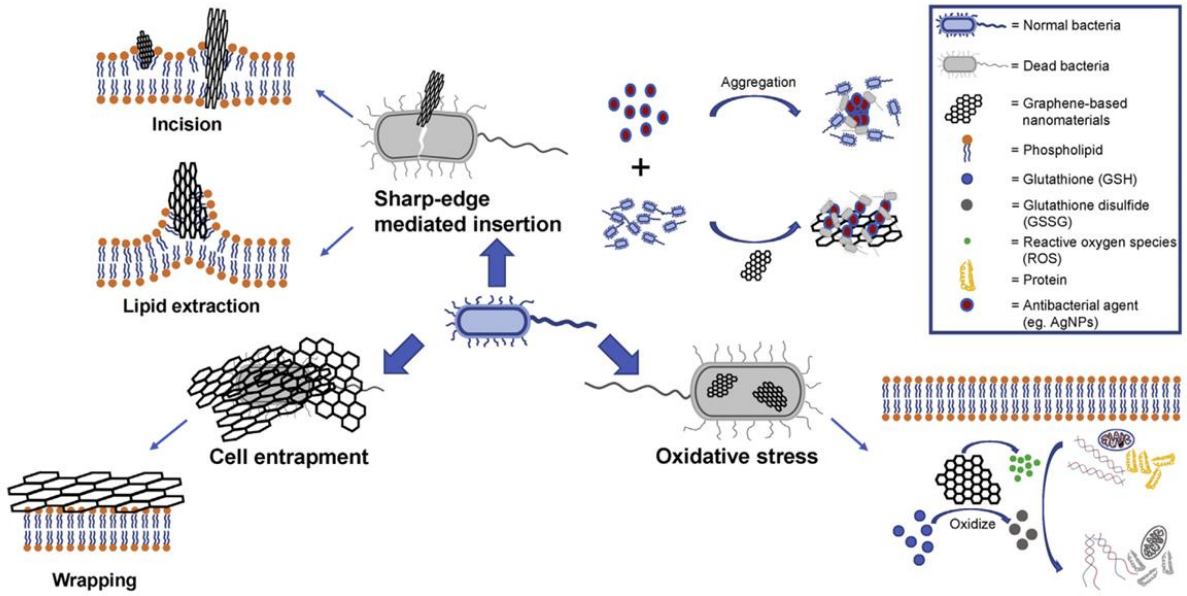

Figure 7: Schematic of the well-recognized antibacterial mechanisms of graphene-based nanomaterials, including sharp edge cutting effect, oxidative stress, and cell entrapment. Reprint with the permission from ref [117]

1.4.2 Structural and physio-chemical properties of GMs

Production methods of GMs have significant effects on their physicochemical properties. These properties play a significant role in the interaction of GMs for biological applications.[118] Graphene produced from CVD has lower structural defects compared to other methods, such as mechanical cleavage, chemical exfoliation, and synthesis.[119] These defects include oxygen moieties (hydroxyl, carboxylic, and epoxide functional groups) and/or damage in the basal plane structure.[120] The incorporation of these defects results in localized active regions on the sheets that enhance interactions with ions, molecules, and materials.[118]

1.5 Functionalization of GMs.

GMs have been functionalized with various materials to improve their processability and attain desired properties.[121] Although carbon-based nanomaterials exhibit innate antimicrobial activity, the effect is only feasible for some practical applications due to problems such as weaker interactions and longer exposure times.[122] Different functionalization approaches with various materials have been studied to enhance the interactions.[123] Generally, GMs can be functionalized with covalent and non-covalent functionalization.[124] Different strategies of the functionalization for GMs, along with different materials, will be discussed in the following section.

1.5.1 Non-Covalent functionalization of GMs.

Non-covalent interactions are those interactions that do not involve the formation of chemical bonds.[125] These interactions arise due to attractive and repulsive forces between different chemical species. It includes ion-ion, ion-dipole, dipole-dipole, hydrogen bonding, van der Waals, hydrophobic and π-π interactions.[126] GMs are repetitive aromatic rings forming a network that has π bonds perpendicular to the basal plane.[127] Hunter and Sander developed a model for aromatic systems in which they proposed the positively charged σ-framework of aromatic structures is sandwiched between the negatively charged cloud of π electron density. This gives rise to distinct electrostatic domains within the structures.[128] The geometry of those aromatic stacks in terms of orientations is shown in the figure 8.

Face-to-face stacking is the least favorable orientation in which aromatic systems can stack because of the electrostatic repulsion between the π electron density. As the aromatic systems are displaced slightly into the slip orientation, the electrostatic attraction between the σ-framework and negatively charged π electron is amplified while reducing the electrostatic repulsion between the π electrons.[128] Edge face conformations occur due to C-H-π interactions (electrostatic attraction between the π electron density of an aromatic ring and proton).[128] Due to its π-π conjugated system, graphene can immobilize a large number of molecules on its surface.[129] π-π interactions have lower dissociation energy if considered individually. However, due to the 2D planar structure of graphene, many of these interactions can take place, which can bind molecules on both sides.[130]

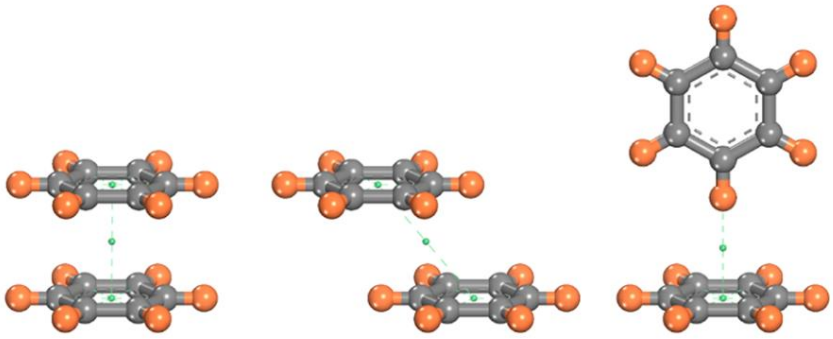

Figure 8: π-π stacking of conjugated systems face to face (left), slipped (middle) edge-face (right). Gray atoms represent carbon atoms, and orange represents hydrogen atoms. Reprint with the permission from ref [129]

Hydrophobic interactions are also used in immobilizing hydrophobic molecules non-covalently on graphene.[131] Organic molecules like surfactants, ionic liquids, or polymers can be fully or partially hydrophobic. Upon interactions with hydrophobic materials, water

molecules try to rearrange themselves to maximize the hydrogen bonding, consequently minimizing the contact with hydrophobic materials. This results in segregation of water and hydrophobic materials.[132] Surfactant molecules are immobilized on GMs to improve their dispersibility in an aqueous medium. The aliphatic chains of surfactant are attached to GMs due to hydrophobic interactions, and the hydrophilic head group can help stabilize the dispersions.[133] Bourlinos et al. reported increased dispersibility by functionalizing pristine graphene sheets with albumin or sodium carboxymethyl cellulose in water.[134]

Ionic interactions can also attach molecules to GMs.[135] GO has carboxylic and hydroxyl functional groups that can interact with positively charged molecules because of electrostatic attraction. Liang et al. have immobilized tetradecyl-trimethylammonium bromide on GO and rGO.[135] The electrostatic attraction between the positively charged trimethyl ammonium head and the negatively charged carboxylic groups binds the surfactant to the GMs. The GO/rGO polymer composites have improved dispersibility in organic solvents due to the lipophilicity of the aliphatic chains.[135]

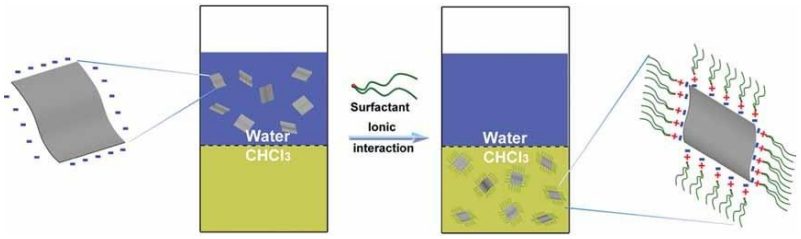

Figure 9: Illustration of the process for transferring graphene sheets from water to chloroform solutions. Reprint with the permission from ref [135]

1.5.2 Covalent functionalization of GMs.

Covalent functionalization involves combining chemical species with GMs by the formation of covalent bonds.[136] It can be achieved either by reacting with the carbon skeleton of GMs or with the oxygen-containing functional groups on their surface. Different addition (free radical,[137] nucleophilic,[138] and cycloadditions[139]) and substitution (electrophilic) reaction[140] strategies for the covalent functionalization of GMs have been reported, which will be discussed in the following section.

GO has a considerable number of epoxy functional groups on its surface that are vulnerable to nucleophilic attack.[138] A nucleophile such as primary amine (-NH_2) with an electron lone pair can easily attack those functional groups. This results in the opening of the epoxy ring and the incorporation of those molecules.[141] Nucleophilic epoxy ring opening is

an effective strategy for covalently functionalizing large number of molecules such as amino acids,[142] aliphatic amines,[143] ionic liquids,[144] biomolecules[145] and polymer[146] with amine functional groups on to the GO.

Electrophilic substitution reactions have also been used for covalent functionalization of GMs.[147] An electrophilic attack on graphene can take place on the sp^2 C–H bond sites, which will end up substituting the hydrogen with the electrophile. Lai et al. reported a simple approach for bromination of rGO with N-bromosuccinimide. N-bromosuccinimide decomposes in acidic conditions to produce bromine cations that act as electrophilic reagents and covalently attach to the defect sites, primarily on the edges of the graphene sheets, via electrophilic substitution reaction.[148] Bekyarova et al. functionalized a few graphene layers by reducing 4-nitrophenyl diazonium tetrafluoroborate. They confirm the covalent bond formation with various characterization techniques.[149]

Carboxylic and hydroxyl functional groups provide ample possibilities for the covalent functionalization of GO. Condensation reactions between a carboxylic and hydroxyl function group have been reported to functionalize various GO polymers. Yu et al. reported the functionalization of GO via an esterification reaction between the CH_2OH-terminated poly(3-hexylthiophene).[150] Salavagione et al. tried two different synthetic routes for functionalizing graphite oxide with PVA (polyvinyl alcohol) by esterification and reported successful conjugation.[151] The condensation reaction between carboxylic and amine functional groups results in the formation of amide bonds. Liu et al. utilized the strategy of amide coupling to functionalize nano-graphene oxide with aminated polyethylene glycol (PEG). Carbodiimide-catalyzed amide coupling reaction between carboxylic acid GO, and amine PEG groups resulted in successful conjugation.[152]

Hu et al. prepared chitosan functionalized graphene nanosheets by amidation reaction between amines of chitosan and carboxylic groups of graphene oxide under microwave irradiation followed by the reduction with hydrazine.[153] Isocyanate can react with carboxyl and hydroxyl groups to form amides and carbamate esters, respectively. Stankovich et al. functionalized graphite oxide with various isocyanates, which, upon further exfoliation into GO nanoplatelets, form a stable suspension in polar solvents.[154]

Due to its π conjugated system, the basal plane is the least reactive part of GMs.[125] However, there are several additional reactions that can functionalize many chemical species. [2+1] cycloaddition reactions were initially reported for functionalization of carbon nanotubes without breaking its π conjugated network.[155] Bingel reaction is one of the earliest methods of [2+1] nucleophilic cycloaddition reaction functionalizing GMs. It was initially reported for

functionalization of fullerenes using diethylmalonate derivatives in the presence of a base.[156] Carbanion of deprotonated malonate acts as a nucleophile attacking the electron-deficient carbon of fullerenes. Formation of the intermediate state transfer carbanion on the 2nd carbon of the fullerene, which displaces bromine by nucleophilic aliphatic substitution, forming a cyclopropane ring.[156] Bingel reaction conditions have been used in exfoliating and functionalizing graphene in situ.[157]

Choi et al. functionalized graphene with azidotrimethylsilane. Under thermal or photoactivation, azide dissociates into nitrogen and nitrene moieties that are highly reactive. These nitrene can react with the C=C, forming aziridine derivatives.[158] Faghani et al. developed a strategy for functionalizing GMs that provides an option for post-modification in mild conditions. They established a single-pot synthesis of thermally reduced graphene oxide (TRGO), sodium azide, and 2,4,6-trichloro-1,3,5-triazine that functionalized TRGO with azido dichloro triazine. Nucleophilic aromatic substitution of chlorine at different temperatures allows controlled biofunctionalization of the functionalized TRGO.[159]

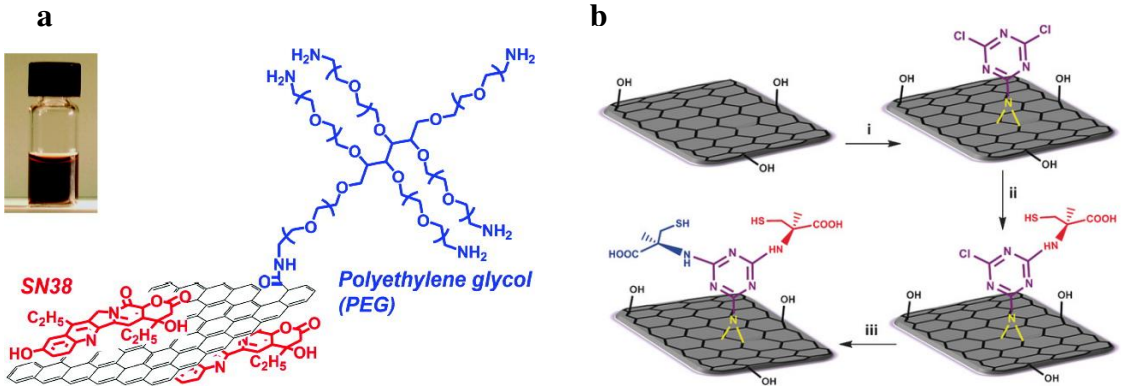

Figure 10: a) amide coupling to functionalize nanographene oxide with aminated polyethylene glycol. **b)** schematic illustration of functionalization of TRGO by a nitrene [2+1] cycloaddition reaction and controlled post-modification of the product (TRGO-Trz) by stepwise attachment of L- and D-Cysteine to its triazine functional groups. Reprint with the permission from ref [152] and [159]

Diels-Alders cycloaddition reaction (DACR) also known as [4+2] cycloaddition, has also been shown for functionalization of GMs.[160] DACR takes place between an electron-rich diene and an electron-deficient dienophile. Munirasu et al. studied the reactivity of different carbon materials, including single and multiwall carbon nanotubes with various diene and dienophile reactants via the DA mechanism.[161] They demonstrated successful functionalization of carbon nanotubes with both types of reactants. This shows that GMs have unique flexibility to act either as diene or dienophile, depending upon the reacting species.[161]

Li et al. have reported the functionalization of graphene with dihydro naphthalene via DACR.[162] [2+2] cycloaddition for functionalization GMs has also been investigated by scientists. The reaction of an aryne with C=C of graphene results in the formation of a four-carbon cycle. Zhong et al. utilized [2+2] cycloaddition to functionalize graphene with 2-triflatophenyl silane benzyne under mild conditions.[163]. 1,3-dipolar cycloaddition was initially reported for the functionalization of fullerenes by azomethine ylides by thermal decarboxylation of N-methylglycine in the presence of paraformaldehyde. Azomethine yildes reacts with the π-system, forming pyrrolidine rings on fullerenes.[164] Zhang et al. used 1,3-dipolar cycloaddition to conjugate tetraphenyl porphyrin with graphene and proved covalent functionalization with various characterization methods, including fluorescence quenching.[165]

Radical addition reactions can functionalize GMs with small and macromolecules. Radical species produced via thermal, photo, or electrochemical initiation can react with non-radical species (typically double bonds) to initiate the reaction. The reaction continues as a growing chain unless another radical species reacts with a propagating chain and terminates the radical. Bahr et al. demonstrated the functionalization of carbon nanotubes with a range of aryl diazonium salts. Electrochemical reduction of aryl diazonium salts in solution produces highly reactive aryl radicals that react with the C=C of carbon nanotubes.[166] Kan et al. functionalized GO with several polymers. They used various vinyl monomers with azobisisobutyronitrile (AIBN) initiator via free radical polymerization to produce 2D polymer brushes.[167] Shen et al. immobilized polystyrene-polyacrylamide copolymer onto graphene. Reduce graphene sheets produced by the Hummers' method were allowed to react with styrene and acryl amide monomers in the presence of benzyl peroxide radical initiator to produce amphiphilic graphene nanoplatelets.[168]

1.6 Functionalized graphene-based antimicrobial composites

Since GMs' innate antimicrobial activity is insufficient for most practical applications,[122] various composite materials have been synthesized and investigated by researchers. Graphene-metal conjugates are one of the most researched categories.[169] GMs loaded with different metallic oxides (e.g., iron oxide, zinc oxide, silver, or titanium dioxide) can be used as a two-dimensional carrier for the bactericidal agent.[170] Hu et al. used diallyl-dimethyl-ammonium chloride to immobilize silver nanoparticles (AgNPs) on GO. The resulting composite of GOPDDA-AgNPs exhibits significantly enhanced antibacterial activity in comparison to AgNPs.[171] The synergistic effect of two effective antimicrobial materials

demonstrated a considerable increase in antibacterial activity.[172] Zinc oxide is another commonly used antibacterial material whose properties depend on the active surface area where molecules can adsorb.[173] Aggregation of nanoparticles hinders the effective antibacterial activity of these materials.[173] To prevent their agglomeration, zinc oxide nanoparticles were immobilized on GO, yielding higher stability in aqueous medium and enhanced antibacterial capacity than individual materials.[174] Zinc oxide-graphene quantum dots produced by hydrothermal method exhibit potent antibacterial activity against *E. coli* with increased ROS production under ultraviolet irradiation.[175]

Gold nanoparticle composites with GMs have also been studied, which showed increased antibacterial activity. Gold nanoparticles can attach to the bacterial cell membrane by electrostatic forces and disturb membrane integrity. Gold NPs wrapped by rGO with polyethylene glycol have been used for photothermal ablation of bacterial cells. This unique biocompatible pathogen ablation technology offers a new therapy option for urinary infections.[176] Iron oxide nanoparticles are well-considered for biomedical applications, such as tissue repair, tissue detoxification, and magnetic resonance imaging resolution development. These nanoparticles exhibit moderate antibacterial activities against both gram-negative and gram-positive pathogenic bacteria. The rGO and iron oxide nanorods composites were produced by one-pot calcination of pre-synthesized iron oxide nanoparticles with rGO. The nanorods were infused between the layers of rGO. The composite material exhibits better antibacterial activity towards methicillin-resistant Staphylococcus aureus (MRSA), vancomycin-resistant Staphylococcus aureus, and ciprofloxacin-resistant Staphylococcus aureus compared to rGO.[177]

GMs with organic moieties like neutral amines, mannose, lactose, or cationic quaternary compounds improve the target specificity and interactions with bacteria. Since the bacteria carry negatively charged surfaces due to the presence of numerous phosphate groups, electrostatic attraction with positively charged surfaces can bind the negatively charged bacteria and effectively kill them. Venkatesan et al. developed chitosan-carbon nanotubes hydrogels by the freeze-lyophilization method and reported that the composite showed higher antimicrobial activity depending upon the concentration of carbon nanotubes.[178] Tan et al. functionalized graphene sheets with zwitterionic properties by stepwise conjugating polyglycerol sulfate and polyglycerol amine on the surface of triazine-functionalized graphene sheets. They used switchable characteristic of zwitterionic material under physiological conditions to trap and agglomerate bacteria from the solution.[179] Single-walled carbon nanotubes composite with poly (lactic-co-glycolic acid) was investigated by Aslan et al. They

reported a substantial decrease in viability of *E. coli* and *Staphylococcus epidermidis* cells when exposed to the composite material.[180] Duri et al. explored the combination of fullerenes with polysaccharides such as chitosan, cellulose, and γ-cyclodextrin. Their results showed the mixed γ-cyclodextrin/fullerene/chitosan film had significant antimicrobial action against vancomycin-resistant enterococci. This emphasized the compatibility of chitosan and γ-cyclodextrin with fullerenes in combined films for applications including food packaging. [181]

1.7 Water filtration membrane technologies for bacteria

Common chemical water treatment methods are chlorination or ozonization.[182] These methods need steady chemical input or energy to work and are known to produce hazardous by-products.[183] Membrane filtration is the most viable technology for dealing with current water problems because it needs little chemical products or energy input and produces no notorious by-products.[184] Membrane technology is well-known as an efficient water separation method because it gives a superior quality of water by removing a maximum number of contaminants.[185] Membrane filtration has several benefits, which include feasible operative techniques, easy maintenance, concise modular structure, and lower leaching levels of chemical sludge while treating wastewater from several different mediums.[186] Membranes work on the principle of size exclusion of particles from the fluid. Separating membranes are classified into microfiltration tubes and nanofiltration tubes on the basis of the pore size.[187] Membranes are classified as organic or inorganic membranes based on their structure. Organic membranes are composed of polymers or composite materials, while inorganic membranes are fabricated of ceramics, metals, and glass.[188] Several outstanding properties of polymer nano-composites are recognized, including elevated flexibility, compact storage space, structural and chemical firmness, permeability, and effective eradication of wastewater products.[189]

1.7.1 Membrane fouling

Fouling is a major concern in membrane filtration systems [190]. Polymeric membranes are inherently hydrophobic, which makes them prone to fouling.[191] Foulants cling to the surface of the polymeric membrane, reducing the pore size and eventually blocking the filter completely. Fouling is classified as organic[192] (e.g., oils, polyelectrolytes, humic), inorganic (precipitates of metal hydroxides),[193] and biofouling (bacteria, fungi, algae).[194] Biofouling is still a significant challenge in commercial membrane water filtration systems. It begins with the binding of microbial cells to the membrane surface, leading to the biofilm layer formation.[195] The biofilm can comprise various microbial species (e.g., bacteria, algae,

protozoa, and fungi). Electrokinetic and hydrophobic interactions are involved in the initial microbial attachment.[196] In a biofilm, the microbial community resides in a matrix of hydrated extracellular polymeric substances that serve as their immediate environment. Microorganisms account for less than 10% of the dry mass in most biofilms, while the extracellular matrix, formed mainly by the organisms themselves, can account for over 90%.[197] Various approaches, including different cleaning methods, have been proposed and adopted to deal with the challenge of stopping the biofilm formation in membranes.[198] These methods can diminish 99% of bacterial growth, but the remaining 1% of the bacterial community can grow back rapidly. To improve the antibacterial potential of these membranes, they are fabricated with other antimicrobial agents to double-fold their action.[199]

1.7.2 Nano-composite fabricated antibacterial polymeric membranes

Nanotechnology in membrane manufacturing not only imposes antibacterial effects but also provides structure and durability to the membrane system for efficient output in the water treatment process.[200] The membranes are categorized into conventional and surface-located nano-composite membranes depending on the manufacturing techniques.[201] In conventional nano-composite membranes, the blending technique is used.[201] In contrast, in the surface-located nano-composite membrane, the nanoparticles are immobilized on the surface of the membrane by using the grafting method or interfacial polymerization techniques [202].

1.7.3 Blending Technique for Antibacterial Polymer Membrane

In the conventional blending technique, the polymer matrix is blended with any antibacterial material like nanomaterials (silver, zinc, titanium, and carbon nanotubes) to have an antibacterial polymer membrane.[203] Using the physical technique of mixing and incorporating the antibacterial ability into the polymer membrane via nanomaterial is one of the most feasible techniques so far. A homogenous polymer matrix mixture is blended with the selected nanomaterial to form composite polymer membranes.[204] A significant disadvantage of using the blending technique is that most of the nanomaterial is in bulk and, therefore, does not come in direct contact with the bacteria on the surface of the membrane, resulting in eventual biofouling.[205] The gradual and continuous leaching of the nanoparticles during the filtration process also results in the loss of the nanomaterial.[206]

1.7.4 Membrane Surface Coating with Antibacterial Agents

This method of membrane formation overcomes the hurdle of non-exposure of the nanoparticles to the membrane surface.[204] A wide range of physical and chemical techniques have been applied to ensure the presence of antibacterial agents on the top-exposing surface of

the membrane.[207] The polymer membrane can be coated with an antibacterial agent by dip coating and/or spin coating processes. In the dipping method, the substrate is dipped in the antibacterial agent. After that, it is thoroughly rinsed with sterilized water, ensuring the attachment of NPs on the surface of the membrane. In the spinning method, the substrate is spun. The antibacterial agent is passed through it, resulting in thinner, smoother, and finer coating surfaces [208].

1.7.5 Interfacial Polymerization of NPs

Interfacial polymerization is the most advanced and refined method of incorporating antibacterial properties onto a membrane.[209] It ensures maximum exposure of antibacterial agents with low possibility of its leaching.[210] This method is effective for constructing thin-film composites (TFCs). TFCs comprise the support of porous substrates comprising thin and ultrafine polyamide sheets of films.[211] In this method, the porous substrate is exposed to an aqueous solution of diamines like m-phenylenediamine followed by the pouring of the organic solution containing monomers, i.e., chloride trimesoyl chloride on the pre-saturated porous substrate layer [212]. To make TFCs antibacterial, the aqueous solution is pre-deposited with the antibacterial NPs before the polymerization with the chloride trimesoyl chloride [213].

Titanium oxide fabricated membranes show antibacterial effects by producing ROS. The major pros of using titanium oxide as a nanomaterial in membrane fabrication include its non-degradation during microbial degradation.[214] Under UV radiation, the electrons in the nanomaterials get excited and react with the atmospheric oxygen. As a result of this reaction, the ROS are generated, rendering anti-effects on bacterial and viral growth.[214] These are very promising membranes in eradicating biofouling from the membrane surface.[215] Silver-based nanoparticles (AgNPs) are famous for their exceptional antibacterial activity. They interfere with the bioactivity of the bacteria by releasing silver ions. Silver ions cause bacterial cell lysing and negatively impact the respiration of the bacterial cell.[216] Although AgNPs are attractive due to their excellent antimicrobial ability, one of the drawbacks of using them in the membrane is their instability. The AgNPs can dissolve in water during the treatment procedures, which is a significant drawback.[217]

2 Scientific Goals

The development of new methods and materials for antibacterial water filtration applications remains highly important because of MDR and the limitations of current water filtration technologies. The aim of this scientific research is to develop a novel approach with flexible 2D material that captures bacteria via electrostatic interaction. Flexible sheets can adapt to the shape of bacteria, and matching oppositely charged surfaces should bind the particles efficaciously. Furthermore, the developed material will be used to design and produce a filtration device and perform quantitative testing to determine the effective removal of bacteria from water.

Graphene materials have been studied for their antibacterial properties. Among many GMs, GO is a flexible, low-cost, 2D material. Furthermore, its higher dispersibility in various solvents makes it a suitable candidate for wet chemistry. The main goals of this study are:

i) to synthesize and characterize micrometer sized GO sheets with poly 2-(dimethylamino)ethyl methacrylate (PDEMA). A grafting-to approach via radical polymerization will be used to functionalize the GO sheets with different polymer chains.

ii) to flip the charge of the functionalized sheets from negative to positive using a quaternization reaction. The methylation of dimethylamines of GO-PDEMA forms quaternary ammonium groups to provide poly[2-trimethylammoniumethyl methacrylate chloride] (GO-PTEMA). Protocols will be developed and performed to determine the charge per unit surface area of the flexible GO PTEMA sheets, and their interaction with bacteria will be examined.

iii) the positively charged GO PTEMA sheets will be immobilized on cellulose fibers (GOX fibers), and quantitative biological studies will be performed to determine effective bacterial filtration under various conditions. GOX fibers will be characterized with various microscopy techniques to verify the immobilization of GO PTEMA sheets and their interaction with bacterial particles. A filtration device will be designed and produced, and protocols will be developed to test GOX fibers in bacteria filtration experiments to evaluate their filtration performance in parameters such as flow rate, loading capacity, and reduction of colony-forming units.

3 Publication and Manuscripts

In the following section, the scientific outcomes of this doctoral research are listed, and the contributions of the authors are specified.

3.1 Multivalent bacteria binding by flexible polycationic micro sheets matching their surface charge density.

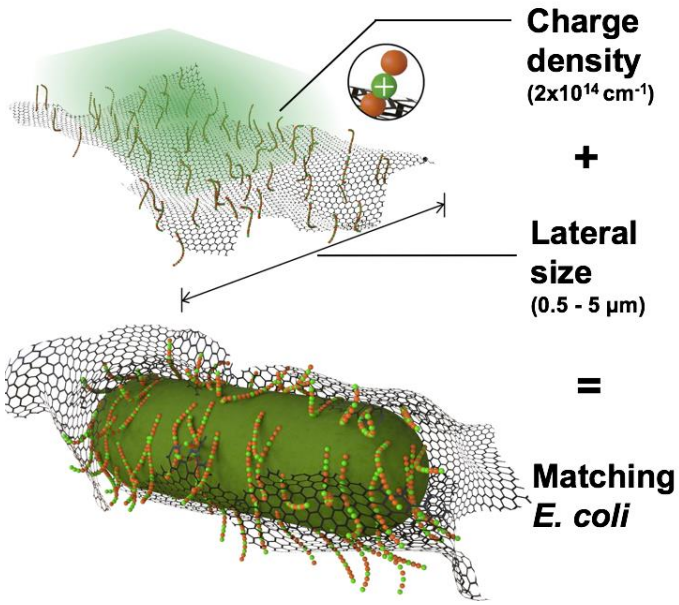

Rameez Ahmed, Ankita Vaishampayan, Jose Luis Cuellar-Camacho, Darren J. Wight, Ievgen Donskyi, Wolfgang Unger, Elisabeth Grohmann, Rainer Haag, Olaf Wagner

Adv. Mater. Interfaces **2020**, *7*, 1902066.

https://doi.org/10.1002/admi.201902066

Author contributions

Rameez Ahmed performed the synthesis and characterization experiments and wrote the manuscript. Ankita Vaishampayan performed biological experiments. Jose Luis Cuellar-Camacho performed AFM. Darren J. Wight performed confocal microscopy. Ievgen Donskyi and Wolfgang Unger performed XPS. Rainer Haag conceptualized and discussed the project. Olaf Wagner conceptualized and supervised the project and co-authored the manuscript.

ADVANCED MATERIALS INTERFACES
www.advmatinterfaces.de

Multivalent Bacteria Binding by Flexible Polycationic Microsheets Matching Their Surface Charge Density

*Rameez Ahmed, Ankita Vaishampayan, Jose Luis Cuellar-Camacho, Darren J. Wight, Ievgen Donskyi, Wolfgang Unger, Elisabeth Grohmann, Rainer Haag, and Olaf Wagner**

Aiming at the overall negative surface charge of bacteria, a new strategy of antibacterial agents based on large polymer-modified graphene oxide (GO) sheets is assessed. The presented flexible, polycationic sheets match the size and charge density of the *Escherichia coli* surface charge density (2×10^{14} cm^{-2}). These matching parameters create an unspecific but very strong bacteria adsorber by multivalent, electrostatic attraction. Their interaction with bacteria is visualized via atomic force and confocal microscopy and shows that they effectively bind and wrap around *E. coli* cells, and thereby immobilize them. The incubation of Gram-negative and -positive bacteria (*E. coli* and methicillin-resistant *Staphylococcus aureus*, MRSA) with these polycationic sheets leads to the inhibition of proliferation and a reduction of the colony forming bacteria over time. This new type of antibacterial agent acts in a different mode of action than classical biocides and could potentially be employed in medicinal, technical, or agriculture applications. The presented microsheets and their unspecific binding of cell interfaces could further be employed as adsorber material for bacterial filtration or immobilization for imaging, analysis, or sensor technologies.

1. Introduction

Pathogenic bacteria remain an important medical and scientific challenge for society. Apart from the development of chemical drugs like antibiotics, new strategies to fight bacteria are currently being developed by targeting pathogens physically via nanotechnology.[1–3] Bacteria are dependent on making contact with other surfaces during the first phase of an infection or colony formation.[4] Blocking bacterial surfaces results in their inhibition and ultimately in nonproliferation.[5]

Graphene materials have been shown to act as antibacterial compounds by blocking the bacteria surface.[6,7] They are flexible, nano- or micrometer-sized sheets that can be employed as basis material for various 2D macromolecular architectures. Graphene oxide (GO) is the most commonly used 2D material, as it is the oxidized and exfoliated product from the low-cost resource graphite. GO is not a defined molecule but a collective term for oxidized graphene sheets.[8] The properties of these macromolecular structures are defined by many variable parameters: sheet size, oxidation degree, shape, number of aggregated layers, etc. Therefore, a huge variety of properties for different GO batches is possible. These variable properties can lead to various effects on bacterial cells.[9,10] The reported antibacterial mechanisms of GO include chemical damage via oxidative stress,[11] physical damage from sharp edges,[12,13] extraction of lipid molecules via attracting, and disruptive forces[12,14] or wrapping and trapping by 2D sheets.[6,7] GO can also be employed as a 2D carrier for biocidal compounds that are loaded onto the sheets (e.g., silver,[15,16] zinc oxide,[17,18] iron oxide,[19] or titanium dioxide[20]). Furthermore, IR-laser irradiation after GO sheet binding has been shown to heat up the material as well as the bacterial cell, leading to immediate bacterial cell death.[19,21]

In order to optimize the targeting function of the GO carrier, several research groups have enhanced the binding affinity to bacteria by introducing chemical binding moieties onto the GO sheets (for example, mannose,[22,23] lactose,[23] neutral amines,[23–25] or cationic quaternary amines).[26,27] However, the number of studies on graphene derivatives binding bacteria is still relatively low, compared to the vast number of variable property parameters (lateral size, concentration, exposure time, or bacteria cell

R. Ahmed, Dr. J. L. Cuellar-Camacho, Dr. I. Donskyi, Prof. R. Haag, Dr. O. Wagner
Freie Universität Berlin
Institute of Chemistry and Biochemistry
Takustr. 3, Berlin 14195, Germany
E-mail: olaf.wagner@fu-berlin.de
A. Vaishampayan, Prof. E. Grohmann
Beuth Hochschule für Technik
Seestraße 64, Berlin 13347, Germany
Dr. D. J. Wight
Freie Universität Berlin
Institute of Virology
Robert-von-Ostertag Str. 7-13, Berlin 14163, Germany
Dr. I. Donskyi, Prof. W. Unger
Bundesanstalt für Materialforschung
Unter den Eichen 44-46, Berlin 12203, Germany
The ORCID identification number(s) for the author(s) of this article can be found under https://doi.org/10.1002/admi.201902066.

DOI: 10.1002/admi.201902066

type) that define the experimental outcome.[9,10,28] Therefore, it is crucial to precisely determine and adjust the 2D material parameters to match the bacterial counterpart that should be bound. A universal binding strategy should cover several bacteria cell types including those of different cell shape (e.g., spherical or rodlike) and cell surface composition. A physical property that almost all bacteria share (including Gram-positive and Gram-negative bacteria) is their overall negative surface charge[29] due to the high number of phosphate groups on their surface. Positively charged surfaces can therefore immobilize a wide variety of bacteria via an electrostatic attraction mechanism.[30] It has been shown that surfaces with the exact same charge density of opposing charges ($\approx 10^{14}$ cm^{-2}) not only bind bacteria but also impose a rapid cell death.[31–33] Transferring this concept onto flexible sheets that can further adapt to the pathogen surface, could potentially create a new class of antibiotics that block the pathogen surface and prevent infection or proliferation.

Therefore, we aimed to design a universal counterpart to bacteria surfaces to meet their physicochemical properties as a flexible 2D sheet. As GO is negatively charged, due to its hydroxyl and carboxyl groups, it would repulse bacteria[34] and the surface charge of the sheets needs to be switched to positive. To realize this macromolecular "umpolung," polycationic polymer chains were grafted to the GO sheets. This adds further flexibility as the positive charges in the polymer chains can also move to find their negatively charged counterparts on the bacterial surface. *Escherichia coli* (*E. coli*) and methicillin-resistant *Staphylococcus aureus* (MRSA) were used in incubation experiments to evaluate the effect of flexible polycationic sheets on bacteria cells. By aiming at a general property of bacteria interfaces we assess a new strategy for antibacterial agents that could physically capture and inactivate bacterial cells.

2. Results

2.1. Synthesis and Characterization

2.1.1. Starting Material Property Analysis

In order to achieve the best interaction between GO sheets and bacteria, they should be of same size and charge density. This means that the average lateral size of GO sheets should be in the range of 1–5 µm to suitably interact with bacteria such as *Escherichia coli* (*E. coli*; ≈2 µm). Therefore, micrometer-sized GO sheets were purchased as a starting material that could be directly dispersed and chemically modified. In order to avoid hydrophobic interaction effects and sheet aggregation, the GO raw material was chosen with a high oxidation degree of ≈48 wt% and a C=C to C—O ratio of 2:1 (see elemental analysis, EA, Table S1 and highly resolved C1s X-ray photoelectron spectroscopy (XPS), Figure S5 in the Supporting Information). To determine the average size of the GO flakes scanning electron microscopy (SEM) images (Figure S1, Supporting Information) were acquired and analyzed with ImageJ software. The average lateral size was determined to be 3.0 ± 2.4 µm (Figure S2, Supporting Information). 86% of the sheets had a size in between 0.5 and 5 µm and therefore fit well to the typical size range of bacteria.

2.1.2. Polymer Grafting onto GO and Subsequent Amine Quaternization

The cationic polymer-functionalized GO sheets were prepared via a two-step synthesis. First, the methacrylate polymer chains were introduced by a radical "grafting from" polymerization based on the work of Kan et al.[35] who reported a high polymer density for several methacrylate monomers via free radical polymerization on GO. After the polymer grafting, positive charges were introduced via methylation of the dimethylamines to form quaternary ammonium groups, as shown in Figure S3 (Supporting Information). The detailed synthesis is described in the experimental section. To verify the grafting process and determine the amount of grafted functional groups on GO, EA, XPS, and atomic force microscopy (AFM) were performed. As the GO-starting material contained only traces of nitrogen in its structure (0.01 wt%), the amount of nitrogen was used to determine the polymer functionalization of the dimethylamine polymer. The nitrogen content of the polymer-functionalized GO (GO-poly[2-(dimethylamino)ethyl methacrylate], GO-PDEMA) was determined by EA as 5.5 wt%, which calculates to a degree of polymer functionalization of 62 wt% (**Table 1**).

AFM was used to visualize the functionalization of the GO sheets, as height and surface structure of the polymer-modified

Table 1. Summary of the determined material properties.

Parameter	Numeric value		
Materials	GO	GO-PDEMA	GO-PTEMA
Average lateral size	3.0 ± 2.4 µm	3.0 ± 2.4 µm	3.0 ± 2.4 µm
Average height	1.7 ± 0.18 nm	2.8 ± 0.87 nm	4.78 ± 0.48 nm
Polymer content[a)]	–	62 wt%	62 wt%
Average polymer length[b)]	–	16.4 kDa (104 rep. units ≈25 nm)	16.4 kDa (104 rep. units ≈25 nm)
No. of ammonium groups[c)]	–	–	3.93 mmol g^{-1}
Theoretical charge density[d)]	–	–	8.3×10^{14} cm^{-2} = 8.3 nm^{-2}
Experimental charge density[e)]	–	–	2.3×10^{14} cm^{-2} = 2.3 nm^{-2}
Zeta potential	–39.5 ± 7 mV	+14.5 ± 5 mV	+ 34 ± 4 mV

[a)]Degree of polymer functionalization calculated by elemental analysis; [b)]Molecular weight of polymer chains determined by GPC; [c)]Number of ammonium groups per gram; [d)]Calculated number of charges per unit area; [e)]Experimentally determined number of charges by fluorescein experiment.

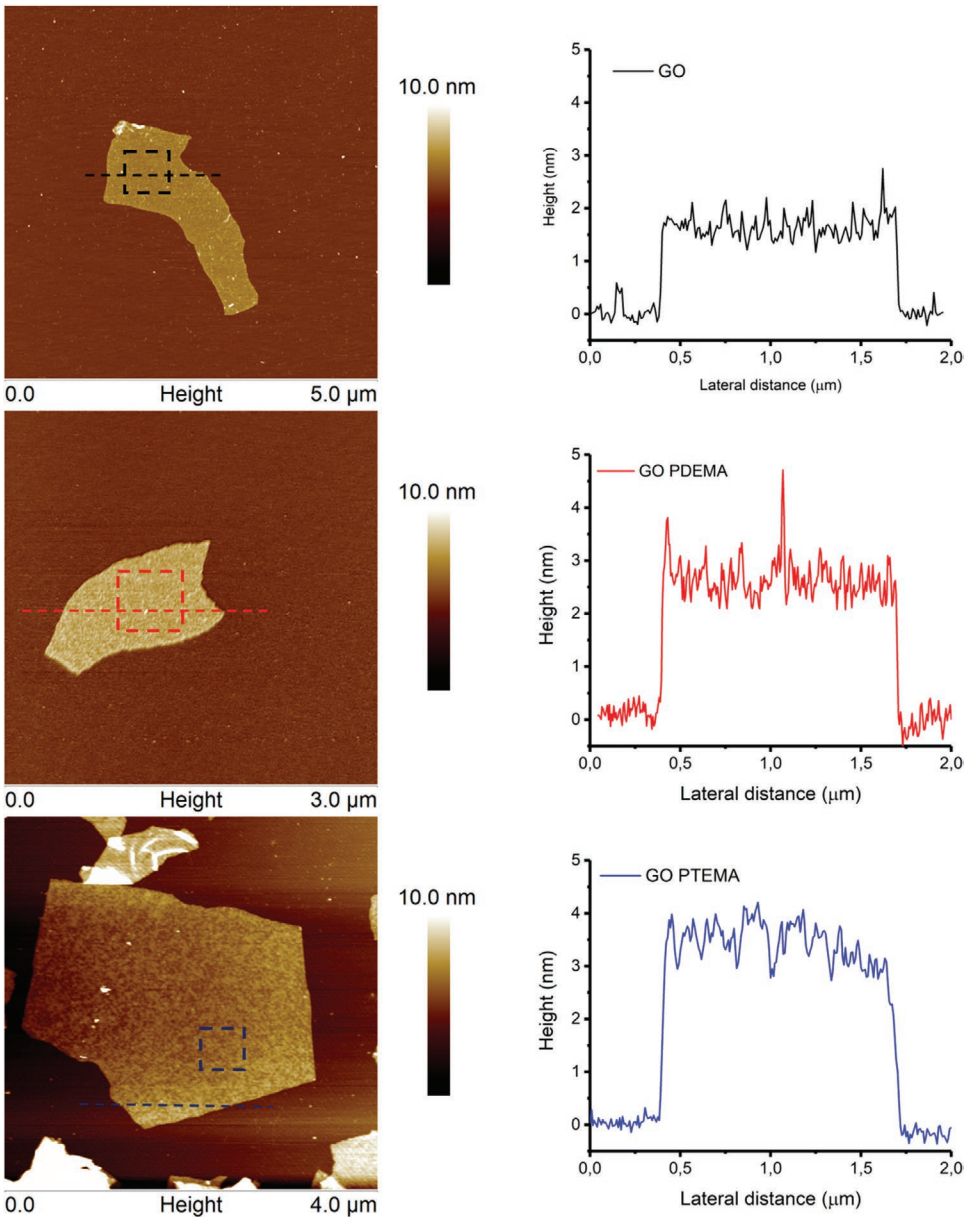

Figure 1. Atomic force microscopy (AFM) images and height profiles of GO, GO-PDEMA, and GO-PTEMA.

GO flakes becomes altered upon functionalization (**Figure 1**). The AFM images show that the GO sheets have a height of ≈1.7 nm, which is typical for GO flakes, and that the polymer-modified GO-PDEMA has a height of ≈2.8 nm. The quaternized sheets with positive charges (GO-poly[2-trimethylammoniumethyl methacrylate chloride] (GO-PTEMA)) were measured and shown to have a height of ≈3.7 nm, suggesting further modification had occurred. The average sheet thickness of GO-PTEMA was determined by measuring twenty sheets by AFM, which gave an average height of 4.78 ± 0.48 nm. These values confirmed the successful grafting of the polymer chains onto the GO starting material.

The compounds were also analyzed by XPS as shown in Figures S5 and S6 (Supporting Information), which further verified the successful polymer modification. To determine the average polymer chain length of polymer-modified GO, the molecular weight (M_w) of nongrafted free polymer was determined by gel permeation chromatography (GPC). A molecular weight of 16 400 g mol^{-1} was determined, which corresponds to 104 monomers per polymer chain (Figure S7, Supporting Information). With a polymer functionalization of 62 wt% of GO-PDEMA, the amount of dimethylamino groups was calculated as 3.93 mmol g^{-1} (Equation S1, Supporting Information). The theoretical number of dimethylamino groups and therefore charges per surface area of the quaternized GO-PTEMA were calculated as 8.36 nm^{-1} = 8.36 × 10^{14} cm^{-1} (Equations S2 and S3, Supporting Information).

2.1.3. Charge Density Calculation

In order to experimentally assess the surface charge of GO-PTEMA their zeta potential was determined. The zeta potential

of the GO starting material was measured to be –40 ± 7 mV, which can be explained by negatively charged hydroxyl or carboxyl groups. The di-amino polymer-modified GO-PDEMA showed a positive value of +15 ± 6 mV. After methylation in excess by methyl iodide, the neutral dimethylamino groups were converted to positively charged ammonium groups and the zeta potential of GO-PTEMA was measured to be +34 ± 4 mV (Figure S8, Supporting Information; Table 1). Compared to that, the corresponding negative zeta potential values of *E. coli* were reported in literature to be –16 to –47 mV.[30,36]

In order to experimentally quantify the number of positive surface charges per surface area, the materials were evaluated in a dye adsorption experiment with a negatively charged dye (fluorescein sodium salt). The amount of the negatively charged dye binding electrostatically to the positive charges of GO-PTEMA was determined by UV–vis spectroscopy (Figure S9, Supporting Information). This revealed the number of charges per mass of GO-PTEMA and was calculated to be 2.3×10^{14} charges cm^{-2} (Equation S6, Supporting Information). It should be noted that the surface charge density of *E. coli* was reported to be 90 µC cm^{-2},[31] which equals 5×10^{14} cm^{-2} (Table 1). Therefore, the charge density on the GO-PTEMA sheets was in the same order of magnitude as determined for bacteria and therefore promising for investigating their bacterial interaction.

2.2. Bacteria Interaction with GO-PTEMA

2.2.1. Interaction with Life/Dead-Stained E. coli Visualized by Confocal Microscopy

In order to assess the effect of GO-PTEMA on bacteria, we stained *E. coli* with two dyes to identify live (SYTO-9; green) and dead (propidium iodide; red) cells and incubated them with 250 µg mL^{-1} GO and GO-PTEMA. Images of bacterial cells were taken using a confocal microscope and showed no dead cells for the control or the GO-treated bacteria. Only the GO-PTEMA treatment showed red-stained cells, indicating disrupted bacterial cell walls by the GO-PTEMA sheets (**Figure 2**a).

Furthermore, stained *E. coli* cells could be seen moving around under the confocal microscope. *E. coli* BL21 (DE3) are nonmotile bacteria but move by random Brownian motion. In order to visualize if GO-PTEMA could affect this Brownian motion, time-lapse images of the SYTO-9-stained live *E. coli* were captured using a confocal microscope. *E. coli* cells could be seen to move around, when they were left untreated or incubated with 250 µg mL^{-1} GO sheets. Interestingly, treatment with 250 µg mL^{-1} GO-PTEMA completely prevented bacteria from moving, suggesting that they were immobilized by being wrapped inside the polycationic GO-PTEMA sheets, and thus preventing their movement by Brownian motion (Figure 2b). This data was also confirmed over a longer time frame of analysis (Figure S10, Supporting Information).

To quantify this observation, all bacterial tracks (>20 consecutive frames in length) from the time lapse were analyzed and showed that the mean velocity of bacterial movements incubated with GO-PTEMA was much lower than the control (Figure 2c). Taken together, this data suggests that GO-PTEMA binds tightly to bacterial cells and wrapping them as a major part of its antimicrobial effect.

2.2.2. Wrapped E. coli Visualized by AFM

In order to further confirm the wrapping of *E. coli* by the GO-PTEMA sheets, AFM was utilized to study the interaction of bacteria and GO-PTEMA in a fluid chamber. Briefly, live *E. coli* on the slightly negatively charged mica substrates were used after depositing a layer of polycationic poly-L-lysine to ensure immobilized bacteria by electrostatic attraction. In case of the *E. coli* samples incubated with GO-PTEMA sheets, bare mica substrates were used without polycationic poly-L-lysine film. The *E. coli* wrapped in positively charged sheets exhibited a positively charged surface and therefore stuck to the mica substrates without further modification (**Figure 3**). The height profiles of GO-PTEMA-treated and free *E. coli* differed and showed an average height of 687 ± 7 nm for *E. coli* alone and

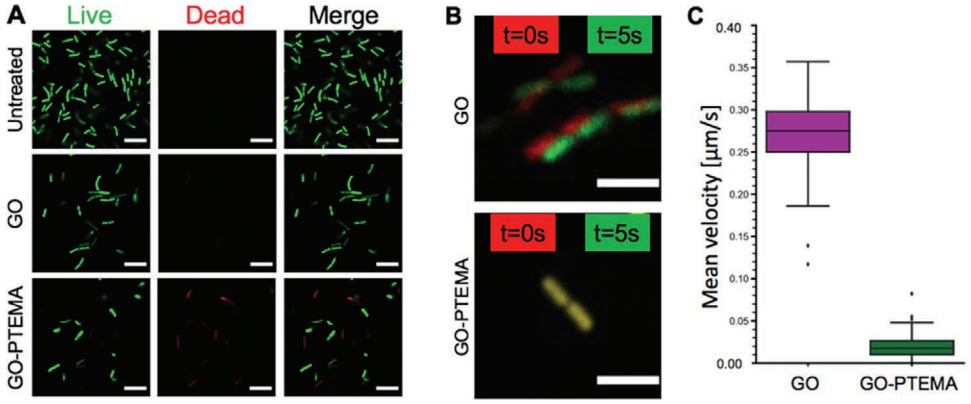

Figure 2. Confocal microscopy of stained and treated *E. coli* BL21 (DE3). *E. coli* were subjected to either no treatment or treatment with GO or GO-PTEMA. Shown are single *z*-plane images of A) *E. coli* stained as live (SYTO-9; green dye) and dead (propidium iodide; red dye) (scale bars equal 10 µm); B) *E. coli* stained with SYTO-9 (green) with time-lapse images with frame 0 (postcolored red) and after 5 s (postcolored green) and then overlaid to show bacterial movement (scale bar = 4 µm); and C) all bacterial tracks (>20 consecutive frames in length) from the time lapse quantified and analyzed. Bar charts show the mean velocity of bacterial movements (GO, nTracks = 65; GO-PTEMA, nTracks = 42).

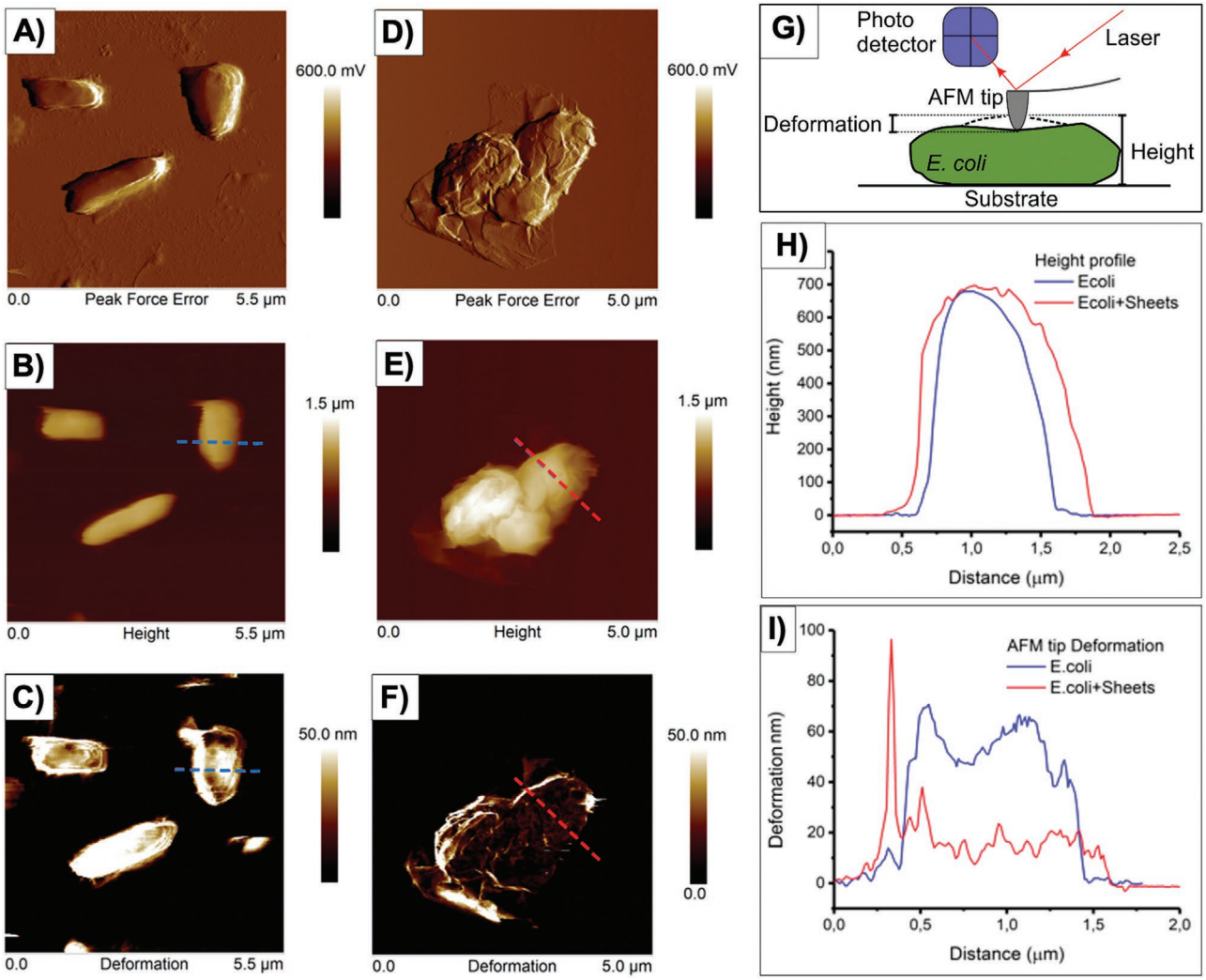

Figure 3. Atomic force microscopy (AFM) images of A–C) *E. coli* and D–F) wrapped *E. coli* after incubation with GO-PTEMA. The height and deformation measurement principle is shown in schematic image (G). Images (A) and (D) are shown in peak force error mode. Images (B) and (E) are shown in height mode. Images (C) and (F) are shown in deformation mode. Images (H) and (I) depict examples of the height and deformation profiles of the free and wrapped *E. coli*.

758 ± 80 nm for *E. coli* with GO-PTEMA. The height difference of ≈70 nm suggests that multiple sheets of 4.8 nm thickness must be wrapped around the bacteria. No wrapping of bacteria could be found for *E. coli* incubated with raw material GO sheets.

Furthermore, the samples were imaged in PeakForce mode under constant maximal loading force by the tip (6 nN). By this nanomechanical mapping method, the deformation profiles obtained for free and treated *E. coli* were compared by the degree of deformation. The samples revealed a clear difference in the induced deformation depth. While the deformation depth of *E. coli* alone was 53.1 ± 3.4 nm, GO-PTEMA-treated *E. coli* seemed to provide a structural reinforcement during indentation by the AFM tip, which led to a decreased deformation depth of 15.8 ± 5.3 nm. Therefore, the deformation profiles obtained for free bacteria and wrapped bacteria could be used to differentiate the two states (Figure 3I).

2.2.3. Growth Inhibition of Gram-Positive and Gram-Negative Bacteria

The antibacterial activity of graphene materials as well as their antibacterial mechanisms have been discussed controversially in many publications.[28] In order to evaluate the antibacterial activity of GO-PTEMA, we conducted incubation and bacterial proliferation experiments. To preclude that toxic compounds, which might have been adsorbed onto the graphene sheets during synthesis, could leach out of the testing materials and thereby kill bacteria, a disc diffusion assay was performed. After 24 h as well as 5 days of incubation, no inhibition zone was observed for the tested materials (GO, GO-PDEMA, and GO-PTEMA), therefore ruling out an antibacterial activity by desorbed toxins (Figure S11, Supporting Information).

The growth inhibition was further tested in liquid phase with varying concentrations of GO, GO-PDEMA, and GO-PTEMA to determine the minimal inhibition concentration (MIC) against

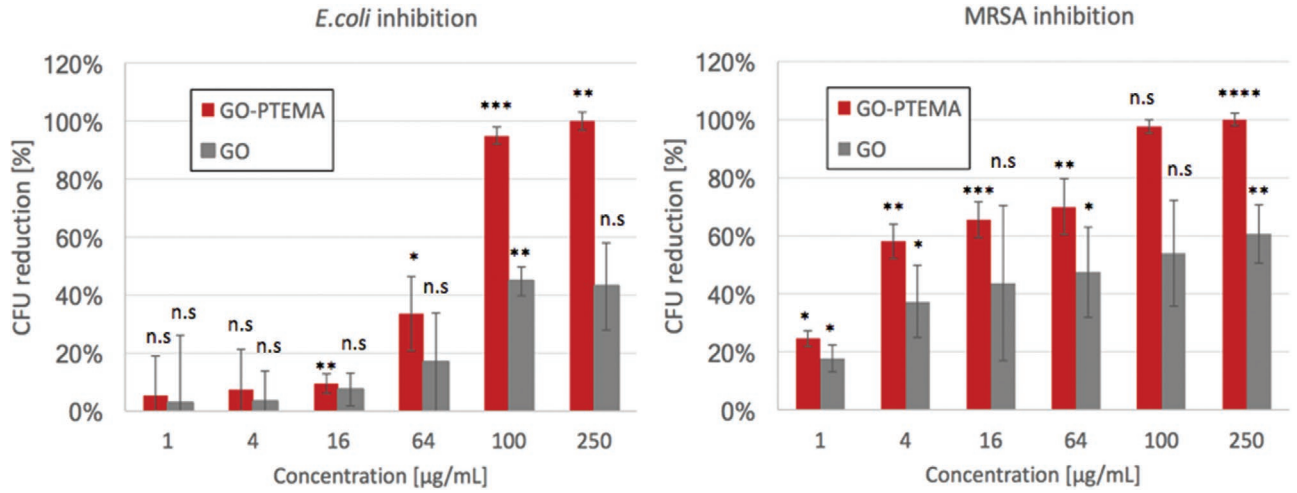

Figure 4. Bacteria inhibition at different concentrations of GO-PTEMA and GO. *E. coli* (Gram-negative) (left) and MRSA (Gram-positive).

E. coli BL21 (DE3) and MRSA (04-02981). Briefly, the effect on bacteria was determined by counting the colony forming units (CFU) on agar plates, which allowed an accurate determination of viable bacterial cells. *E. coli* cultures (CFU = 10^7) were incubated with different concentrations of GO-PTEMA and GO as control. The reduction of the CFU compared to the control (only *E. coli*, without sample) was calculated in percent and is shown in **Figure 4**. It is shown that after 6 h of incubation in growth medium, GO-PTEMA concentrations of 100 µg mL^{-1} and higher resulted in a reduction of the number of *E. coli*, as well as MRSA, of more than 99% compared to the control culture without an antibacterial compound. Furthermore, the antibacterial effect of GO-PTEMA sheets was much stronger compared to GO sheets, even at concentrations of 250 µg mL^{-1} GO could reduce the CFU of both *E. coli* and MRSA by only 60%.

In order to monitor the growth inhibition over time, the above MIC test was repeated with a constant GO or GO-PTEMA concentration of 250 µg mL^{-1}. Briefly, ≈10^5 CFU mL^{-1} *E. coli* or MRSA solution were incubated with the two compounds at 37 °C and samples were taken every 2 h to determine the CFU mL^{-1} by counting the colonies on agar plates. GO-PTEMA showed a significant inhibition of the bacterial growth for both *E. coli* and MRSA. By incubating with 250 µg mL^{-1} of GO-PTEMA the bacterial number reduction is visible after 2 h for both bacteria. For MRSA the CFU shows a 100-fold reduction, which reflects the 5 times lower surface area and thus higher susceptibility to surface blocking compared to *E. coli*.[29] Further incubation time resulted in a slow decrease in CFU values for both bacteria over the period of 6 h, while the control culture as well as the GO-incubated bacteria continued to grow. The GO-incubated bacteria only showed a marginally slower proliferation than the control without any compound. After 6 h incubation the CFU reduction of GO-PTEMA (99.96% *E. coli*; 99.99% MRSA), calculated against the control culture in percent, was much higher than that of GO (60% *E. coli*; 60% MRSA) as shown in **Figure 5**.

2.2.4. Electrostatic Binding Mechanism Test by Salinity-Dependent Growth Inhibition Assay

In order to confirm that the main mechanism of bacterial inhibition is based on electrostatic attraction between the GO-PTEMA and the bacteria, *E. coli* were incubated in medium with increasing sodium chloride (NaCl) concentrations, which changes the ionic strength of the surrounding solution. The binding affinity based on electrostatic interaction of the GO-PTEMA sheets to *E. coli* should therefore decrease and result

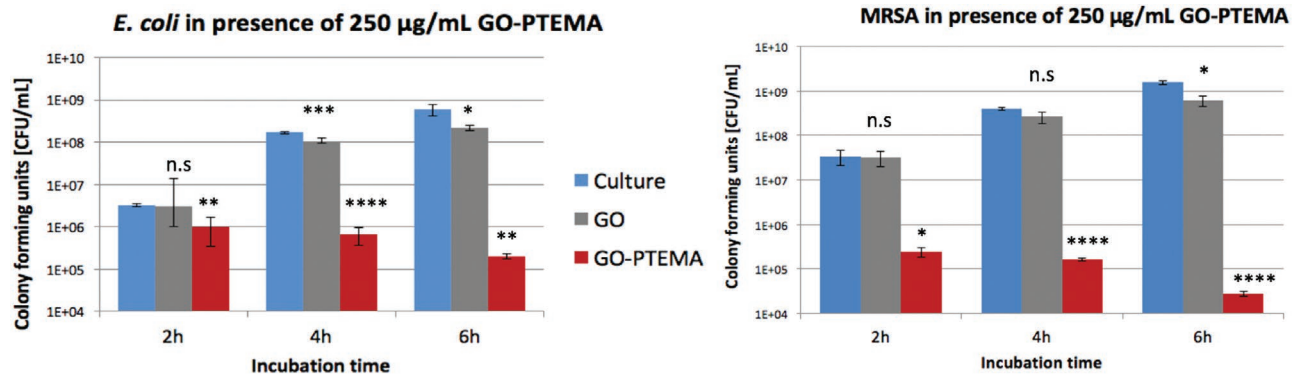

Figure 5. Growth inhibition experiment of MRSA (Gram-positive) and *E. coli* (Gram-negative) bacterium.

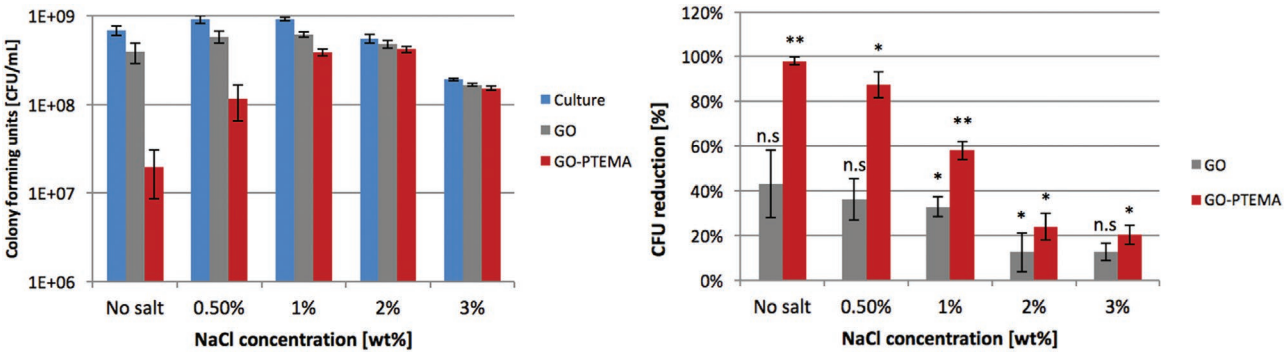

Figure 6. Salinity-dependent growth inhibition. Colony count graph (left) and CFU reduction in percent (right).

in lower bacteria inhibition. Briefly, *E. coli* (10^4 CFU mL^{-1}) were incubated with GO-PTEMA (250 µg mL^{-1}) for 6 h in medium with NaCl concentrations of 0, 0.5, 1, 2, and 3 wt%. The maximum inhibition activity of 99% was observed for the medium without NaCl (0 wt%) (**Figure 6**). An increase in the salt concentration resulted in reduced inhibition activities of 87%, 58%, 24%, and 20%, in the respective order shown above. These results indicate that the electrostatic attraction of GO-PTEMA is the main binding mechanism and cause of bacterial growth inhibition.

Furthermore, as the electrostatic binding mechanism is reversible at high salt concentrations, these polycationic sheets could be used for bacterial enrichment experiments that could be utilized in a number of future studies.

3. Conclusion

We assess a multivalent type of antibacterial agent and presented its design and synthesis based on defined target parameters. These parameters (lateral size and charge) were chosen for optimal bacteria binding and were confirmed by SEM, AFM, zeta potential, and a dye adsorption assay. The charge density of 2×10^{14} cm^{-2} matched the negatively charged bacterial surface density known from literature.[31]

We could show by AFM and confocal microscopy that the GO-PTEMA sheets bind tightly to *E. coli* and wrap around the bacteria cells, thereby immobilizing them. In contrast, this was not the case for the unmodified GO sheets, which did not wrap bacterial cells or inhibited bacteria movement. The incubation of Gram-negative and -positive bacteria (*E. coli* and MRSA) with GO-PTEMA resulted in the inhibition of proliferation and a slow reduction of the number of colony forming bacteria. This effect can be attributed to the observed wrapping of bacteria cells that might result in the blockade of metabolic exchange pathways. The salt concentration dependency of the inhibition experiment, as well as the fact that unmodified negatively charged GO sheets did not inhibit bacteria, confirm that the main driving force of the antibacterial effect is based on electrostatic attraction.

The presented compound binds and wraps bacteria cells, which inhibits proliferation and results in a slow cell death. Therefore, it can be described as an antibacterial agent acting on a different mode of action than classical antibiotics or biocides. Besides the antibacterial property that has potential use in medicinal, technical, or agriculture applications, the multivalent binding could also be applied for adsorbing bacteria or other cell types. The presented GO-PTEMA and its unspecific binding of cell interfaces could be employed as adsorber material for bacterial filtration or immobilization methodology in cell analysis and imaging applications. The graphene-sheet-based immobilization furthermore offers electroconductive materials that can be used to transmit electrical signals in sensor setups.

4. Experimental Section

Materials and Methods: Used chemicals were purchased from following sources: 2-(dimethylamino)ethyl methacrylate (98%, Aldrich), 2,2′-azobis(2-methylpropionitrile) (98%, Aldrich), aluminum oxide (50–200 µm, Acros Organics) 3-dimethylaminopropylamin (99%, Aldrich), methyl iodide (99%, Acros Organics) dimethylformamide (99.5%, Acros Organics), tetrahydrofuran (99.9%, VWR chemicals), fluorescein sodium salt (Sigma-Aldrich), poly-L-lysine (MW 75–150 kDa, from Sigma-Aldrich, LB-Broth or LB-Agar (Carl Roth GmbH & Co. KG, Karlsruhe, Germany). The graphene oxide (GO) sheets were purchased as paste from "graphene-supermarket.com," 0.5–5 µm, 80%).

GO-PDEMA Synthesis: GO was functionalized based on the method reported by Kan et al.[35] 300 mg GO was dispersed in 350 mL of *N*,*N*-dimethylformamide (DMF) in a 500 mL Schlenk flask and sonicated (35 kHz, 160 W) for 30 min. 15.6 g (100 mmol) of DEMA monomer was added to the reaction mixture. The DEMA monomer was previously cleared from the quinoline stabilizer by filtration through 1 g aluminum oxide (ALOX). The reaction mixture was then flushed with nitrogen for 30 min to remove oxygen. Under nitrogen flow protection and constant stirring, 820 mg (5 mmol) of AIBN was added. The reaction mixture was stirred at 65 °C for 48 h. Then it was transferred to 50 mL falcon tubes for purification via centrifugation at 9000 rpm and 15 °C 3–4 times with DMF and 3–4 times with DI water for purification. After extensive purification the product was dispersed in 200 mL DI water and lyophilized to obtain 600 mg of a dry black solid.

GO-PTEMA Synthesis: To introduce permanent positive charges, the dimethylamine groups of GO-PDEMA were methylated to form quaternary ammonium ions.[37] 150 mg GO-PDEMA (0.59 mmol repeating unit) was dispersed in 80 mL THF via 15 min of ultrasonication. Methyl iodide (MeI) (1 mL, 16 mmol) in excess was added under constant stirring for 24 h. The reaction mixture was transferred to 50 mL falcon tubes for purification via centrifugation 3–4 times with THF and 3–4 times with DI water. It was dispersed in 50 mL DI water and lyophilized to obtain 155 mg as a dry black solid.

Scanning Electron Microscopy: The GO sheets were imaged with a field emission scanning electron microscope (FE-SEM, Hitachi SU8030)

at 20 kV, a current of 10 µA and a working distance (WD) of around 8.3. The samples were coated with a gold layer by using a sputter coater (Emscope SC 500, Quorum Technologies, UK).

Atomic Force Microscopy: Imaging of functionalized graphene sheets and their interaction with bacteria was carried out with an atomic force microscope Multimode 8 from Bruker in PeakForce QNM mode (Quantitative NanoMechanics) with a NanoScope V controller. All experiments were performed in a closed fluid chamber in Milli-Q water. The NanoScope software 1.5 from Bruker was used for image analysis where plane fit and flatten tools with order 1 were used. To identify the effective interaction between GO-PTEMA sheets and bacteria, both samples were first imaged independently. Discs of muscovite mica of about 1 cm in diameter were cleaved with regular tape and used as substrates for sample deposition. SNL tips from Bruker were used with nominal radius in the range of 2–12 nm and cantilever spring constant of 0.35 N m^{-1}. Before any imaging was performed, the sensitivity of the cantilever was acquired from a force distance curve after compression on the hard surface of mica and subsequently the thermal noise method was applied to extract its spring constant. Images were taken with a resolution of 512 points per line and 0.7 Hz scan rate.

10 µL of a GO sample (1–3 mg mL^{-1}) was deposited on cleaved mica and allowed to dry. The sample was rinsed repeatedly with Milli-Q water and imaged in a closed chamber. Although it is well known that GO is mostly negatively charged, it was observed that a few flakes remained attached to the surface of cleaved mica when substrate was rehydrated. On the other hand, positively charged functionalized GO sheets (GO-PTEMA) that were precipitously bound on the mica surface were driven by the strong electrostatic interaction to silanol groups present on its surface. For this reason, the original sample concentration was 10-fold diluted before deposition followed by 15 min of incubation. Maximal loading forces during imaging were 0.5–1 nN. Imaging of live bacteria was achieved on cleaved mica substrates after deposition of a layer of a cationic polymer. 5 µL of poly-L-lysine (MW 75–150 kDa, from Sigma-Aldrich) was deposited at the center of cleaved mica and allowed to dry. Afterward, the surface was rinsed with Milli-Q water, allowed again to dry, and used as substrate for deposition of the sample. A sample with *E. coli* BL21 (DE3) was centrifuged at 5000 rpm, the supernatant (culture medium) was removed, and 100 µL of Milli-Q water was added and mixed. Then 15 µL of the prepared sample was deposited at the center of the poly-L-lysine-coated mica and incubated for at least 10 min. After incubation, the sample was slightly blotted with a filter paper to reduce the amount of liquid in the sample to only a very thin film but without allowing to dry. The sample was mounted on the AFM head and the liquid chamber was assembled. Maximum loading forces were optimized to avoid shadowing effects present due to the high bacteria lateral cross section and its interaction with the conical AFM tip. Therefore, maximal loading forces were 6 nN, which were still within the elastic reversible response of the bacterial cell wall and allowed to repeatedly image. Also, this applied force setpoint induced a defined degree of deformation on the cells, which could be easily monitored and further compared with the case of cells trapped within GO-PTEMA sheets, as described below. To monitor the binding of GO-PTEMA sheets with bacteria, bare mica substrates were used, because the wrapped bacteria should have exhibited a positively charged surface compared to nonwrapped bacteria. Imaging conditions were kept constant as in the case of imaging live bacteria. The samples were diluted in a similar ratio as when measured individually. 10 µL of each sample was added to 80 µL of Milli-Q water and incubated for at least 40 min. Finally, 10 µL of the sample with the mixture was deposited at the center of cleaved mica and incubated for 15 min, followed by slight blotting to leave a thin film and then mounted to the AFM head for measurement.

X-Ray Photoelectron Spectroscopy: The gold substrates for XPS analysis were cleaned in a piranha solution (1:4) 30% H_2O_2:98% H_2SO_4 (v/v) during ultrasonication at room temperature for 10 min. Then they were washed with the DI water 5 times and with acetone 2 times. After drying overnight, the studied compounds were dissolved in methanol and evenly distributed dropwise over the surface of gold substrates. Synchrotron XPS was carried out at the high-energy spherical-grating monochromator (HE-SGM) dipole beamline at BESSY II in Berlin, Germany. A fixed analyzer transmission mode at pass energy of 50 eV and the following excitation energies were used: survey scan 750 eV, O 1 s 620 eV, N 1 s 500 eV, and C 1 s 385 eV. The spectra were recorded at an electron emission angle of 60°. All XPS spectra were processed with the UNIFIT program (version 2017). A Gaussian/Lorentzian product function peak shape model GL (30) was used in combination with a Shirley background. If not otherwise denoted, the L–G mixing for component peaks in all spectra was constrained to be identical. Peak fitting of C1s spectra was performed by using an asymmetric peak shape model for the graphene C1s component peak and a symmetric peak shape model for all other component peaks. After peak fitting of the C1s spectra, all the binding energies were calibrated in reference to the graphene C1s' component at a binding energy of 284.6 eV. High-resolution, core-level spectra were recorded in FAT (fixed analyzer transmission) mode at pass energy of 20 eV using excitation energy of 1486.69 eV for all elements: O1s, N1s, and C1s.

Elemental Analysis: EA was carried out on a VARIO EL III instrument (Elementar, Hanau, Germany) using sulfanilic acid as the standard.

Gel Permeation Chromatography: GPC measurements were performed on an Agilent 1100 Series HPLC series, equipped with a PSS SUPREMA 1000 Å providing a separation range from 100 to 1 000 000 Da. Eluent was H_2O + 0.3 M formic acid and calibration was performed with pullulan obtained from PSS. Analysis was performed with WinGPC.

Zeta Potential: The zeta potential measurements were performed by a Malvern Zetasizer Nano machine (Brookhaven Instruments Corp.) at 25 °C. All measurements were performed in disposable capillary cell (DTS1070) from Malvern instruments. 0.1 g mL^{-1} samples in Millipore quality water were used in all the measurements.

Confocal Microscopy: *E. coli* BL21 (DE3) were inoculated into fresh LB culture media to ≈10^4 CFU mL^{-1} and grown for 2 h at 37 °C (180 rpm). The culture was then split into three tubes and treated with i) LB media, ii) GO, or iii) GO-PTEMA at a final concentration of 250 µg mL^{-1}. After 20 min of incubation at 37 °C with shaking (180 rpm) the samples were then stained with BacLight Live/Dead staining kit (ThermoFisher) according to the manufacturer's instructions, resuspended in 50% glycerol and briefly centrifuged onto µ-Slide 8-well chambered cover glass (ibidi). Single Z-plane confocal images were acquired through a ×100 NA1.45 objective on a VisiScope Confocal FRAP System (VisiTron systems). Images were recorded on an iXON 888 EMCCD (Andor) using the same laser intensities, EMCCD gain, and exposures between samples. Images were all processed equally in the Fiji distribution of ImageJ using a custom written IJ1 script.[38] Time-lapse images of the live bacteria on the glass surface were quantified and analyzed.

Disc Diffusion Assay: *E. coli* BL21 (DE3) was prepared in LB-Broth or LB-Agar [Carl Roth GmbH & Co. KG, Karlsruhe] at 37 °C with constant shaking at 150 rpm. Agar diffusion tests were performed according to CLSI guidelines.[39] Bacteria cultures (OD_{600} = 0.2) were distributed with a sterile cotton swab on an agar plate. The Whatman filter paper discs (6 mm diameter) were immersed in corresponding concentrations (2, 4, 8, 16, 32, 64, and 100 µg mL^{-1}) of the test samples and placed on the agar plate. A paper disc was immersed in sterile deionized water as reference. The plates were incubated at 37 °C and checked after 24 h and 5 days.

Bacterial Growth Inhibition Assay (MIC): Due to the turbidity of graphene oxide solutions, all bacteria concentrations were determined by counting the CFU, instead of determining the OD_{600} values. *E. coli* BL21 (DE3) (CFU = 10^7) as well as with *S. aureus* 04-02981 (MRSA) were incubated in LB medium with 0.001 wt% NaCl at 37 °C for 6 h with different concentrations of GO and GO-PTEMA. The reduction of the CFU values compared to the control (only bacteria) was calculated in percent.

Growth Inhibition Assay (Time Dependent): The time-dependent inhibition assay was performed with *E. coli* BL21 (DE3) and *S. aureus* 04-02981 in presence of GO or GO-PTEMA to elucidate the mechanism of action of GO-PTEMA with respect to different incubation times. For this, overnight cultures of *E. coli* and MRSA were prepared in LB broth and tryptic soy broth (TSB) without addition of sodium chloride, respectively. Overnight cultures were incubated at 37 °C with a constant agitation at 150 rpm, subsequently set to ≈10^5 CFU mL^{-1}, and exposed

to 250 μg mL^{-1} of GO or GO-PTEMA in a total volume of 6 mL. The samples were incubated at 37 °C, 150 rpm and samples were taken after 2, 4, and 6 h. The samples were serially diluted and spread on LB agar plates to determine their CFU mL^{-1}. The reduction of the CFU values in percent in presence of GO or GO-PTEMA was calculated with reference to the untreated cultures of *E. coli* and MRSA.

Growth Inhibition Assay (Salinity Dependent): This inhibition assay was performed to determine the susceptibility of *E. coli* BL21 (DE3) to GO and GO-PTEMA at different NaCl concentrations. Overnight cultures of *E. coli* BL21 (DE3) were prepared in LB broth without NaCl and incubated at 37 °C with a constant agitation at 150 rpm, subsequently set to ≈10^4 CFU mL^{-1}, and exposed to 250 μg mL^{-1} of GO or GO-PTEMA at varying NaCl concentrations of 0, 0.5, 1, 2, and 3 wt%. The total volume of each sample was 6 mL. The samples were incubated for 6 h at 37 °C, 150 rpm followed by serial dilution and spreading on LB agar plates to determine the CFU mL^{-1}. The reduction in *E. coli* CFU values in percent in presence of GO or GO-PTEMA was calculated with reference to untreated *E. coli* cultures and is presented in dependence of the sample salinity.

Supporting Information

Supporting Information is available from the Wiley Online Library or from the author.

Acknowledgements

This work was supported by the SFB765 funded by the Deutsche Forschungsgemeinschaft (DFG) and ProFIT funded by Europäische Fonds für regionale Entwicklung (EFRE). The authors also acknowledge support by the team at the BESSY II synchrotron radiation facility as well as Dr. A. Nefedov (Karlsruhe Institute of Technology, KIT) from the HE-SGM Collaborate Research Group. The authors thank their colleagues Andrés Velázquez for artwork and Dr. Pamela Winchester for language polishing.

Conflict of Interest

The authors declare no conflict of interest.

Keywords

antibacterial, *Escherichia coli*, graphene, inhibition, *Staphylococcus aureus*

Received: December 11, 2019
Revised: May 11, 2020
Published online: June 17, 2020

[1] P. V. Baptista, M. P. McCusker, A. Carvalho, D. A. Ferreira, N. M. Mohan, M. Martins, A. R. Fernandes, *Front. Microbiol.* **2018**, *9*, 1441.
[2] R. Singh, M. S. Smitha, S. P. Singh, *J. Nanosci. Nanotechnol.* **2014**, *14*, 4745.
[3] L. Rizzello, R. Cingolani, P. P. Pompa, *Nanomedicine* **2013**, *8*, 807.
[4] D. H. Stones, A. M. Krachler, *Biochem. Soc. Trans.* **2016**, *44*, 1571.
[5] G. Y. Zhu, B. Y. Lu, T. X. Zhang, T. Zhang, C. L. Zhang, Y. Li, Q. Peng, *Nanomedicine* **2018**, *13*, 1093.
[6] O. Akhavan, E. Ghaderi, A. Esfandiar, *J. Phys. Chem. B* **2011**, *115*, 6279.
[7] S. Liu, M. Hu, T. H. Zeng, R. Wu, R. Jiang, J. Wei, L. Wang, J. Kong, Y. Chen, *Langmuir* **2012**, *28*, 12364.
[8] A. M. Dimiev, E. Siegfried, *Graphene Oxide: Fundamentals and Applications*, John Wiley & Sons, Ltd, Chichester, West Sussex, UK **2017**.
[9] H. Ji, H. Sun, X. Qu, *Adv. Drug Delivery Rev.* **2016**, *105*, 176.
[10] X. Zou, L. Zhang, Z. Wang, Y. Luo, *J. Am. Chem. Soc.* **2016**, *138*, 2064.
[11] S. Gurunathan, J. W. Han, A. A. Dayem, V. Eppakayala, J.-H. Kim, *Int. J. Nanomed.* **2012**, *7*, 5901.
[12] V. T. Pham, V. K. Truong, M. D. Quinn, S. M. Notley, Y. Guo, V. A. Baulin, M. Kobaisi, R. J. Crawford, E. P. Ivanova, *ACS Nano* **2015**, *9*, 8458.
[13] S. Xiao, X. Lu, L. Gou, J. Li, Y. Ma, J. Liu, K. Yang, B. Yuan, *Carbon* **2019**, *149*, 248.
[14] W. Hu, C. Peng, W. Luo, M. Lv, X. Li, D. Li, Q. Huang, C. Fan, *ACS Nano* **2010**, *4*, 4317.
[15] J. Tang, Q. Chen, L. Xu, S. Zhang, L. Feng, L. Cheng, H. Xu, Z. Liu, R. Peng, *ACS Appl. Mater. Interfaces* **2013**, *5*, 3867.
[16] J. Ma, J. Zhang, Z. Xiong, Y. Yong, X. S. Zhao, *J. Mater. Chem.* **2011**, *21*, 3350.
[17] Y. -W. Wang, A. Cao, Y. Jiang, J. -H. Liu, Y. Liu, H. Wang, *ACS Appl. Mater. Interfaces* **2014**, *6*, 2791.
[18] L. Zhong, K. Yun, *Int. J. Nanomed.* **2015**, *10*, 79.
[19] W. Y. Pan, C. C. Huang, T. T. Lin, H. Y. Hu, W. C. Lin, M. J. Li, H. W. Sung, *Nanomedicine* **2016**, *12*, 431.
[20] Y. N. Chang, X. M. Ou, G. M. Zeng, J. L. Gong, C. H. Deng, Y. Jiang, J. Liang, G. Q. Yuan, H. Y. Liu, X. He, *Appl. Surf. Sci.* **2015**, *343*, 1.
[21] Z. Qi, P. Bharate, C. H. Lai, B. Ziem, C. Böttcher, A. Schulz, F. Beckert, B. Hatting, R. Mülhaupt, P. H. Seeberger, R. Haag, *Nano Lett.* **2015**, *15*, 6051.
[22] W. Zhan, T. Wei, L. Cao, C. Hu, Y. Qu, Q. Yu, H. Chen, *ACS Appl. Mater. Interfaces* **2017**, *9*, 3505.
[23] P. Subramanian, F. Barka-Bouaifel, J. Bouckaert, N. Yamakawa, R. Boukherroub, S. Szunerits, *ACS Appl. Mater. Interfaces* **2014**, *6*, 5422.
[24] K. H. Tan, S. Sattari, I. S. Donskyi, J. L. Cuellar-Camacho, C. Cheng, K. Schwibbert, A. Lippitz, W. E. S. Unger, A Gorbushina, M. Adeli, R. Haag, *Nanoscale* **2018**, *10*, 9525.
[25] M. Lin, L. Chunlei, C. Fengyi, Y. Dehong, J. Xu, H. Sijie, M. Xiaomei, W. Pengfei, *Appl. Nano Mater.* **2019**, *2*, 2902.
[26] L. Xiao, J. Sun, L. Liu, R. Hu, H. Lu, C. Cheng, Y. Huang, S. Wang, J. Geng, *ACS Appl. Mater. Interfaces* **2017**, *9*, 5382.
[27] S. Omidi, A. Kakanejadifard, F. Azarbani, *J. Mol. Liq.* **2017**, *242*, 812.
[28] I. Barbolina, C. R. Woods, N. Lozano, K. Kostarelos, K. S. Novoselov, I. S. Roberts, *2D Mater.* **2016**, *3*, 025025.
[29] J. S. Dickson, M. Koohmaraie, *Appl. Environ. Microbiol.* **1989**, *55*, 832.
[30] B. Gottenbos, D. W. Grijpma, H. C. van der Mei, J. Feijen, H. J. Busscher, *J. Antimicrob. Chemother.* **2001**, *48*, 7.
[31] S. L. Walker, J. E. Hill, J. A. Redman, M. Elimelech, *Appl. Environ. Microbiol.* **2005**, *71*, 3093.
[32] R. Kügler, O. Bouloussa, F. Rondelez, *Microbiology* **2005**, *151*, 1341.
[33] H. Murata, R. R. Koepsel, K. Matyjaszewski, A. J. Russell, *Biomaterials* **2007**, *28*, 4870.
[34] S. Romero-Vargas Castrillón, F. Perreault, A. F. de Faria, M. Elimelech, *Environ. Sci. Technol. Lett.* **2015**, *2*, 112.
[35] L. Kan, Z. Xu, C. Gao, *Macromolecules* **2011**, *44*, 444.
[36] E. Kłodzinska, M. Szumski, E. Dziubakiewicz, K. Hrynkiewicz, E. Skwarek, W. Janusz, B. Buszewski, *Electrophoresis* **2010**, *31*, 1590.
[37] V. Bütün, S. P. Armes, N. C. Billingham, *Macromolecules* **2001**, *34*, 1148.
[38] J. Schindelin, I. Arganda-Carreras, E. Frise, V. Kaynig, M. Longair, T. Pietzsch, S. Preibisch, C. Rueden, S. Saalfeld, B. Schmid, J. Y. Tinevez, D. J. White, V. Hartenstein, K. Eliceiri, P. Tomancak, A. Cardona, *Nat. Methods* **2012**, *9*, 676.
[39] T. Naas, B. Coignard, A. Carbonne, K. Blanckaert, O. Bajolet, C. Bernet, X. Verdeil, P. Astagneau, J. C. Desenclos, P. Nordmann, *Emerging Infect. Dis.* **2006**, *12*, 1214.

ADVANCED MATERIALS INTERFACES

Supporting Information

for *Adv. Mater. Interfaces,* DOI: 10.1002/admi.201902066

Multivalent Bacteria Binding by Flexible Polycationic Microsheets Matching Their Surface Charge Density

*Rameez Ahmed, Ankita Vaishampayan, Jose Luis Cuellar-Camacho, Darren J. Wight, Ievgen Donskyi, Wolfgang Unger, Elisabeth Grohmann, Rainer Haag, and Olaf Wagner**

((Supporting Information can be included here using this template))

Supporting Information

Multivalent bacteria binding by flexible polycationic micro-sheets matching their surface charge density

*Rameez Ahmed, Ankita Vaishampayan, Luis Cuellar-Camacho, Darren J. Wight, Ievgen Donskyi, Elisabeth Grohmann, Rainer Haag, Olaf Wagner**

Table of contents

References

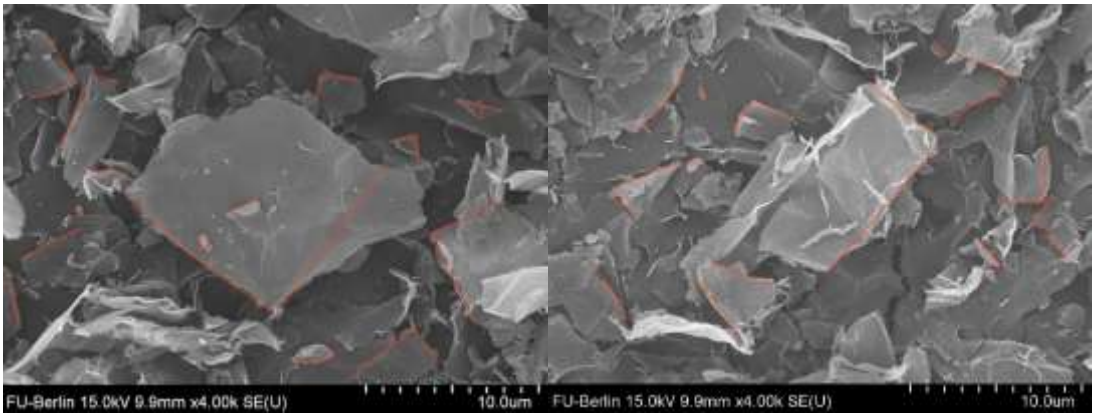

Figure S1. SEM images of GO sheets and the measured lateral dimensions marked in red.

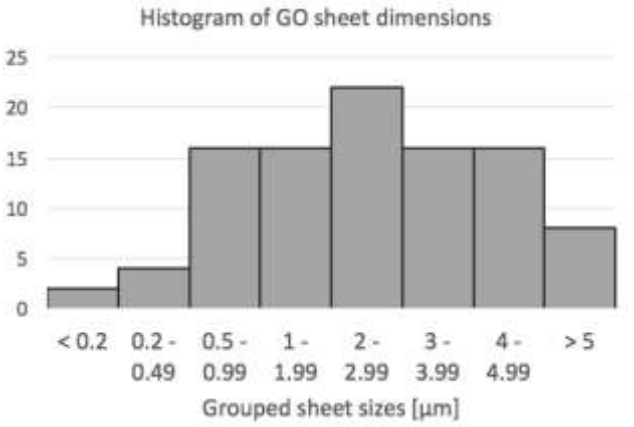

Figure S2. Histogram of sheet lateral dimensions.

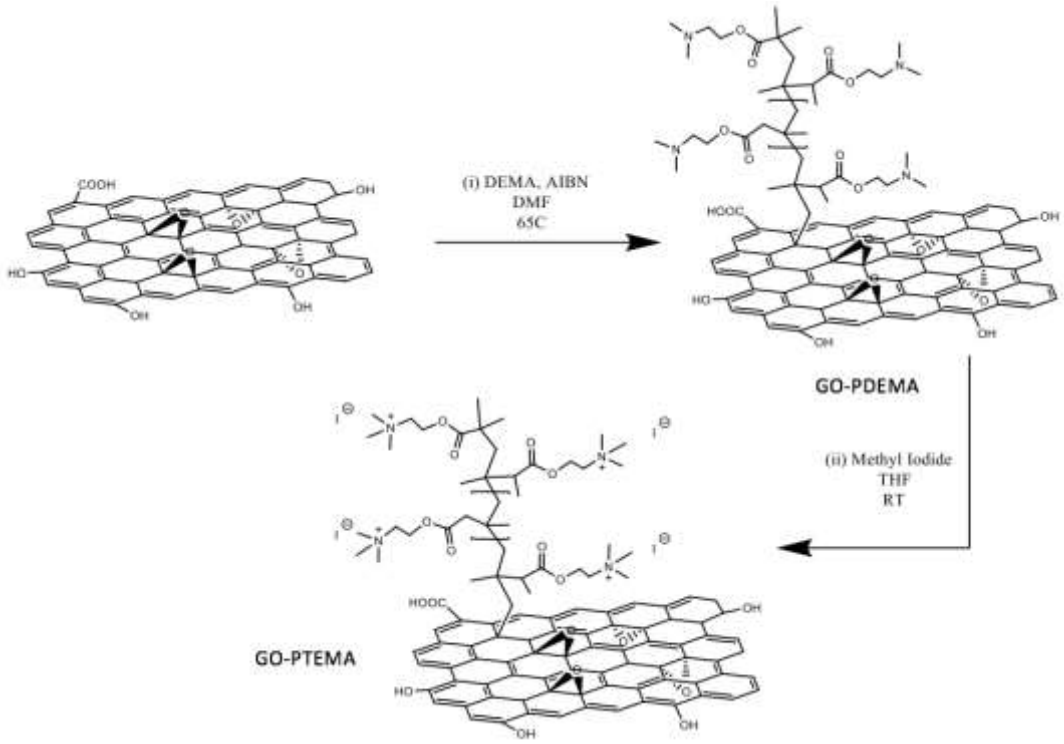

Figure S3. Synthesis scheme of the 2-step GO-PTEMA synthesis.

Figure S4. Photograph of GO-PTEMA.

To analyze the amount of grafted functional groups on GO, elemental analysis (EA) was performed on GO and GO-PDEMA. The results of EA are shown in **Table S1**.

Table S1. C/H/N elemental analysis results of GO and GO-PDEMA.

Sample	C%	H%	N%
GO (control)	48.2	3.2	0.01
GO-PDEMA	60	6.5	5.5

GO and GO-PDEMA were also characterized by XPS. Figure S5 shows the XPS carbon spectra (C1s) and survey spectra of GO. The signal at 284.6 eV corresponds to the C=C sp2 component in GO. The signal at binding energy 286.7 eV corresponds to the C–O component in GO that occurs due to the presence of a large amount of oxygen species. The ratio of the integrals of C=C and C–O component is 2:1. No nitrogen signal was detected in the survey spectrum of GO (b). The low energy C 1s component peak is due to differential charging at the surface of the heterogeneous sample. There was no active charge compensation used in the experiment.

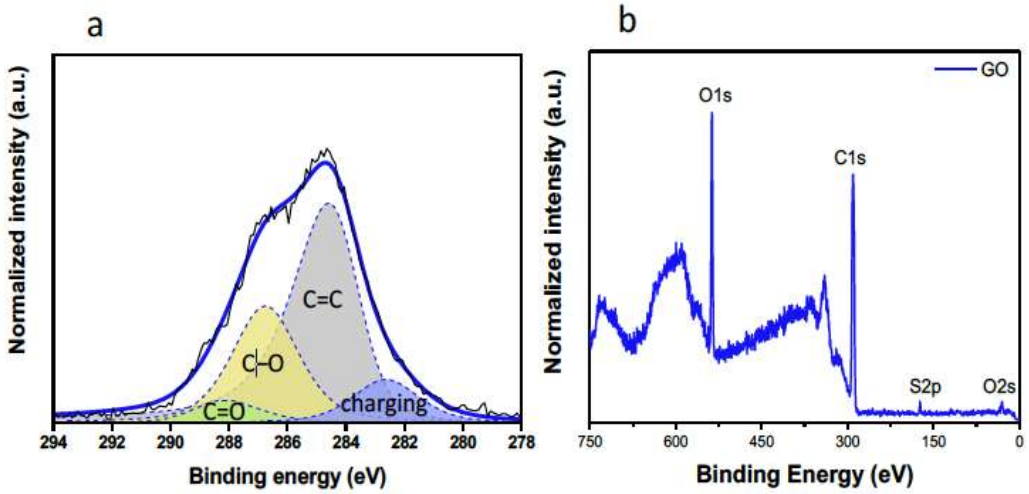

Figure S5. (a) Highly resolved C1s XPS spectrum and (b) survey XPS spectrum of GO. The S2p signal presumably originates from sulfur residues of sulfuric acid used for the preparation of GO by using a Hummers' type method.

The XPS spectra of GO-PDEMA are presented in Figure S6. The typical signal of C=C sp2 component in GO is at 284.6 eV. The signal at binding energy 285.3 eV corresponds to the C-N component. The C–N signal appears because of the PDEMA polymer side chains, since it is the only constituent containing nitrogen. A distinct signal appears at the binding energy of 288.4 eV. This peak corresponds to the presence of carboxylic groups of the attached polymer. The integral ratio of O–C=O and C–N component is almost 1:1, which matches the chemical structure of the attached polymer. The signal of nitrogen can also be observed in the survey spectrum of GO-PDEMA. Therefore, we can conclude that the synthesis of GO-PDEMA via free radical polymerization was successful.

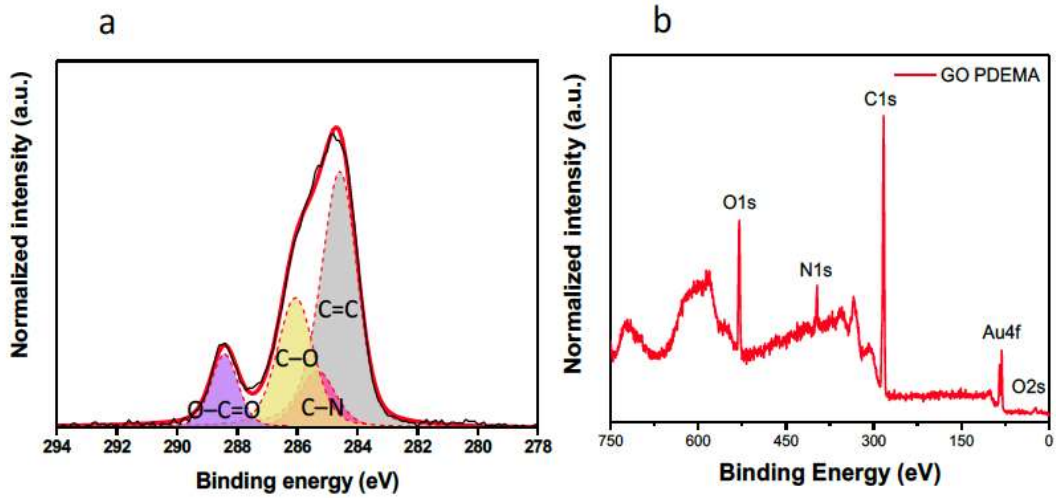

Figure S6. (a) Highly resolved C1s XPS spectrum and (b) overall XPS spectrum of GO-PDEMA. The Au 4f signal originates from the not fully covered Au/Si wafer substrate where the GO-PDEMA was deposited on.

The chain length of unattached polymer is similar to the grafted polymer brushes. [SI1] Therefore GPC was performed on unattached polymer to determine the length of the polymer brushes of GO-PDEMA. The results of GPC are shown below. Number average molecular weight of 6700 (Mn) and weight average molar mass (Mw) is 16,400 with a poly dispersity

index of 2.4. From the Mw the average number of repeating units (Mw = 157.21) per polymer chain was calculated to be 104.

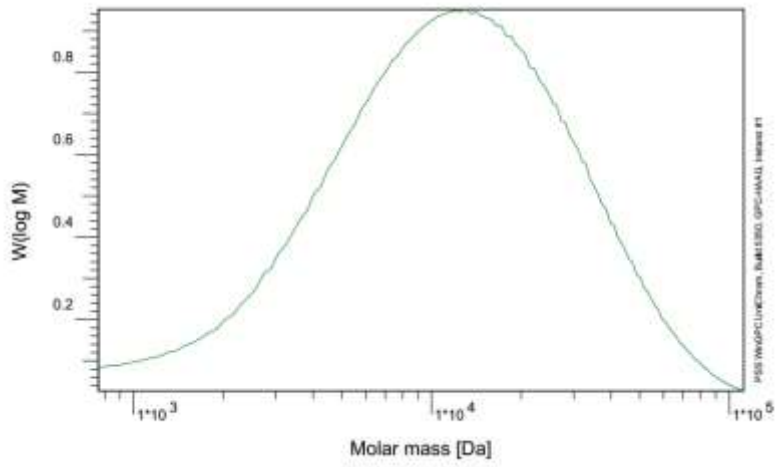

Figure S7. GPC measurement of non-covalently bound PDEMA polymer chains separated from the GO-PDEMA synthesis.

Calculation of dimethylamino groups per g of GO-PDEMA:

$$\frac{No.\ of\ rep.\ units \times degree\ of\ polymer\ funct.}{MW\ Polymer} = \frac{104 \times 0.62}{16400\ g\ mol^{-1}} = 0.00393\ mol\ g^{-1} \quad (1)$$

By Equation 1 the amount of dimethylamino groups in 1 g of GO-PDEMA was determined to be 3.93 mmol.

Calculation of theoretical surface area of GO-PDEMA via the theoretical value of the surface area of GO[SI2]:

$$Surf.area\ GO_{PDEMA} = Surf.area\ GO \times (1 - degree\ of\ polymer\ funct.) =$$

$$745\ m^2 g^{-1} \times 0.38 = 283\ m^2 g^{-1} \quad (2)$$

Calculation of dimethylamino groups per area of GO-PDEMA:

$$\frac{No.of\ dimethylamino\ groups\ per\ g}{Surf.area\ GO_{PDEMA}} \times N_A = \frac{0.00393\ mol\ g^{-1}}{283\ m^2 g^{-1}} \times 6.022 \cdot 10^{23} mol^{-1} =$$

$$8.36 \cdot 10^{18}\ m^{-2} = 8.36\ nm^{-2}$$

(3)

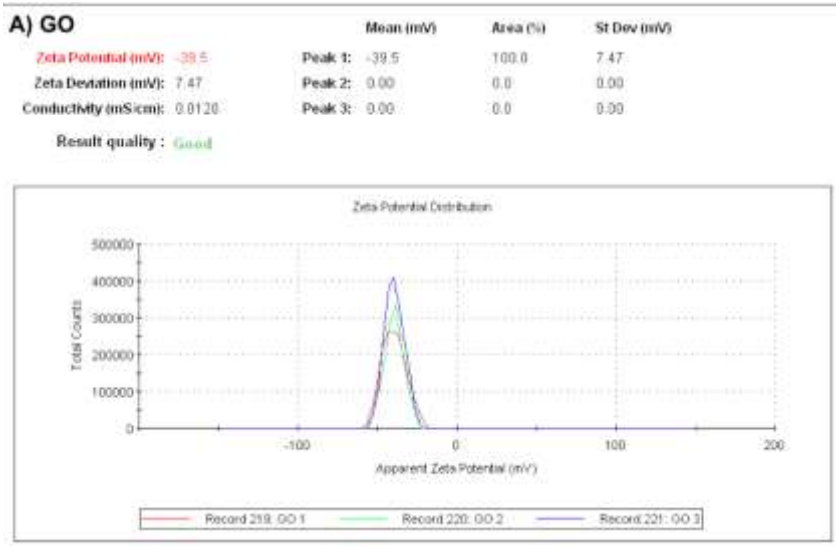

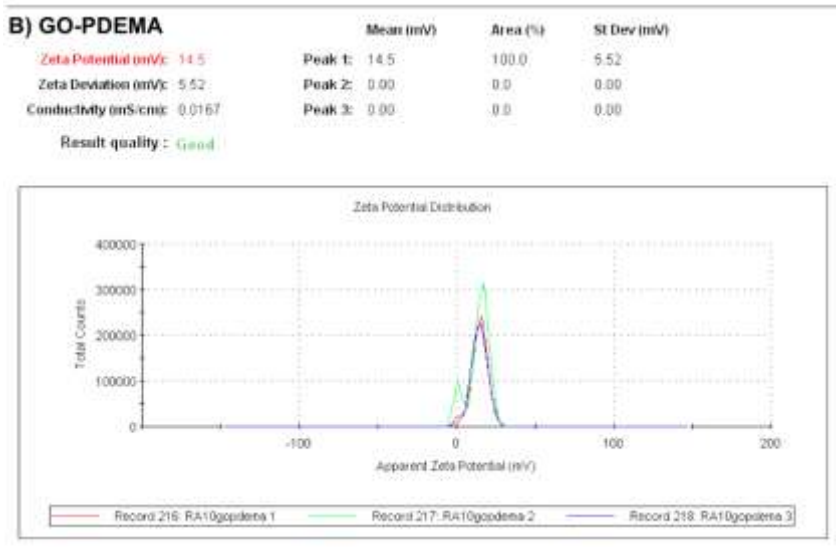

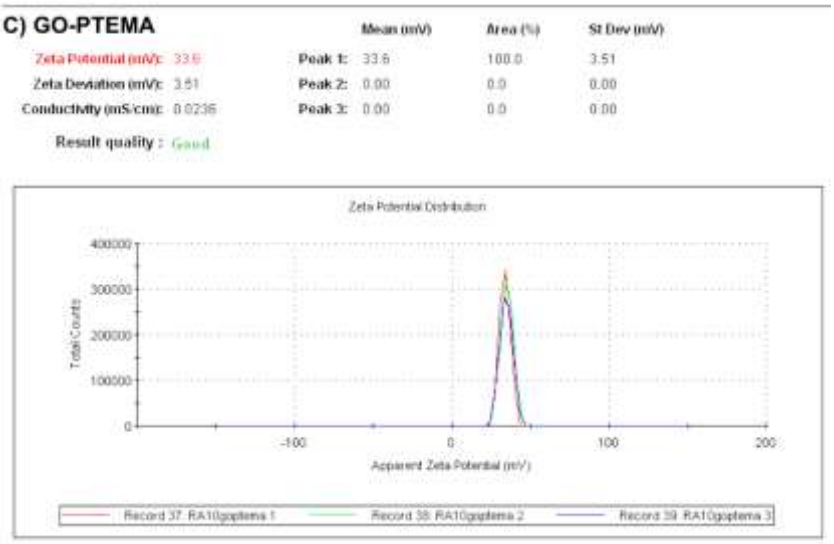

Figure S8. Zeta potential of (A) GO, (B) GO-PDEMA, and (C) GO-PTEMA.

To determine the surface charge per area of GO-PTEMA, a modified colorimetric method based on UV-VIS spectroscopy, as described by Tilleret al. (2001), was used for this measurement.[SI3] Fluorescein sodium salt in solution dissociates into negative ions of fluorescein and positive sodium ions. The negative fluorescein ions bind to the positively charged material by electrostatic interactions. The absorbance of known fluorescein concentrations was plotted to obtain the calibration curve. The slope of the calibration curve was then used to calculate the concentration of unknown samples by using absorbance values from the measurements of UV-VIS spectroscopy. GO, GO-PDEMA, and GO-PTEMA were dispersed in fluorescein solutions (0.5 g/l) and kept for 24 h with shaking for the samples to bind the dye. The samples were then centrifuged and the supernatant was collected. The stock solution and supernatants were diluted in equal ratio to bring the absorption signal into the measurement range of the UV-VIS spectrometer. The resulting concentrations of the solutions were determined by UV-VIS spectroscopy (**Figure S9**).

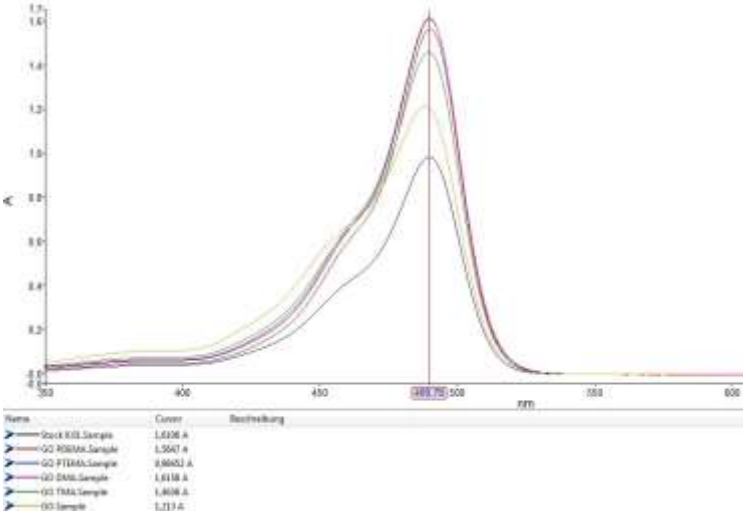

Figure S9. UV-VIS absorbance measurement of fluorescein stock solution 0.01 g/L (black) and fluorescein solution after adsorption of the test samples: GO (yellow), GO-PDEMA (red), GO-PTEMA (blue) determined by UV-VIS spectroscopy.

The absorption of the GO supernatant, which was determined to be 1.213, was significantly less than 0.01 g/l stock solution (1.61). This could be explained by unspecific adsorption of fluorescein on GO, for instance, via π-π interactions. The GO-PDEMA supernatant showed an absorption of 1.565, which means a lower fluorescein adsorption than for GO. This could be because of the reduction of double bonds during the functionalization via radical polymerization as explained in the synthesis strategy. The absorption of the GO-PTEMA supernatant shows a decreased value of 0.984, which reflects the high amount of negatively charged fluorescein bound to the positively charged quaternary amines of the GO-PTEMA. Therefore, no binding of fluorescein onto the material was observed.

The surface charge per mg of GO-PTEMA based on the measured UV-VIS absorbance is shown in **Table S1**. The diluted supernatant concentrations of the samples were determined via matching the calibration curve.

$$Concentration = \frac{Absorbance - 0.048}{159} \quad (4)$$

The initial concentration of the stock solution was calculated by multiplying the concentrations of the diluted samples and stock solution with a dilution factor of 50. The amount of fluorescein attached per mg of sample was then calculated by Equation 5.

$$\frac{Amount\ of\ fluorescein}{mg\ of\ sample} = \frac{volume\ (\ Stock\ conc. - supernatant\ conc.)}{Amount\ of\ sample} \quad (5)$$

The amount of fluorescein in mol per mg of sample was determined. The amount of fluorescein salt adsorbed to the non-quaternized samples of the GO-PDEMA sheets (0.05 mg/mg) was subtracted from charged sample values (0.41 mg/mg) to only account for the electrostatic nature of the adsorption. The resulting value of 0.36 g/g, which was divided by the molecular weight of fluorescein (332.31 g mol^{-1}), was 0.00108 mol g^{-1} = 1.08 mmol g^{-1} of charged units per 1 g of GO-PTEMA. Multiplied with the Avogadro constant to calculate the charges per g of GO-PTEMA were 6.52 x 10^{20} charges per g. Divided by the theoretical surface area of polymer-modified GO (calculated as 283 m^2g^{-1}) gave the number of charges per m^2 as 2.3 x 10^{18} m^{-2} = 2.3 x 10^{14} cm^{-2} = 2.3 nm^{-2}.

$$Specific\ surface\ charge = \frac{(Charge\ per\ g\ of\ sample)}{(Specific\ surface\ area\ of\ functionalized\ GO)} \quad (6)$$

Table S2. Summary of the fluorescein adsorption results and the calculated surface charge of GO-PTEMA.

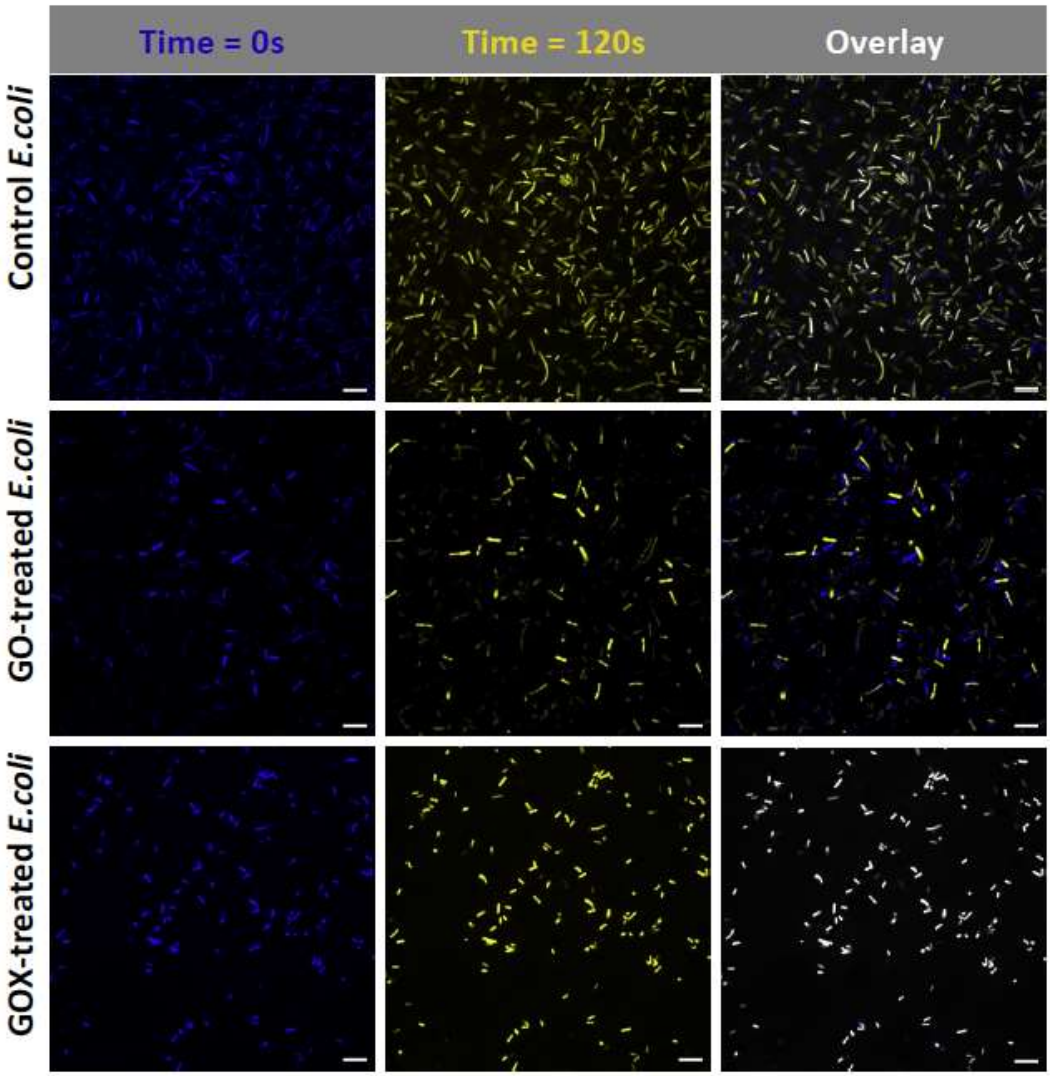

Sample	Diluted supernatant Concentration (g/l)	Supernatant concentration (g/l)	Amount of fluorescein per mg of sample (mg)	charge per g of sample	Specific surface charge per cm^2
GO	0.0073	0.365	0.27	---	---
GO PDEMA	0.0095	0.475	0.05	---	---
GO PTEMA	0.0059	0.295	0.41	6.52×10^{20}	2.3×10^{14}

Figure S10. Time-lapse recording of live-stained (SYTO-9) *E. coli*. Time point 0s was artificially colored blue and time point 120s was artificially colored yellow. In the time overlay (third column), it resulted in white or grey color. Scale bar = 10 µm.

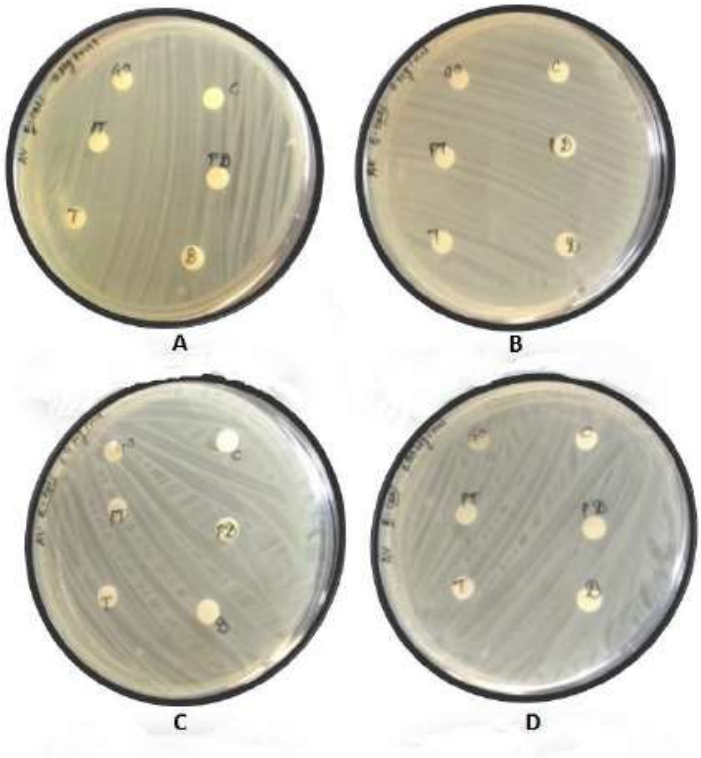

Figure S11. Disc diffusion assay with *E. coli* BL21 (DE3) and GO and its derivatives GO-PDEMA and GO-PTEMA. Petri dishes A-D contained all disc samples after 24 hours with four different incubation concentrations: (A) 2 µg/mL, (B) 8 µg/mL, (C) 64 µg/mL, and (D) 100 µg/mL. No inhibition zone was observed at all tested concentrations for GO or the GO derivatives.

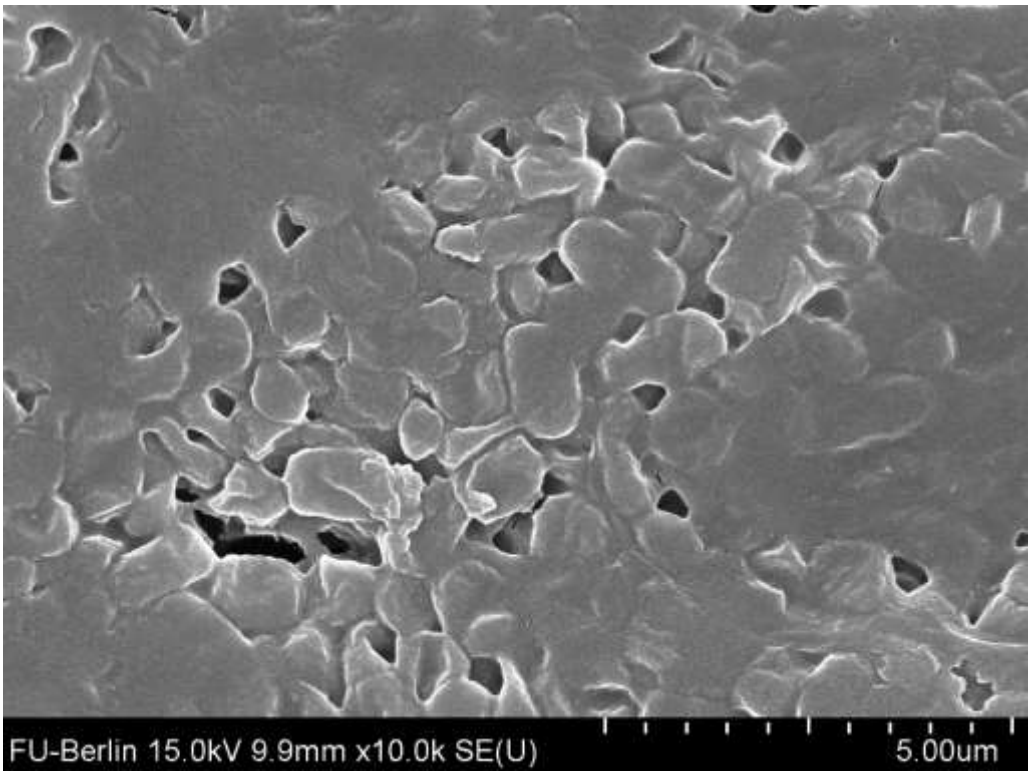

Figure S12. SEM image of vacuum dried *E. coli* BL21 (DE3) after incubation with GO-PTEMA sheets.

References

SI1) N. Azizi, M. R. Saidi, *Organic letters* **2005**, *7*, 3649.

SI2) H.N. Tien, N.T.M. Hien, E.S. Oh, J. Chung, E.J. Kim, W.M. Choi, S.H. Hur, *J. Mater. Chem. A* **2013**, *1*, 208.

SI3) J. C. Tiller, C. J. Liao, K. Lewis, A. M. Klibanov, *Proc. Natl. Acad. Sci*. **2001**, *98*, 5981.

3.2 Graphene-Based Bacterial Filtration via Electrostatic Adsorption

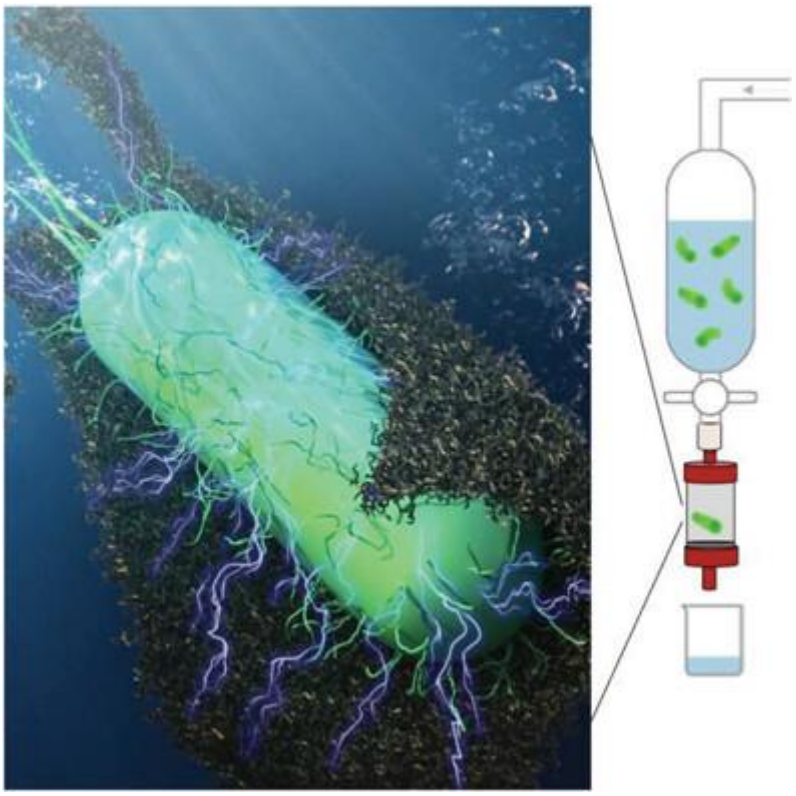

Rameez Ahmed, Ankita Vaishampayan, Katharina Achazi, Elisabeth Grohmann, Rainer Haag, Olaf Wagner

Adv. Mater. Interfaces **2022**, *9*, 2101917.

https://doi.org/10.1002/admi.202101917

Author contributions

Rameez Ahmed performed the synthesis and characterization experiments and wrote the manuscript. Ankita Vaishampayan performed biological experiments. Katharina Achazi performed fluorescence microscopy. Elisabeth Grohmann and Rainer Haag discussed the project and corrected the manuscript. Olaf Wagner conceptualized and supervised the project and corrected the manuscript.

ADVANCED MATERIALS INTERFACES
www.advmatinterfaces.de

Graphene-Based Bacterial Filtration via Electrostatic Adsorption

*Rameez Ahmed, Ankita Vaishampayan, Katharina Achazi, Elisabeth Grohmann, Rainer Haag, and Olaf Wagner**

Flexible graphene oxide (GO) microsheets with attached positively charged polymers, termed GOX microsheets, are efficient at bacterial adsorption, as they bind electrostatically to bacterial membranes' negative surface charge. The authors explore an antimicrobial water filter application for GOX's extremely high surface area and its previously described efficient bacterial adsorption. Cellulose-fiber carrier material is functionalized with GOX microsheets to create an adsorption-based bacteria filtration material. The morphology and charge density (7.8×10^{19} g^{-1}) of the prepared GOX fibers are determined by scanning electron microscopy and dye adsorption assay, and widefield fluorescence microscopy is used to visualize the adsorption of stained *Escherichia coli* bacterial cells on the fibers. GOX fibers are tested in filtration setups to investigate their bacteria removal performance. The experimental results, with 100 mg of GOX fibers filtering 2.4×10^9 colony-forming units (CFU) from an *E. coli* bacterial culture with 99.5% bacterial reduction, demonstrate the fibers' high bacteria loading capacity. The electrostatic adsorption-based filtration mechanism allows the filter to be operated at higher flow rates than micropore membrane filters, while maintaining 3-log bacterial reduction. GOX filter materials removing bacteria via adsorption are a high flow rate alternative to current water filtration processes that rely on size-exclusion.

1. Introduction

The water crisis is a serious global dilemma of the 21st century. The world's population is rapidly increasing, placing unprecedented strain on clean water supplies. By 2030, around half the world's population will be living in extreme water-deficient conditions, according to a recent United Nations World Water Development report.[1] Especially when people in crowded conditions lack clean water, fecal-oral diseases can proliferate rapidly. Diarrhea may not seem deadly to those who have access to improved sanitation, but it kills 750 000 children every year that is more than malaria, AIDS, and measles combined.[2]

Waterborne pathogens are also of great concern in the hospital environment, as the water temperatures and the complex structure of hospital water systems are suitable for bacterial growth and biofilm formation.[3,4] These pathogens in connected devices (such as sinks, showers, ice machines, water baths, eyewash stations, and dental units) can lead to severe infections, especially with the rising number of multidrug-resistant bacteria.[5,6]

The faucet micropore filters that are used to prevent this outcome must be replaced after a few weeks of use, making them very costly. Novel antibacterial technologies may offer practical and cost-effective prevention strategies for these concerns.

Graphene materials have been reported to exhibit antibacterial activity by physically interacting with bacterial cells.[7–9] These flexible, single-atom-thick, nano-micrometer sized sheets feature an extremely large surface area.[10,11] Among the variety of different graphene materials, graphene oxide (GO) is frequently used due to its inexpensive preparation from graphite[12–16] as well as its hydrophilic functional groups, which enhance its dispersibility in polar solvents and offer multiple options for chemical post-modification.[17,18]

In a previous work we demonstrated that polymer post-modification of micrometer-sized GO can be used to create polycationic microsheets.[19] These flexible GO microsheets matched the size and surface-charge density of opposite charged *E. coli* bacterial cells. Incubating them with gram-positive methicillin-resistant *Staphylococcus aureus* (MRSA) and gram-negative *Escherichia coli (E. coli)* led to wrapping and immobilization of bacterial cells in both cases.[19] Based on multivalent electrostatic attraction, these GO derivates (GOX) also showed antibacterial activity when they were attached to a carrier material.[20,21]

Although many polycationic polymers like chitosan,[22,23] polyethylene imine,[24,25] ε-polylysine,[26] polysiloxanes,[27,28] polyionenes[29,30] as well as modified GO materials with various conjugated moieties like mannose,[31] lactose,[32] quaternary ammonium compounds[33,34] and zwitterionic systems[35] have been shown to bind and inhibit bacteria, investigation

R. Ahmed, K. Achazi, R. Haag, O. Wagner
Freie Universität Berlin
Institute of Chemistry and Biochemistry
Takustr. 3, 14195 Berlin, Germany
E-mail: olaf.wagner@fu-berlin.de
A. Vaishampayan, E. Grohmann
Berliner Hochschule für Technik
Seestraße 64, 13347 Berlin, Germany
The ORCID identification number(s) for the author(s) of this article can be found under https://doi.org/10.1002/admi.202101917.

DOI: 10.1002/admi.202101917

of these materials as water purification materials remains quite limited. Ottenhall et al. reported *E. coli* reduction by cellulose-based filter papers functionalized with polycationic polyvinylamine in single-layer or multilayer systems with polyanionic polyacrylic acid.[36] Musico et al. reported increase in reduction of *E. coli* and *Bacillus subtilis* by modifying commercially available membrane filters with poly(N-vinylcarbazole)-graphene oxide.[37]

By far the most common technology for addressing bacterial water problems is membrane filtration. It is considered a very effective method, as it removes the targeted contaminants from water via the employed membrane pore size.[38] However, it has been reported that this is not true for bacteria with spirillum-shaped morphology. Wang et al. performed a quantification study to evaluate the filtration ability of commercially available membrane filters with 0.45, 0.22, and 0.1 µm pore sizes against freshwater bacterial communities. They reported that an average of 50% of the spirillum-shaped *Hylemonella gracilis* strains managed to pass through the 0.45 µm membrane filter.[39] Although this strain is not pathogenic it demonstrates the limitation of size exclusion filtration.

Another drawback of the size exclusion working principle of membrane filters is their low flow rate due to the small pore sizes and continuously decreasing permeability due to accumulated filtrate or biofouling.[40] Commercially available 0.45 µm, 0.2 µm, and 0.1 µm pore size polytetrafluorethylene (PTFE) filters from Sterlitech have maximum flowrates of 40, 20 and 14 mL min^{-1} cm^{-2}, according to the product data sheet.[47] Membrane filters with these low flow rates require very high filter cross sections or specially designed high surface area filter geometries. In addition, membrane filtration systems require regular maintenance, backwash cycles, or membrane replacement to keep them operational.

While size exclusion filtration is used against bacteria, other water contaminants (i.e., heavy metals, biocides, pharmaceuticals) are usually removed by adsorption materials like activated carbon[41] or ion exchange resins.[42]

In this work, we present a universal antimicrobial filter material that removes bacteria by adsorption based on electrostatic interaction. This was realized by covalently coating the above mentioned polycationic GO sheets (GOX) onto cellulose fibers as a carrier material. The GOX-functionalized fibers were tested in bacterial filtration experiments to evaluate their filtration performance in parameters such as flow rate, loading capacity, and reduction of colony-forming units.

2. Results

2.1. Filter Material Synthesis

The polycationic GO sheets (GOX) were prepared by a method described in our previous work.[19] Briefly, GOX was prepared from GO via a two-step synthesis. First, the polymer chains were grafted onto the surface of GO via radical polymerization of a dimethylamino-ethylmethacrylate monomer, based on the work of Kan et al.[43] After the polymerization, the dimethylamine side groups were quaternized by methyl iodide to form quaternary ammonium groups to render GOX polycationic microsheets (**Figure 1**).

The cellulose fibers were selected as carrier material because it is one of the most abundant natural polymers on earth. It is a renewable, biodegradable, nontoxic material with excellent mechanical properties, which is available in different size.[44,45] Cellulose fibers were initially dried to remove adsorbed water from the surface. Methylene bisphenyl diiscoyanate was dissolved in dry DMF and the dried fibers were immersed into the solution to homogeneously distribute the fibers. GOX in a 10 wt% ratio to the fibers was dispersed in dry DMF and then added to the diisocyanate surface-activated cellulose dispersion to covalently bind to them.

2.2. Characterization of Filter Materials

2.2.1. Appearance and Morphology

A change in appearance of the cellulose fibers from a bright white to darker brown to black can be observed after the functionalization with GOX (**Figure 2**a,d). Scanning electron microscopy (SEM) was used to examine the cellulose fibers before and after immobilization with the GOX microsheets. The cellulose fibers have a smooth surface morphology with random orientation (Figure 2b,c). The GOX-functionalized fibers are also in

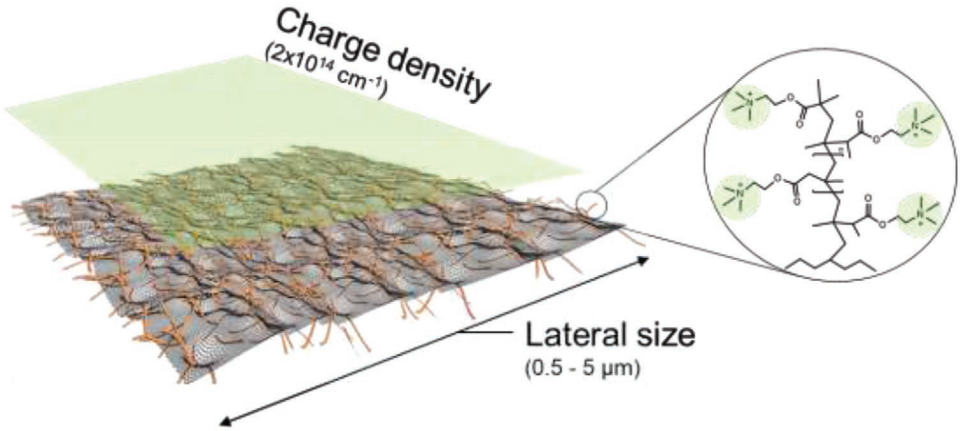

Figure 1. Illustration of GOX microsheets and its dimensions and polycationic surface charge density.

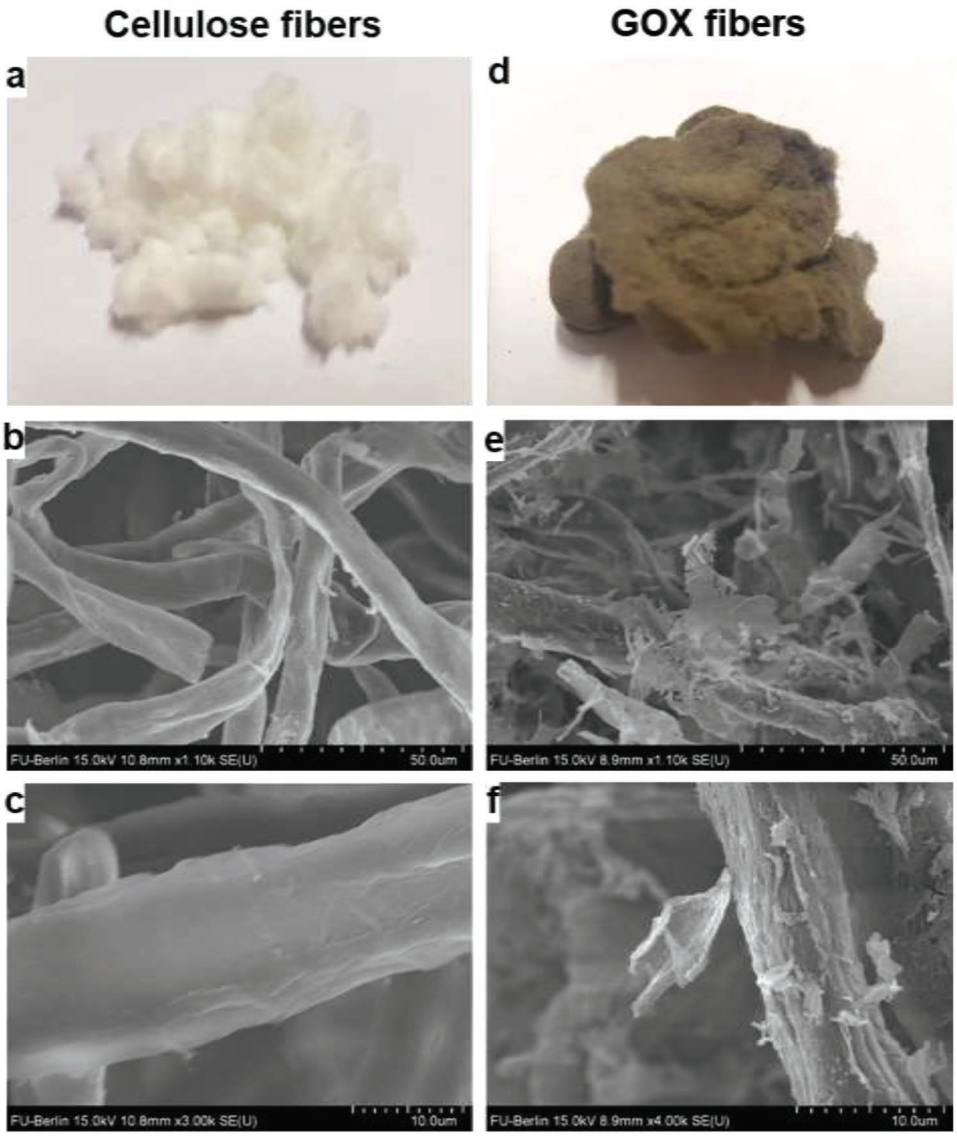

Figure 2. Images of cellulose fibers (left column) and cellulose fibers with GOX microsheet coating (right column). Images (a) and (d) are photographs, while the images below are SEM images at b,e) 10k, c) 300k and f) 400k magnification.

random orientation and GOX microsheets are attached along the fiber surfaces increasing their overall surface area (Figure 2e,f).

2.2.2. Polycationic Charge Density

The number of positive charges on GOX (6.5×10^{20} per gram) was quantified in our previous work via a colorimetric method.[19] The method is based on the electrostatic adsorption of a negatively charged dye (fluorescein), which binds to the positive charges of the sample. The concentration decrease via bound dye is determined by UV–Vis spectroscopy and the difference of initial and final concentration is used to calculate the number of positive charges on the sample. The charge density of the 10 wt% GOX-functionalized cellulose fibers was quantified by the same assay (see Supporting Information) and was calculated to be 7.8×10^{19} charges per gram. This value is around 10% of the GOX charge density and validates the successful immobilization of 10 wt% GOX microsheets on cellulose fibers (**Table 1**).

2.2.3. Adsorption of Bacterial Cells on GOX Fibers

The binding effect of GOX-functionalized cellulose fibers on bacteria was visualized with a widefield microscope using *E. coli* with a live/dead staining kit. The attraction of *E. coli* to GOX cellulose fibers was visible as the *E. coli* cells stuck to the GOX cellulose fibers (**Figure 3**). The fibers had no immediate toxic effect on the bacteria, as all bacteria appeared alive, showing a fluorescence in the green spectra. However, the membranes of some bacteria seemed to be affected, as some bacteria appeared in the orange/red spectra due to the orange/red fluorescent ethidium homodimer-III (EthD-III) dye that can enter a leaky

Table 1. Summary of charge calculations per unit amount of GOX fibers.

Sample	Adsorbed dye on fibers [mg]	Cellulose control subtracted [mg][a)]	Adsorbed dye [mmol][b)]	No. of charges per GOX fibers[c)]
Cellulose Fibers	0.0050	-	-	-
GOX fibers	0.0480	0.0430	0.129	7.8×10^{19}

[a)]Amount of adsorbed dye on fibers after subtraction of cellulose control; [b)]Amount of adsorbed dye/molecular weight of dye; [c)]Adsorbed dye [mol] * Avogadro's constant

bacterial membrane. The unmodified cellulose fibers did not show this interaction with the *E. coli* cells, which were homogenously distributed in the suspension. Therefore, the immobilization of *E. coli* bacterial cells can be attributed to the positive charges of the GOX-functionalized cellulose fibers.

2.2.4. Bacterial Cell Filtration Experiments

To determine the filtration effectivity and capacity of GOX fibers, several experiments have been performed. The initial test was performed to determine the effective amount of material to reduce the number of bacteria in colony forming units (CFUs) by three orders of magnitude (3 logs), which is a common minimal requirement for commercial membrane filters.[46] Different amounts of GOX fibers were loaded in a syringe volume and 2 runs of 10 mL of a 1.6×10^7 CFU mL^{-1} *E. coli* bacterial culture was filtered through them. **Figure 4** summarizes the reduction of colony-forming *E. coli* bacteria for the different tested GOX fiber amounts.

The results demonstrate that bacterial reduction increased with increasing amounts of GOX fiber material. 33 mg GOX fibers

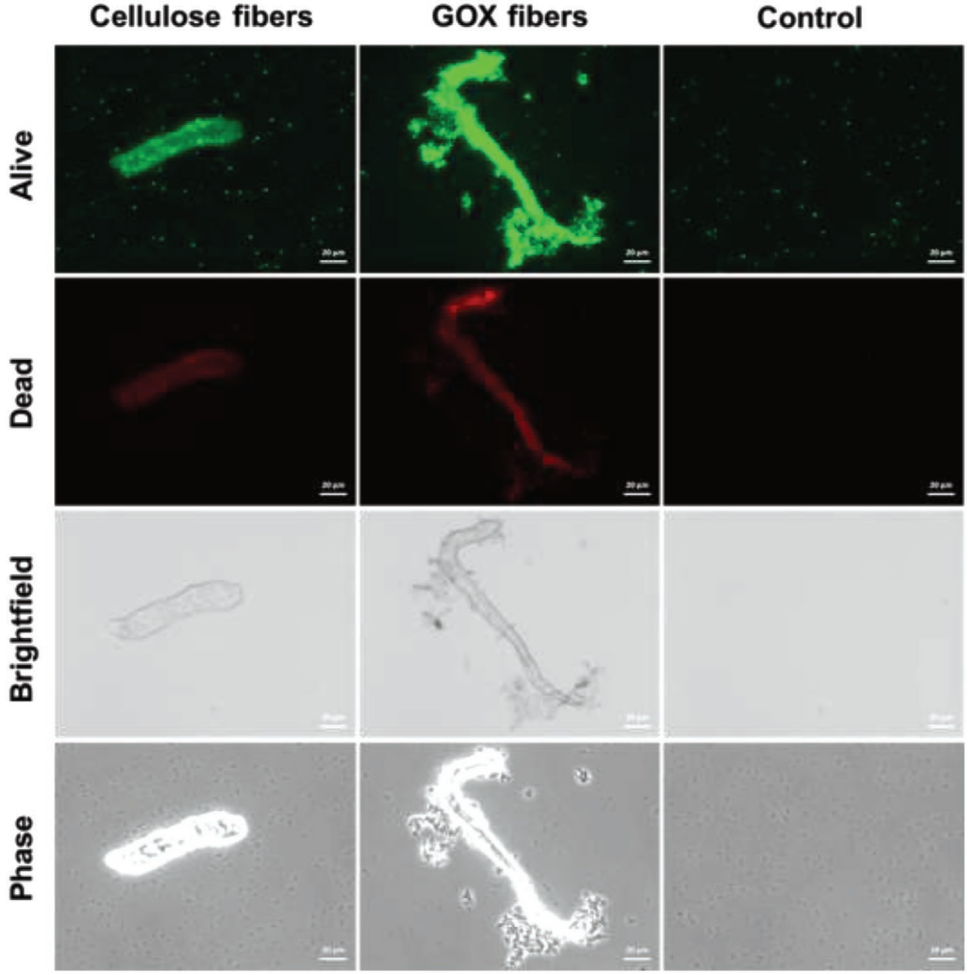

Figure 3. Microscopy images of cellulose fibers (left column); GOX cellulose fibers (middle column) incubated with *E. coli* bacteria (strain ORN208, K12 derivative); and bacteria only, without fibers, as control (right column). Bacteria were stained with the Bacteria Live/Dead Staining Kit live/dead staining kit from PromoCell GmbH (Heidelberg). In the fluorescence images live bacteria are shown in green (first row) and dead bacteria in red (second row). In the brightfield images (third row) fibers and attached GOX microsheets are visible. Using phase contrast microscopy (bottom row) the bacteria as well as fibers can be visualized. (The scale bar is 20 µm in all images.)

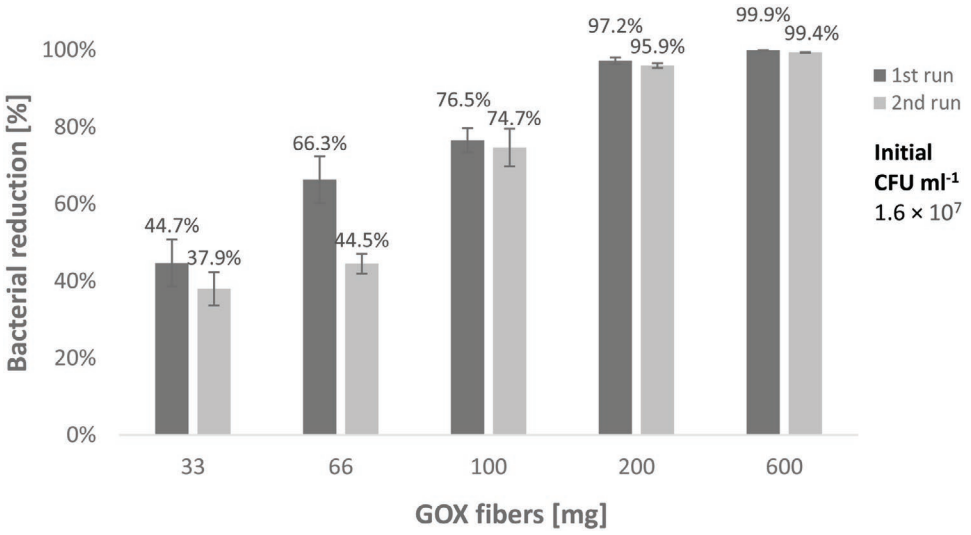

Figure 4. Summary of the two *E. coli* bacterial filtration runs of increasing GOX fiber amounts. The Y-axis values represent the percent reduction of colony-forming bacteria in the filtrate as compared to the initial concentration of 1.6×10^7 CFU mL^{-1}.

caused the lowest CFU reduction at 45%, whereas the filtrate from 600 mg GOX fibers showed a 99.9% reduction of CFU. The amount of 100 mg of GOX fiber was selected for further experiments because of its moderate bacterial reduction performance of 75%, in order to allow the detection of samples with higher CFU reduction, as well as the convenient handling for varying flow rate and pressure experiments, in lab scale environment.

To elucidate to what extent the GOX microsheets on the cellulose fibers were responsible for the filtration of bacteria, control experiments were performed with unfunctionalized cellulose fibers. The procedure is described in detail in the experimental section, and the experimental setup is shown in **Figure 5**. Briefly, 1000 mL of *E. coli* bacterial culture (9.1×10^4 CFU mL^{-1}) was filtered through 100 mg of GOX-functionalized fibers and

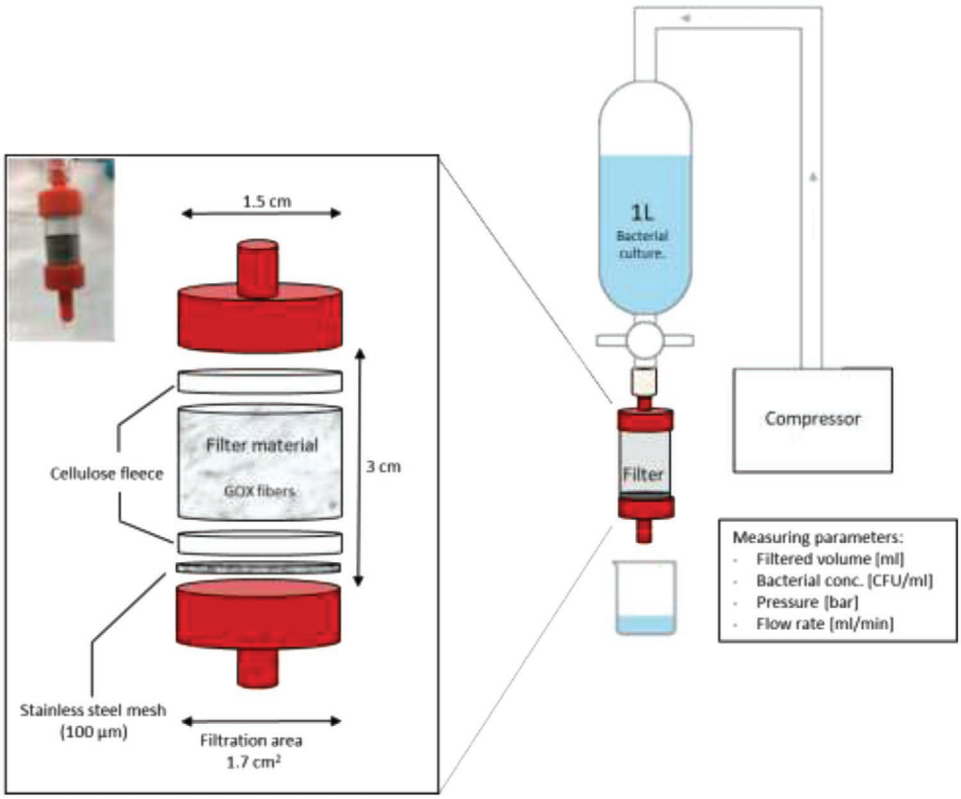

Figure 5. Scheme of experimental setup for GOX fiber filtration experiment.

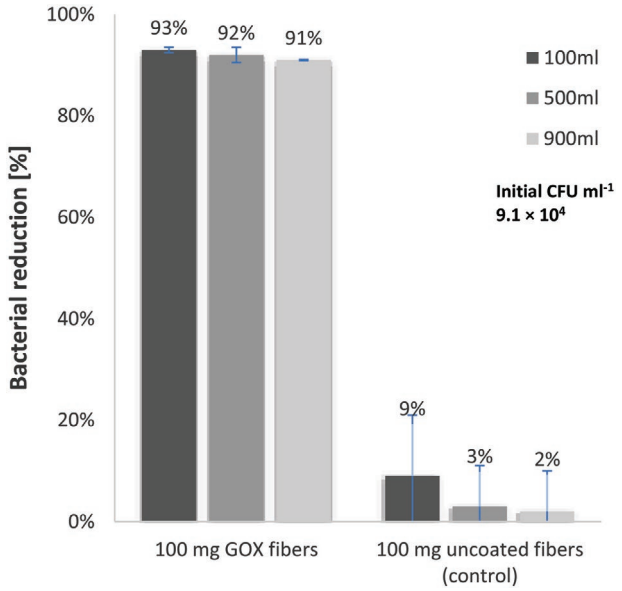

Figure 6. Bacterial reduction by 100 mg GOX fibers and uncoated fibers (control). The 3 bars for each material represent the 3 sampling points (100, 500, 900 mL).

control cellulose fibers, at 35 ± 5 mL min^{-1} respectively. Samples were collected during filtration at 100 mL, 500 mL and 900 mL flow through and plated on agar to determine the CFU concentration and the percentage of bacterial reduction (**Figure 6**). GOX-functionalized fibers reduced the CFU concentration more than 90% in all 3 fractions of the 1 L filtered bacterial culture. On the other hand, cellulose fibers reduced the amount of bacteria in the solution by only 2–10%. This result demonstrated that the GOX microsheets on the fibers were responsible for the high bacterial filtration performance.

2.2.5. GOX Fiber Bacterial Loading Capacity

To evaluate the bacterial loading capacity of the GOX fiber material, 3 L of bacterial culture of increasing concentration (1.0, 2.8 and 3.3 × 10^6 CFU mL^{-1}) was filtered through 100 mg of GOX-functionalized fibers at flowrate of 25 ± 5 mL min^{-1}. For each filtered liter, Two samples were taken from the bacterial culture (at flow points 400 mL and 800 mL) and plated on agar to determine the CFU concentration. The total number of passing bacteria was plotted against the bacterial reduction in the filtrate (**Figure 7**).

The results show that 100 mg of GOX fibers removed more than 99.5% of bacteria from the first 1.4 L of bacterial culture (2.4 × 10^9 CFU). Ottenhallet al. reported maximum 98% bacterial removal by filtering 10^7 CFU bacterial culture with a stack of 5 sheets of single-layer polyvinylamine-coated filter paper.[36] In comparison to this polyvinylamine cellulose filter paper, GOX fibers have 100-fold greater bacteria loading capacity at a higher bacterial reduction efficiency. After the filtration of 1.8 L of bacterial culture (3.6 × 10^9 CFU) the performance dropped to 97%, then further to 83% at 2.4 L (5.1 × 10^9 CFU), and finally to 48% at 6.8 × 10^9 CFU.

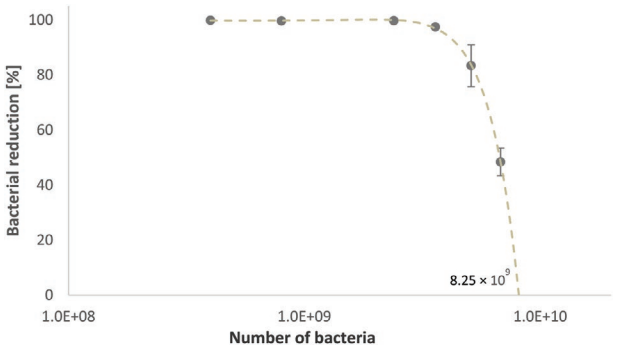

Figure 7. Bacterial loading capacity of 100 mg GOX fibers for 3 L of bacterial culture with increasing CFU concentration per liter. The number of passing bacteria is plotted against the bacterial reduction at each sample point.

The sudden decrease in filtration performance around 5 × 10^9 CFU indicates that the filter surface is saturated at this point, which reflects the maximum bacterial loading capacity of 100 mg GOX fibers. The extrapolation of the data shows that the 100 mg GOX fibers will completely lose their filtration ability at 8.25 × 10^9 CFU. Since the bacteria culture continues passing through the filter, this result further demonstrates that the mechanism of removal is bacterial adsorption and not size exclusion.

2.2.6. Flow Rate and Pressure Dependence

Flow rate and pressure are important parameters for filter applications. Membrane filters have flow rate limitations stemming from the small pore sizes necessary to retain particles. These limitations further increase when retained particles accumulate, tightening the space and clogging the pores, resulting in even lower flow rates and a higher drop in pressure. Therefore we used an experimental setup with increasing water pressure to evaluate the filtration performance of GOX-functionalized fibers at increasing flow rates. In short, 1 L of *E. coli* bacterial culture (1.7 × 10^4 CFU mL^{-1}) was prepared, then forced by an air compressor through a cartridge filled with 100 mg of GOX fibers. The flow rate was determined and, in **Figure 8**, is plotted against the applied pressure. Samples of the filtrate were collected and plated on agar to determine the CFU concentration at the corresponding flow rates.

The results show that increased pressure and flow rate have no negative effect on GOX filtration performance within the range of tested parameters. Even a maximum flow rate of 334 mL min^{-1} allowed for complete removal of bacteria from the filtrate. The maximum flow rate per unit surface area for the GOX fiber filter cartridge is calculated to be 196 mL min^{-1} cm^{-2}, by dividing the maximum flow rate (334 mL min^{-1}) by cartridge filtration area (1.7 cm^2). Commonly used micropore bacterial filters cannot operate at such a high ratio of flow rate to area. Under 0.7 bar of pressure in a clean water environment, commercially available PTFE membrane filters with 0.45 µm pores can reach maximum flow rates of 40 mL min^{-1} cm^{-2}.[47] In contrast, the presented filter material based on polycationic graphene oxide sheets provides 3-log bacteria reduction at flow

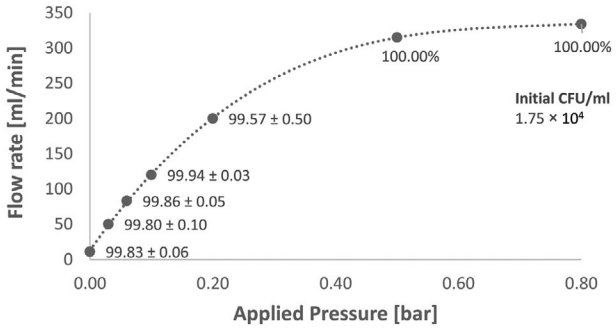

Figure 8. Bacterial filtration at increasing flow rate for 100 mg of GOX-functionalized fibers.

rates of 196 mL min^{-1} cm^{-2}, which is nearly five times higher than typical membrane filters.

3. Conclusion

In this work, a new bacteria-adsorbing material based on electrostatic attraction was developed and investigated for its bacteria reduction performance. The material's functionality is based on a positively charged high-surface-area graphene derivative. The derivative, a GO microsheet with grafted polycationic polymers (GOX), was covalently immobilized on cellulose fibers. 100 mg of the created GOX fibers adsorbed *E. coli* bacteria cells, removing up to 2.4×10^9 CFU with 99.5% filtration efficiency. The filter performance of 3-log CFU reduction was reached even at flow rates of 196 mL min^{-1} cm^{-2}, which is around five times higher than membrane filters. Log-3 bacterial reduction at these flow rates per area validates the potential of these GOX sheets as a simple method to efficiently filter bacteria when directly attached to a faucet. Cartridges with GOX-functionalized filter materials could be installed on the faucets of hospitals or public water sources to ensure drinking water quality without falling short of typical faucet flow rates.

4. Experimental Section

Materials and Methods: Used chemicals were purchased from following sources:

2-(dimethylamino) ethyl methacrylate (98%, Aldrich), 2,2'-azobis(2-methylpropionitrile) (98%, Aldrich), 4,4′-methylene bis (phenyl isocyanate) (98% Aldrich), aluminum oxide (50–200 µm, Acros Organics), 3-dimethylaminopropylamin (99%, Aldrich), methyl iodide (99%, Acros Organics), dimethylformamide (99.5%, Acros Organics), tetrahydrofuran (99.9%, VWR chemicals), fluorescein sodium salt (Sigma-Aldrich), LB-Broth or LB-Agar (Carl Roth GmbH & Co. KG, Karlsruhe, Germany). The graphene oxide sheets were purchased as paste from "graphene-supermarket.com," (0.5–5 µm, 80%). Cellulose fibers were from Vitacell LC 1000, JRS, J. Rettenmaier & Söhne GmbH.

Synthesis of GOX Fibers: The detailed synthesis of GOX and its characterization was reported in the previous work.[18] GOX fibers were produced by drying 1 g of cellulose fibers at 80 °C overnight to remove adsorbed water from the surface. 5 mg of 4,4′-methylenebis (phenyl isocyanate) (4,4′MDI) was dissolved in 5 mL dry DMF. The dried fibers were then immersed into the 4,4′MDI solution to homogeneously distribute and activate the surface of the fibers. 100 mg of GOX was dispersed in 45 mL of dry DMF by ultrasonication and added to the reaction mixture to bind the GOX onto the cellulose fibers. The mixture was allowed to react at room temperature under constant stirring for 24 h. The fibers were then filtered, washed with deionized water, and dried by lyophilization.

Scanning Electron Microscopy: The cellulose fibers and GOX fibers were imaged with a field emission scanning electron microscope (FE-SEM, Hitachi SU8030) at 15 kV, a current of 10 µA and a working distance (WD) of around 8.3 mm. The samples were coated with a gold layer by using a sputter coater (Emscope SC 500, Quorum Technologies, UK).

Fluorescent Microscopy of Bacterial Binding to GOX Cellulose Fibers: For analyzing the binding of *E. coli* bacteria (strain *E. coli* ORN208, K12 derivative) to cellulose fibers and GOX cellulose fibers, a bacterial culture was prepared and stained with the Bacteria Live/Dead Staining Kit (PromoCell GmbH, Heidelberg, Germany) according to the manufacturer's instructions.

In short, 10 mL LB medium was inoculated with *E. coli* (strain ORN208, K12 derivative) and incubated overnight at 37 °C in a shaking incubator. The overnight bacterial culture was divided in 2 mL aliquots and centrifuged at room temperature and 10000 × *g* for 15 min. After discarding the supernatant, 2 mL of 0.85% NaCl solution was added to each aliquot. After resuspending the pellet by vortexing, the aliquots were further incubated at 37 °C under shaking for 1 h and vortexed every 15 min. Then, two times all aliquots were centrifuged at room temperature and 10 000 × *g* for 15 min, the supernatant was discarded, and the pellet was resuspended by vortexing in 2 mL of 0.85% NaCl solution. The optical density (OD) from all aliquots was measured at 670 nm using 0.85% NaCl solution as blank and if needed adjusted to an OD of 0.25-0.3 corresponding to approximately 2×10^8 CFU mL^{-1}. Then, 200 µL of sample suspension either containing 20 mg mL^{-1} of bare cellulose fibers or 20 mg mL^{-1} of GOX-functionalized cellulose fibers was mixed each with 200 µL of the prepared suspension containing living bacteria for at least 15 min at room temperature. 200 µL of each suspension (Bacteria-fiber-mix and bacteria suspension without fibers) was mixed by vortexing 2 µL of freshly prepared staining solution (1 volume of 5×10^{-3} M DMAO in DMSO + 2 volumes of 2×10^{-3} M ethidium homodimer-III in DMSO/H_2O + 8 volumes 0.85% NaCl solution) at room temperature for 15 min in the dark.

For imaging, 5 µL from each stained suspension was mounted on a glass slide and covered with a coverslip. Imaging was done with a Zeiss Axio Observer.Z1 epifluorescence microscope (inverted) with an 40x objective and the Zeiss ZEN software using the fluorescence filter sets for GFP/FITC (live bacteria) and Cy3/Texas Red (dead bacteria) and using also brightfield and phase-contrast imaging.

GOX Fibers Filtration Test: An overnight culture of *E. coli* BL21 (DE3) was prepared in LB broth and incubated at 37 °C with constant agitation at 150 rpm. The culture was then diluted in LB broth to $OD_{600} = 0.05$, approximately, 10^7 colony forming units (CFU mL^{-1}). Initially, the syringe filter was wetted by passing 5 mL deionized water. 10 mL of the diluted culture was passed through syringe filters containing, 33, 66, 100, 200, or 600 mg GOX fibers. The filtrate was collected, serially diluted, and spread on LB agar plates (100 µL culture was spread). The filtration step was replicated by filtering 10 mL of the diluted culture. The LB agar plates were incubated for 16–24 h at 37 °C, colonies were counted, and CFU mL^{-1} was calculated. To flush out all the bacteria that were retained in the filter, a final step in the filtration process was performed by filtering 5 mL LB broth containing 1% NaCl. The filtrate was serially diluted and plated on LB agar plates to calculate the CFU mL^{-1} as described above.

Filter Cartridge Preparations: Cylindrical filter cartridges of 1.7 cm^2 surface area consist of 100 µm stainless steel mesh as base layer. Thin layer of cellulose fleece was placed on top of it as support layer for the fibers. 100 mg of GOX fibers or cellulose fibers were dispersed in water and filtered through the cartridge to load the fibers. Cellulose fleece layer was then deposited on top to sandwich the fibers. 500 mL of water was

made to flow through the cartridge under 0.05 bar pressure to settle down the fibers in the support layers.

1 L Bacterial Culture Filtration Test: An overnight culture of *E. coli* BL21 (DE3) was prepared in LB broth and incubated at 37 °C with constant agitation at 150 rpm. The culture was diluted in LB broth to $OD_{600} = 0.05$, equal to approximately 10^7 CFU mL^{-1}. The diluted culture of $OD_{600} = 0.05$ was further diluted 1:1000 in LB broth to obtain the desired 10^4 CFU mL^{-1} cell density. One liter of diluted culture of 10^4 CFU mL^{-1} was passed through the cartridge filter containing 100 mg GOX fibers or 100 mg cellulose fibers. Three fractions of the flow-through were collected after 100 mL, 500 mL, and 900 mL of bacterial culture and spread on LB agar plates. The plates were incubated for 16–24 h at 37 °C, colonies were counted, and CFU mL^{-1} was calculated.

GOX Fiber Bacterial Loading Test: An overnight culture of *E. coli* BL21 DE3 was prepared in LB broth without salt and incubated at 37 °C with constant agitation at 150 rpm. The overnight culture was diluted to $OD_{600} = 0.1$ (in LB broth without salt) corresponding to a bacteria concentration of approximately 10^8 CFU mL^{-1}. The bacterial culture was further diluted in deionized water to yield 3 L of a solution with 10^6 CFU mL^{-1}. Three samples were collected from the bacterial culture to determine the initial CFU of each liter, by spreading it on an LB agar plate. The GOX fibers filter cartridge was flushed with 200 mL of deionized water. Three liters of bacterial culture were then filtered through the cartridge by applying external pressure with the help of an air compressor at steady flow rate. Two samples were collected from the filtrate for each liter, after passing 400 mL and 800 mL bacterial culture. The samples were serially diluted and spread on LB agar plates. The agar plates were incubated for 16–24 h at 37 °C before colonies were counted and the corresponding CFU mL^{-1} plated bacterial culture was calculated.

Flowrate and Pressure Dependence: An overnight culture of *E. coli* BL21 (DE3) was prepared in LB broth (devoid of salt) and incubated at 37 °C with constant agitation at 150 rpm. The overnight culture was diluted in LB broth to $OD_{600} = 0.05$, equal to approximately 10^7 CFU mL^{-1}. This diluted culture was further diluted 1:1000 in deionized water to obtain the desired 10^4 CFU mL^{-1} cell density. One liter of diluted culture was filtered through a 100 mg GOX fibers filter cartridge. Pressure was applied to the culture by using an air compressor. Samples were collected from the filtrate at atmospheric pressures of 0.03, 0.06, 0.10, 0.20, 0.50, and 0.80 bar. The flow rate was calculated by dividing the passing bacterial culture volume (mL) by time (min). The samples were serially diluted and spread on LB agar plates. They were incubated for 16–24 h at 37 °C, colonies were counted, and CFU mL^{-1} was calculated.

Supporting Information

Supporting Information is available from the Wiley Online Library or from the author.

Acknowledgements

Open access funding enabled and organized by Projekt DEAL.

Conflict of Interest

The authors declare no conflict of interest.

Data Availability Statement

The data that support the findings of this study are available from the corresponding author upon reasonable request.

Keywords

flow rate, graphene oxide, polycationic microsheets, water filter, water purification

Received: October 5, 2021
Revised: December 10, 2021
Published online: January 23, 2022

[1] A. Otte, D. Coates, R. Connor, G. Roder, D. Hebart-Coleman, M. Klimes, E. Yaari, M. Gutierrez, N. Crawhall, R. Kinna, *The United Nations World Water Development Report* **2021**, pp. 97–106.
[2] L. Liu, H. L. Johnson, S. Cousens, J. Perin, S. Scott, J. E. Lawn, I. Rudan, H. Campbell, R. Cibulskis, M. Li, *Lancet* **2012**, *379*, 2151.
[3] B. K. Decker, T. N. Palmore, *Curr. Opin. Infect. Dis.* **2013**, *26*, 345.
[4] A. Breathnach, M. Cubbon, R. Karunaharan, C. Pope, T. Planche, *J. Hosp. Infect.* **2012**, *82*, 19.
[5] F.-A. Pitten, B. Panzig, G. Schröder, K. Tietze, A. Kramer, *J. Hosp. Infec.* **2001**, *47*, 125.
[6] H. Kanamori, D. J. Weber, W. A. Rutala, *Clin. Infect. Dis.* **2016**, *62*, 1423.
[7] M.-Y. Xia, Y. Xie, C.-H. Yu, G.-Y. Chen, Y.-H. Li, T. Zhang, Q. Peng, *J. Controlled Release* **2019**, *307*, 16.
[8] O. Akhavan, E. Ghaderi, A. Esfandiar, *J. Phys. Chem. B* **2011**, *115*, 6279.
[9] S. Liu, M. Hu, T. H. Zeng, R. Wu, R. Jiang, J. Wei, L. Wang, J. Kong, Y. Chen, *Langmuir* **2012**, *28*, 12364.
[10] A. Tiwari, M. Syväjärvi, *Graphene Materials: Fundamentals and Emerging Applications*, John Wiley & Sons, New York **2015**.
[11] S. Liu, T. H. Zeng, M. Hofmann, E. Burcombe, J. Wei, R. Jiang, J. Kong, Y. Chen, *ACS Nano* **2011**, *5*, 6971.
[12] S. Hermanová, M. Zarevúcká, D. Bouša, M. Pumera, Z. Sofer, *Nanoscale* **2015**, *7*, 5852.
[13] S. You, J. Yu, B. Sundqvist, A. V. Talyzin, *Phys. Status Solidi* **2012**, *249*, 2568.
[14] W. S. HummersJr, R. E. Offeman, *J. Am. Chem. Soc.* **1958**, *80*, 1339.
[15] C. K. Chua, Z. Sofer, M. Pumera, *Chem. - Eur. J.* **2012**, *18*, 13453.
[16] D. R. Dreyer, S. Park, C. W. Bielawski, R. S. Ruoff, *Chem. Soc. Rev.* **2010**, *39*, 228.
[17] A. M. Dimiev, S. Eigler, *Graphene Oxide: Fundamentals and Applications*, John Wiley & Sons, New York **2016**.
[18] H. Ji, H. Sun, X. Qu, *Adv. Drug Delivery Rev.* **2016**, *105*, 176.
[19] R. Ahmed, A. Vaishampayan, J. L. Cuellar-Camacho, D. J. Wight, I. Donskyi, W. Unger, E. Grohmann, R. Haag, O. Wagner, *Adv. Mater. Interfaces* **2020**, *7*, 1902066.
[20] A. Vaishampayan, R. Ahmed, O. Wagner, A. de Jong, R. Haag, J. Kok, E. Grohmann, *Mater. Sci. Eng., C* **2021**, *119*, 111578.
[21] D. Wischer, D. Schneider, A. Poehlein, F. Herrmann, H. Oruc, J. Meinhardt, O. Wagner, R. Ahmed, S. Kharin, N. Novikova, *Front. Microbiol.* **2020**, *11*, 1626.
[22] M. Rinaudo, *Prog. Polym. Sci.* **2006**, *31*, 603.
[23] N. Sudarshan, D. Hoover, D. Knorr, *Food Biotechnol.* **1992**, *6*, 257.
[24] C. Z. Chen, N. C. Beck-Tan, P. Dhurjati, T. K. van Dyk, R. A. LaRossa, S. L. Cooper, *Biomacromolecules* **2000**, *1*, 473.
[25] N. Bourne, L. Stanberry, E. Kern, G. Holan, B. Matthews, D. Bernstein, *Antimicrob. Agents Chemother.* **2000**, *44*, 2471.
[26] M. Hyldgaard, T. Mygind, B. S. Vad, M. Stenvang, D. E. Otzen, R. L. Meyer, J. Björkroth, *Appl. Environ. Microbiol.* **2014**, *80*, 7758.
[27] J. Jońca, C. Tukaj, W. Werel, U. Mizerska, W. Fortuniak, J. Chojnowski, *J. Mater. Sci.: Mater. Med.* **2016**, *27*, 55.

[28] Q. Zhang, H. Liu, X. Chen, X. Zhan, F. Chen, *J. Appl. Polym. Sci.* **2015**, *132*, 14.
[29] S. R. Williams, T. E. Long, *Prog. Polym. Sci.* **2009**, *34*, 762.
[30] S. Liu, R. J. Ono, H. Wu, J. Y. Teo, Z. C. Liang, K. Xu, M. Zhang, G. Zhong, J. P. Tan, M. Ng, *Biomaterials* **2017**, *127*, 36.
[31] W. Zhan, T. Wei, L. Cao, C. Hu, Y. Qu, Q. Yu, H. Chen, *ACS Appl. Mater. Interfaces* **2017**, *9*, 3505.
[32] P. Subramanian, F. Barka-Bouaifel, J. Bouckaert, N. Yamakawa, R. Boukherroub, S. Szunerits, *ACS Appl. Mater. Interfaces* **2014**, *6*, 5422.
[33] L. Xiao, J. Sun, L. Liu, R. Hu, H. Lu, C. Cheng, Y. Huang, S. Wang, J. Geng, *ACS Appl. Mater. Interfaces* **2017**, *9*, 5382.
[34] S. Omidi, A. Kakanejadifard, F. Azarbani, *J. Mol. Liq.* **2017**, *242*, 812.
[35] K. H. Tan, S. Sattari, I. S. Donskyi, J. L. Cuellar-Camacho, C. Cheng, K. Schwibbert, A. Lippitz, W. E. Unger, A. Gorbushina, M. Adeli, *Nanoscale* **2018**, *10*, 9525.
[36] A. Ottenhall, J. Henschen, J. Illergård, M. Ek, *Environ. Sci.: Water Res. Technol.* **2018**, *4*, 2070.
[37] Y. L. F. Musico, C. M. Santos, M. L. P. Dalida, D. F. Rodrigues, *ACS Sustainable Chem. Eng.* **2014**, *2*, 1559.
[38] M. R. Esfahani, S. A. Aktij, Z. Dabaghian, M. D. Firouzjaei, A. Rahimpour, J. Eke, I. C. Escobar, M. Abolhassani, L. F. Greenlee, A. R. Esfahani, *Sep. Purif. Technol.* **2019**, *213*, 465.
[39] Y. Wang, F. Hammes, N. Boon, T. Egli, *Environ. Sci. Technol.* **2007**, *41*, 7080.
[40] R. Zhang, Y. Liu, M. He, Y. Su, X. Zhao, M. Elimelech, Z. Jiang, *Chem. Soc. Rev.* **2016**, *45*, 5888.
[41] L. Li, P. A. Quinlivan, D. R. Knappe, *Carbon* **2002**, *40*, 2085.
[42] S. D. Alexandratos, *Ind. Eng. Chem. Res.* **2009**, *48*, 388.
[43] L. Kan, Z. Xu, C. Gao, *Macromolecules* **2011**, *44*, 444.
[44] T. G. Van De Ven, A. Sheikhi, *Nanoscale* **2016**, *8*, 15101.
[45] J. K. Pandey, A. N. Nakagaito, H. Takagi, *Polym. Eng. Sci.* **2013**, *53*, 1.
[46] *National systems to support drinking-water, sanitation and hygiene: global status report*, W. H. Organization, **2019**.
[47] https://www.sterlitech.com/ptfe-unlaminated-membrane-filters-hydrophilic-02-micron-90mm-25pk.html (accessed: June 2021).

ADVANCED MATERIALS INTERFACES

Supporting Information

for *Adv. Mater. Interfaces,* DOI: 10.1002/admi.202101917

Graphene-Based Bacterial Filtration via Electrostatic Adsorption

*Rameez Ahmed, Ankita Vaishampayan, Katharina Achazi, Elisabeth Grohmann, Rainer Haag, and Olaf Wagner**

Supporting information

Graphene-Based Bacterial Filtration via Electrostatic Adsorption

Rameez Ahmed, Ankita Vaishampayan, Katharina Achazi, Elisabeth Grohmann, Rainer Haag, and Olaf Wagner *

Scanning electron microscopy (SEM) images

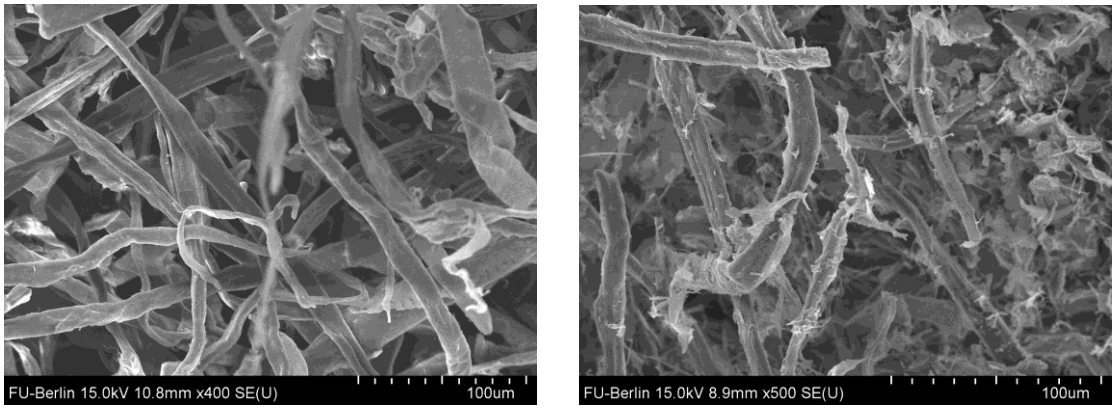

Figure S1. Larger scale SEM images of cellulose fibers and GOX fibers.

Surface charge analysis

Surface charge per unit amount of GOX fiber was determined by a modified colorimetric method based on UV-VIS spectroscopy, as described by Tiller et al. (2001).[SI 1] A stock solution of 0.5 g L^{-1} of fluorescein was prepared. For the calibration curve, a dilution series of the fluorescein stock solution (0.02, 0.015, 0.01, 0.0075, 0.005 0.0025 and 0.001 g L^{-1}) was prepared from the fluorescein stock solution. UV measurements were recorded on the UV-VIS spectrometer Agilent Cary 8454 using a quartz cuvette (Fig. S2). Absorbance was measured between 350 to 750 nm. For the calibration curve, the absorbance of the fluorescein dilution series at the absorbance maxima of 489 nm was plotted against its concentration (Fig. S3)

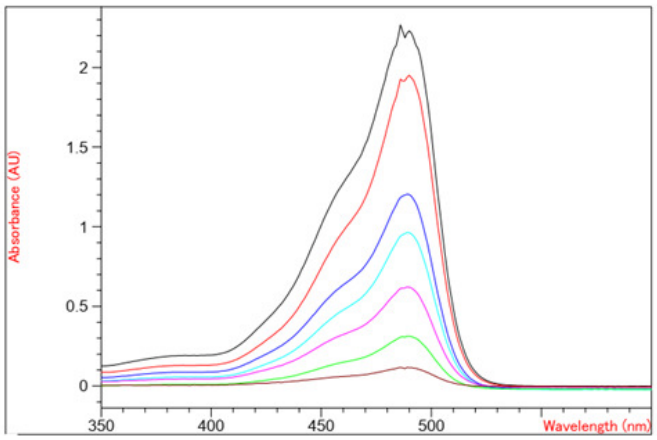

Sample/Result Table

#	Name	Abs<489nm>	#	Name	Abs<489nm>
1	0.02	2.21580	5	0.005	0.62236
2	0.015	1.93870	6	0.0025	0.31338
3	0.01	1.20390	7	0.001	0.11631
4	0.075	0.96351			

Figure S2. UV-VIS absorbance measurement of the dilution series of the fluorescein solution (0.02, 0.015, 0.01, 0.0075, 0.005 0.0025 and 0.001 g L^{-1})

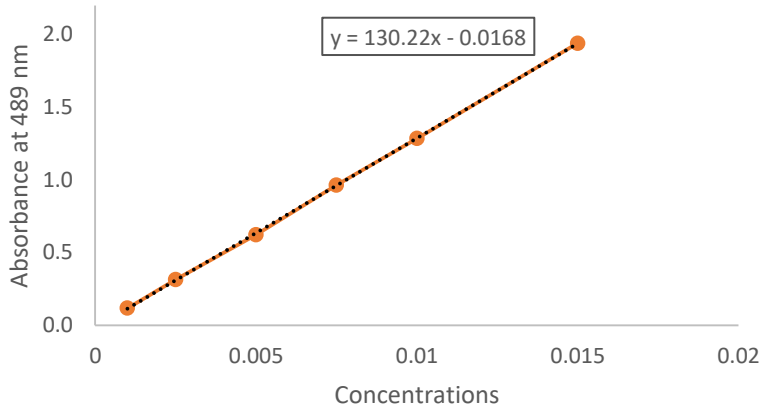

Figure S3. Calibration curve of fluorescein absorbance dilution series at 489 nm.

For the charge calculation of the samples 10 mg cellulose fibers or GOX fibers were dispersed in 10 ml of a 0.1 g L^{-1} fluorescein solution and incubated for 10 minutes. The supernatant was collected from both samples. The stock solution (0.1 g L^{-1}) and collected supernatants samples were diluted by 1:10 (0.01 g L^{-1}) to be in the linear measurement range of the photometer. The absorbance of the diluted solutions was measured between 350 to 750 nm and their corresponding concentration was

calculated by the equation of the calibration curve and the absorbance at the absorbance maxima of 489 nm.

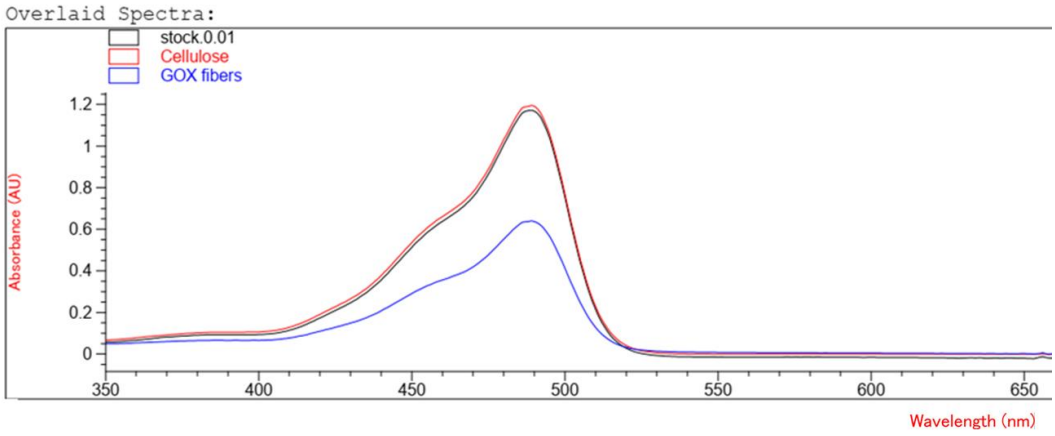

#	Name	Abs<489nm>	#	Name	Abs<489nm>
1	stock.0.01	1.17300	3	GOX fibers	0.64035
2	Cellulose	1.19550			

Figure S4. UV-VIS absorbance measurement of fluorescein stock solution 0.01 g L^{-1} (black) control, cellulose incubated supernatant (red), GOX fibers incubated supernatant, determined by UV-VIS spectroscopy.

$$Concentration = \frac{Absorbance + 0.0168}{130.22} \quad (1)$$

The initial concentrations were calculated by multiplying the concentrations of the diluted samples and stock solution with a dilution factor (10). The amount of fluorescein adsorbed by the unit amount GOX fibers is calculated by the difference between fluorescein amount in supernatants of incubated control cellulose fibers and GOX fibers. The resulting value of 0.043 g, which was divided by the molecular weight of fluorescein (332.31 g mol^{-1}), was 0.00013 mol. It is equal to charged units per g of GOX fibers. Multiplied with the Avogadro constant, the charges per g of GOX fibers were 7.8×10^{19}.

GOX Leaching test

To determine the ability of GOX remain immobilized on the cellulose, 1 L deionized water was filtered through the filter media. Filtrate was collected and the

volume was reduced from 1 L to 10 ml with the help of rota evaporator. Series dilution of 0.01, 0.005 and 0.001 g L^{-1} GOX were also prepared and absorbance was measured between 300 to 700nm. The absorbance spectra confirm the amount of leached GOX in the filtrate is less than 0.001 g L^{-1}. For 1 L filtrate the amount of GOX remains below 10 µg (10 ppm).

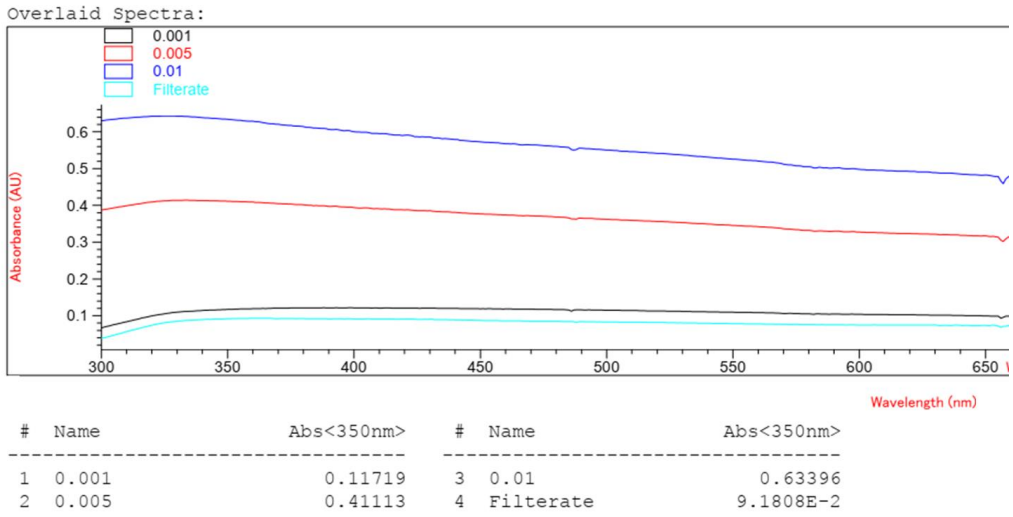

#	Name	Abs<350nm>	#	Name	Abs<350nm>
1	0.001	0.11719	3	0.01	0.63396
2	0.005	0.41113	4	Filterate	9.1808E-2

Figure S5. UV-VIS absorbance measurement of the dilution series of GOX (0.01, 0.005 and 0.001 g L^{-1}) and concentrated filtrate.

Flow rates and pressure values of filtration experiments

Table S1: Summary of the flow rate and pressure dependent filtration experiment.

Sample	Pressure (bar)	Flow rate (ml min^{-1})	Percentage reduction
1	0.00	11	99.83 ± 0.06
2	0.03	50	99.80 ± 0.10
3	0.06	83	99.86 ± 0.05
4	0.10	120	99.94 ± 0.03
5	0.20	200	99.57 ± 0.50
6	0.50	315	100.00%
7	0.80	334	100.00%

References

SI 1) J. C. Tiller, C. J. Liao, K. Lewis, A. M. Klibanov, *Proc. Natl. Acad. Sci*. **2001**, *98*, 11, 5981-5985.

4 Summary and Outlook

The MDR properties of water-borne pathogens will keep them a significant threat to global health and safety. Due to this reason alone, research into preventive methods should be of utmost priority. Current antibacterial and water filtration technologies have drawbacks. Furthermore, they need to be more sustainable. Typically, mainstream water purification strategies are based on two main approaches. Chemical treatment which includes processes like chlorination or ozonization, unfortunately requires energy and chemical input and results in the release of toxins. On the other hand, membrane filtration is a more widely adopted approach to remove bacteria with low energy input and without the release of toxins. However, certain shaped bacteria (such as spirillum-shaped *Hylemonella gracilis*) have been known to pass through it. Since membrane filtration works on the principle of size exclusion, material and maintenance costs due to clogging and biofouling for membranes make it unsustainable.

In this research project, innovative material and strategy were studied to deal with the challenges of bacteria filtration. A flexible 2D material was designed and synthesized that catches bacteria based on electrostatic attraction. Micrometer-sized GO sheets were functionalized with an acrylate polymer with secondary amines via free radical polymerization of 2-(dimethylamino)ethyl methacrylate. Secondary amines of the polymer were quaternized in the second step by methylation reaction to change the charge of flexible sheets from negative to positive. Protocol was developed to quantify the charge per unit surface area of GO-PTEMA sheets. Upon interaction with bacteria, flexible sheets adapt to the shape of bacteria and bind them. AFM confirmed the wrapping of positively charged sheets with live bacteria in liquid cell.

In the second research project, the GO-PTEMA sheets were covalently immobilized on cellulose fiber as support material (GOX fibers) to design and produce a filtration device. The immobilization was confirmed with SEM. Fluorescence microscopy was used to examine the interactions of GOX fiber with bacteria. The filter performance of 3-log CFU reduction was achieved at flow rates around five times higher than membrane filters. 100 mg of the created GOX fibers, removing up to 10^9 CFU/ml with 99.5% filtration efficiency. Since the principle of removing bacteria is based on binding via electrostatic attraction, the typical problem of membrane clogging, and back pressure is not an issue when the filter is entirely loaded with bacteria.

In a broader sense, this project provides a detailed report from the synthesis and characterization of a material for an application to design and manufacture prototypes with

detailed testing. There are reports of polycationic polymers and zwitterionic systems that bind and inhibit bacteria proliferation with minimum inhibition concentration tests. However, there are few studies to take them to the next step of determining their abilities in filtration settings. Protocols developed during this project can be used to test many of the features. This work provides a platform to develop future hybrid materials for filtration applications.

5 Kurzzusammenfassung

Aufgrund der Multiresistenz von Krankheitserregern, die durch Wasser übertragen werden, sind sie eine erhebliche Bedrohung für die globale Gesundheit. Allein aus diesem Grund sollte die Erforschung von Präventivmethoden oberste Priorität haben. Die derzeit gängigen antibakteriellen und Wasserfiltrations-Technologien haben Nachteile und sollten nachhaltiger werden. Herkömmliche Wasserreinigungsstrategien beruhen in der Regel auf zwei Hauptansätzen. Chemische Behandlung, die Verfahren wie Chlorierung oder Ozonisierung umfasst. Leider erfordert diese Methode einen hohen Energie- oder Chemikalieneinsatz und führt zur Freisetzung von Giftstoffen. Andererseits ist die Membranfiltration ein weit verbreiteter Ansatz zur Entfernung von Bakterien mit geringerem Energieaufwand und ohne Freisetzung von Giftstoffen. Es ist jedoch bekannt, dass bestimmte geformte Bakterien (z. B. die spiralförmige Hylemonella gracilis) manche Membranen passieren können. Da die Membranfiltration nach dem Prinzip des Größenausschlusses funktioniert, ist sie aufgrund der Material- und Wartungskosten, die durch Verstopfung und Biofouling der Membranen entstehen, nicht nachhaltig.

In diesem Forschungsprojekt wurden innovative Materialien und Strategien untersucht, um den Herausforderungen der Bakterienfiltration zu begegnen. Es wurde ein flexibles zweidimensionales Material entworfen und synthetisiert, das Bakterien auf der Grundlage elektrostatischer Anziehung auffängt. GO-Folien in Mikrometergröße wurden mit einem Acrylatpolymer mit sekundären Aminen durch radikalische Polymerisation von 2-(dimethylamino)ethyl methacrylate funktionalisiert. Die sekundären Amine des Polymers wurden im zweiten Schritt durch eine Methylierungsreaktion quaternisiert, um die Ladung der flexiblen Blätter von negativ auf positiv zu ändern. Es wurde ein Protokoll entwickelt, um die Ladung pro Oberflächeneinheit der GO-PTEMA-Folien zu quantifizieren. Bei der Interaktion mit Bakterien passen sich die flexiblen Folien an die Form der Bakterien an und binden die Partikel. AFM bestätigte die Umhüllung von positiv geladenen Folien mit lebenden Bakterien in einer Flüssigzelle.

Im zweiten Teil des Forschungsprojekts wurden die GO-PTEMA-Folien kovalent auf Zellulosefasern als Trägermaterial (GOX-Fasern) immobilisiert, um eine Filtrationsvorrichtung herzustellen. Die Immobilisierung wurde mit SEM bestätigt. Mit Hilfe der Fluoreszenzmikroskopie wurden die Wechselwirkungen der GOX-Fasern mit Bakterien untersucht. Die Filterleistung von 3-log CFU-Reduktion wurde bei Durchflussraten erreicht, die etwa fünfmal höher waren als bei Membranfiltern. 100 mg der hergestellten GOX-Fasern entfernten bis zu 10^9 KBE/ml mit einer Filtrationseffizienz von 99,5 %. Da das Prinzip der Bakterienentfernung auf der Bindung durch elektrostatische Anziehung beruht, tritt das typische Problem der Membranverstopfung und des Gegendrucks nicht auf, wenn der Filter vollständig mit Bakterien beladen ist.

Im weiteren Sinne liefert dieses Projekt einen detaillierten Bericht über die Synthese und Charakterisierung eines Materials für eine Anwendung zur Entwicklung und Herstellung von Prototypen mit detaillierten Tests. Es gibt Berichte über polykationische Polymere und zwitterionische Systeme, die Bakterien binden und deren Vermehrung durch Tests der minimalen Hemmkonzentration hemmen. Es gibt jedoch nur wenige Studien, in denen ihre Fähigkeiten in Filtrationsumgebungen untersucht wurden. Mit den im Rahmen dieses Projekts entwickelten Protokollen können viele der Eigenschaften getestet werden, was Zeit und Mühe spart. Diese Arbeit bietet eine Plattform für die Entwicklung zukünftiger Hybridmaterialien für Filtrationsanwendungen.

6 References

[1] E. Cerceo, S. B. Deitelzweig, B. M. Sherman, A. N. Amin, *Microb. Drug Resist.* **2016**, *22*, 412-431.

[2] J.-M. Rolain, C. Abat, M.-T. Jimeno, P.-E. Fournier, D. Raoult, *Clin. Microbiol. Infect.* **2016**, *22*, 408-415.

[3] E. D. Ahire, S. G. Talele, H. S. Shah, in *Applied Pharmaceutical Science and Microbiology*, Apple Academic Press, **2020**, pp. 133-158.

[4] M. Abd Elkodous, S. O. Olojede, S. Sahoo, R. Kumar, *Chemico-Biological Interactions* **2023**, 110517.

[5] J. H. Humphrey, J. Brown, O. Cumming, B. Evans, G. Howard, R. N. Kulabako, J. Lamontagne, A. J. Pickering, E. N. Wang, *The Lancet Planetary Health* **2020**, *4*, e91-e92.

[6] J. Zheng, Z. Wang, J. Ma, S. Xu, Z. Wu, *Environmental science & technology* **2018**, *52*, 4117-4126.

[7] S. S. Bucs, N. Farhat, J. C. Kruithof, C. Picioreanu, M. C. van Loosdrecht, J. S. Vrouwenvelder, *Desalination* **2018**, *434*, 189-197.

[8] W. Pronk, A. Ding, E. Morgenroth, N. Derlon, P. Desmond, M. Burkhardt, B. Wu, A. G. Fane, *Water research* **2019**, *149*, 553-565.

[9] W. W. Wilson, M. M. Wade, S. C. Holman, F. R. Champlin, *Journal of microbiological methods* **2001**, *43*, 153-164.

[10] J. G. Sawyer, N. L. Martin, R. Hancock, *Infection and immunity* **1988**, *56*, 693-698.

[11] H. Fang, J. Kang, D. Zhang, *Microbial cell factories* **2017**, *16*, 1-14.

[12] F. Y. Ramírez-Castillo, A. Loera-Muro, M. Jacques, P. Garneau, F. J. Avelar-González, J. Harel, A. L. Guerrero-Barrera, *Pathogens* **2015**, *4*, 307-334.

[13] N. S. Shah, S. C. Auld, J. C. Brust, B. Mathema, N. Ismail, P. Moodley, K. Mlisana, S. Allana, A. Campbell, T. Mthiyane, *New England Journal of Medicine* **2017**, *376*, 243-253.

[14] H. M. P. Consortium, *nature* **2012**, *486*, 207.

[15] E. K. Costello, C. L. Lauber, M. Hamady, N. Fierer, J. I. Gordon, R. Knight, *science* **2009**, *326*, 1694-1697.

[16] D. Ribet, P. Cossart, *Microbes and infection* **2015**, *17*, 173-183.

[17] Results of round II of the WHO international scheme to evaluate household water treatment technologies, *World Health Organization* **2019**, Licence: CC BY-NC-SA 3.0 IGO.

[18] J. P. S. Cabral, *International Journal of Environmental Research and Public Health* **2010**, *7*, 3657-3703.

[19] K. H. Schleifer, *Systematic and applied microbiology* **2009**, *32*, 533-542.

[20] B. S. Nagoba, A. PICHARE, *Microbiology and Parasitology PMFU - E-BooK*, Elsevier Health Sciences, **2016**.

[21] M.-P. Chapot-Chartier, S. Kulakauskas, *Microbial cell factories* **2014**, *13*, 1-23.

[22] G. Seltmann, O. Holst, *The bacterial cell wall*, Springer Science & Business Media, **2013**.

[23] A. Lin, Y. Liu, X. Zhu, X. Chen, J. Liu, Y. Zhou, X. Qin, J. Liu, *Acs Nano* **2019**, *13*, 13965-13984.

[24] D. Claus, *World journal of Microbiology and Biotechnology* **1992**, 8, 451-452.

[25] L. Pasquina-Lemonche, J. Burns, R. Turner, S. Kumar, R. Tank, N. Mullin, J. Wilson, B. Chakrabarti, P. Bullough, S. Foster, *Nature* **2020**, *582*, 294-297.

[26] K. C. Huang, R. Mukhopadhyay, B. Wen, Z. Gitai, N. S. Wingreen, *Proceedings of the National Academy of Sciences* **2008**, *105*, 19282-19287.

[27] W. Pajerski, D. Ochonska, M. Brzychczy-Wloch, P. Indyka, M. Jarosz, M. Golda-Cepa, Z. Sojka, A. Kotarba, *Journal of Nanoparticle Research* **2019**, *21*, 1-12.
[28] H. Rogers, H. Perkins, J. Ward, in *Microbial Cell Walls and Membranes*, Springer, **1980**, pp. 105-175.
[29] S. L. Walker, J. E. Hill, J. A. Redman, M. Elimelech, *Applied and Environmental Microbiology* **2005**, *71*, 3093-3099.
[30] H. Nikaido, *Annual review of biochemistry* **2009**, *78*, 119-146.
[31] H. De Lencastre, D. Oliveira, A. Tomasz, *Current opinion in microbiology* **2007**, *10*, 428-435.
[32] B. G. Spratt, *Science* **1994**, *264*, 388-393.
[33] R. Benveniste, J. Davies, *Proceedings of the National Academy of Sciences* **1973**, *70*, 2276-2280.
[34] I. T. Paulsen, R. A. Skurray, R. Tam, M. H. Saier Jr, R. J. Turner, J. H. Weiner, E. B. Goldberg, L. L. Grinius, *Molecular microbiology* **1996**, *19*, 1167-1175.
[35] G. Schröder, E. Lanka, *Plasmid* **2005**, *54*, 1-25.
[36] R. Singh, M. Smitha, S. P. Singh, *Journal of nanoscience and nanotechnology* **2014**, *14*, 4745-4756.
[37] B. Brar, S. Marwaha, A. K. Poonia, B. Koul, S. Kajla, V. D. Rajput, *Archives of Microbiology* **2023**, *205*, 62.
[38] S. Cheeseman, A. J. Christofferson, R. Kariuki, D. Cozzolino, T. Daeneke, R. J. Crawford, V. K. Truong, J. Chapman, A. Elbourne, *Advanced Science* **2020**, *7*, 1902913.
[39] V. V. Mody, R. Siwale, A. Singh, H. R. Mody, *Journal of Pharmacy and Bioallied Sciences* **2010**, *2*, 282.
[40] C. Noguez, *The Journal of Physical Chemistry C* **2007**, *111*, 3806-3819.
[41] A. Panáček, L. Kvitek, R. Prucek, M. Kolář, R. Večeřová, N. Pizúrová, V. K. Sharma, T. j. Nevěčná, R. Zbořil, *The Journal of Physical Chemistry B* **2006**, *110*, 16248-16253.
[42] A. T. Simon, D. Dutta, A. Chattopadhyay, S. S. Ghosh, *ACS omega* **2019**, *4*, 4697-4706.
[43] A. Alshareef, K. Laird, R. Cross, *Acta metallurgica sinica (english letters)* **2017**, *30*, 29-35.
[44] T. Kim, Q. Zhang, J. Li, L. Zhang, J. V. Jokerst, *ACS nano* **2018**, *12*, 5615-5625.
[45] C. Loo, A. Lin, L. Hirsch, M.-H. Lee, J. Barton, N. Halas, J. West, R. Drezek, *Technology in cancer research & treatment* **2004**, *3*, 33-40.
[46] J. Chen, C. Glaus, R. Laforest, Q. Zhang, M. Yang, M. Gidding, M. J. Welch, Y. Xia, *Small* **2010**, *6*, 811-817.
[47] P. Pallavicini, A. Dona, A. Taglietti, P. Minzioni, M. Patrini, G. Dacarro, G. Chirico, L. Sironi, N. Bloise, L. Visai, *Chemical Communications* **2014**, *50*, 1969-1971.
[48] M.-T. Hsiao, S.-F. Chen, D.-B. Shieh, C.-S. Yeh, *The Journal of Physical Chemistry B* **2006**, *110*, 205-210.
[49] W. C. Huang, P. J. Tsai, Y. C. Chen, *Small* **2009**, *5*, 51-56.
[50] S. A. Khan, A. K. Singh, D. Senapati, Z. Fan, P. C. Ray, *Journal of Materials Chemistry* **2011**, *21*, 17705-17709.
[51] aS. Liu, T. H. Zeng, M. Hofmann, E. Burcombe, J. Wei, R. Jiang, J. Kong, Y. Chen, *ACS nano* **2011**, *5*, 6971-6980; bZ. Sun, Y. Zhang, H. Yu, C. Yan, Y. Liu, S. Hong, H. Tao, A. W. Robertson, Z. Wang, A. A. Pádua, *Nanoscale* **2018**, *10*, 12543-12553.
[52] A. Laganà, G. Visalli, F. Corpina, M. Ferlazzo, A. Di Pietro, A. Facciolà, *European Review for Medical & Pharmacological Sciences* **2023**, *27*.

[53] E. Hoseinzadeh, P. Makhdoumi, P. Taha, H. Hossini, J. Stelling, M. Amjad Kamal, *Current drug metabolism* **2017**, *18*, 120-128.
[54] K. Gold, B. Slay, M. Knackstedt, A. K. Gaharwar, *Advanced Therapeutics* **2018**, *1*, 1700033.
[55] Y. N. Slavin, J. Asnis, U. O. Häfeli, H. Bach, *Journal of nanobiotechnology* **2017**, *15*, 1-20.
[56] I. Sondi, B. Salopek-Sondi, *Journal of colloid and interface science* **2004**, *275*, 177-182.
[57] J. Renkawitz, M. Sixt, *Developmental cell* **2016**, *38*, 448-450.
[58] B. Ezraty, A. Gennaris, F. Barras, J.-F. Collet, *Nature Reviews Microbiology* **2017**, *15*, 385-396.
[59] S. Ranjan, C. Ramalingam, *Environmental Chemistry Letters* **2016**, *14*, 487-494.
[60] A. Vaishampayan, R. Ahmed, O. Wagner, A. de Jong, R. Haag, J. Kok, E. Grohmann, *Materials Science and Engineering: C* **2021**, *119*, 111578.
[61] Y. Xie, Y. He, P. L. Irwin, T. Jin, X. Shi, *Applied and environmental microbiology* **2011**, *77*, 2325-2331.
[62] O. Choi, Z. Hu, *Environmental science & technology* **2008**, *42*, 4583-4588.
[63] S. Sharmin, M. M. Rahaman, C. Sarkar, O. Atolani, M. T. Islam, O. S. Adeyemi, *Heliyon* **2021**, *7*.
[64] K. A. Willets, R. P. Van Duyne, *Annu. Rev. Phys. Chem.* **2007**, *58*, 267-297.
[65] Y. Yu, J. D. Williams, K. A. Willets, *Faraday discussions* **2018**, *210*, 29-39.
[66] E. Petryayeva, U. J. Krull, *Analytica chimica acta* **2011**, *706*, 8-24.
[67] V. P. Zharov, K. E. Mercer, E. N. Galitovskaya, M. S. Smeltzer, *Biophysical journal* **2006**, *90*, 619-627.
[68] A. H. Morrish, *The physical principles of magnetism*, **2001**.
[69] Z. Hedayatnasab, F. Abnisa, W. M. A. W. Daud, *Materials & Design* **2017**, *123*, 174-196.
[70] L. A. Thomas, L. Dekker, M. Kallumadil, P. Southern, M. Wilson, S. P. Nair, Q. A. Pankhurst, I. P. Parkin, *Journal of Materials Chemistry* **2009**, *19*, 6529-6535.
[71] S. Singh, K. Barick, D. Bahadur, *Powder technology* **2015**, *269*, 513-519.
[72] L. O. Mair, A. Nacev, R. Hilaman, P. Y. Stepanov, S. Chowdhury, S. Jafari, J. Hausfeld, A. J. Karlsson, M. E. Shirtliff, B. Shapiro, *Journal of Magnetism and Magnetic Materials* **2017**, *427*, 81-84.
[73] G. Hwang, A. J. Paula, E. E. Hunter, Y. Liu, A. Babeer, B. Karabucak, K. Stebe, V. Kumar, E. Steager, H. Koo, *Science robotics* **2019**, *4*.
[74] M. Dresselhaus, G. Dresselhaus, R. Saito, *Nanotechnology* **1999**, 285-329.
[75] E. H. Falcao, F. Wudl, *Journal of Chemical Technology & Biotechnology: International Research in Process, Environmental & Clean Technology* **2007**, *82*, 524-531.
[76] M. Endo, M. S. Strano, P. M. Ajayan, *Carbon nanotubes* **2007**, 13-62.
[77] R. E. Smalley, *Reviews of Modern Physics* **1997**, *69*, 723.
[78] S. Lin, J. Tang, K. Zhang, Y. Chen, R. Gao, H. Yin, L.-C. Qin, *Nanoscale Advances* **2023**, *5*, 1163-1171.
[79] J. Gopal, M. Muthu, I. Sivanesan, *Polymers* **2023**, *15*, 701.
[80] H. Chen, F. Zhuo, J. Zhou, Y. Liu, J. Zhang, S. Dong, X. Liu, A. Elmarakbi, H. Duan, Y. Fu, *Chemical Engineering Journal* **2023**, *464*, 142576.
[81] S. K. Bhardwaj, S. Kumar, in *Engineered Nanostructures for Therapeutics and Biomedical Applications*, Elsevier, **2023**, pp. 131-166.
[82] S. Sengupta, S. Pal, A. Pal, S. Maity, K. Sarkar, M. Das, *Inorganica Chimica Acta* **2023**, 121677.

[83] S. K. Tiwari, V. Kumar, A. Huczko, R. Oraon, A. D. Adhikari, G. Nayak, *Critical Reviews in Solid State and Materials Sciences* **2016**, *41*, 257-317.
[84] G. Qin, K.-R. Hao, Q.-B. Yan, M. Hu, G. Su, *Nanoscale* **2019**, *11*, 5798-5806.
[85] A. C. Ferrari, J. C. Meyer, V. Scardaci, C. Casiraghi, M. Lazzeri, F. Mauri, S. Piscanec, D. Jiang, K. S. Novoselov, S. Roth, *Physical review letters* **2006**, *97*, 187401.
[86] K. Novoselov, S. Morozov, T. Mohinddin, L. Ponomarenko, D. Elias, R. Yang, I. Barbolina, P. Blake, T. Booth, D. Jiang, *physica status solidi (b)* **2007**, *244*, 4106-4111.
[87] A. K. Geim, K. S. Novoselov, in *Nanoscience and technology: a collection of reviews from nature journals*, World Scientific, **2010**, pp. 11-19.
[88] K. E. Whitener Jr, P. E. Sheehan, *Diamond and related materials* **2014**, *46*, 25-34.
[89] Q. Yu, J. Lian, S. Siriponglert, H. Li, Y. P. Chen, S.-S. Pei, *Applied Physics Letters* **2008**, *93*, 113103.
[90] M. Eizenberg, J. Blakely, *Surface Science* **1979**, *82*, 228-236.
[91] C. Wen, University of Pennsylvania **2023**.
[92] A. Anwar, T.-P. Chang, C.-T. Chen, *Carbon Letters* **2022**, *32*, 1-38.
[93] P. Trucano, R. Chen, *Nature* **1975**, *258*, 136-137.
[94] B. Jayasena, S. Subbiah, *Nanoscale research letters* **2011**, *6*, 1-7.
[95] M. Yi, Z. Shen, *Journal of Materials Chemistry A* **2015**, *3*, 11700-11715.
[96] S. Park, R. S. Ruoff, *Nature nanotechnology* **2009**, *4*, 217-224.
[97] W. S. Hummers Jr, R. E. Offeman, *Journal of the american chemical society* **1958**, *80*, 1339-1339.
[98] S. Eigler, S. Grimm, M. Enzelberger-Heim, P. Müller, A. Hirsch, *Chemical Communications* **2013**, *49*, 7391-7393.
[99] S. Eigler, M. Enzelberger-Heim, S. Grimm, P. Hofmann, W. Kroener, A. Geworski, C. Dotzer, M. Röckert, J. Xiao, C. Papp, *Advanced materials* **2013**, *25*, 3583-3587.
[100] S. Pei, H.-M. Cheng, *Carbon* **2012**, *50*, 3210-3228.
[101] D. Li, M. B. Müller, S. Gilje, R. B. Kaner, G. G. Wallace, *Nature nanotechnology* **2008**, *3*, 101-105.
[102] G. Reina, J. M. González-Domínguez, A. Criado, E. Vázquez, A. Bianco, M. Prato, *Chemical Society Reviews* **2017**, *46*, 4400-4416.
[103] H. Shen, L. Zhang, M. Liu, Z. Zhang, *Theranostics* **2012**, *2*, 283.
[104] H. Pieper, S. Chercheja, S. Eigler, C. E. Halbig, M. R. Filipovic, A. Mokhir, *Angewandte Chemie International Edition* **2016**, *55*, 405-407.
[105] A. Al-Jumaili, S. Alancherry, K. Bazaka, M. V. Jacob, *Materials* **2017**, *10*, 1066.
[106] M. Dallavalle, M. Calvaresi, A. Bottoni, M. Melle-Franco, F. Zerbetto, *ACS applied materials & interfaces* **2015**, *7*, 4406-4414.
[107] L. Hui, J.-G. Piao, J. Auletta, K. Hu, Y. Zhu, T. Meyer, H. Liu, L. Yang, *ACS applied materials & interfaces* **2014**, *6*, 13183-13190.
[108] O. Akhavan, E. Ghaderi, *ACS nano* **2010**, *4*, 5731-5736.
[109] H. Yao, Y. Huang, X. Li, X. Li, H. Xie, T. Luo, J. Chen, Z. Chen, *Environmental Science: Nano* **2020**, *7*, 782-792.
[110] R. Campos Chiste, M. Freitas, A. Zerlotti Mercadante, E. Fernandes, *Current medicinal chemistry* **2015**, *22*, 4234-4256.
[111] H. W. Harris, M. Y. El-Naggar, O. Bretschger, M. J. Ward, M. F. Romine, A. Obraztsova, K. H. Nealson, *Proceedings of the National Academy of Sciences* **2010**, *107*, 326-331.

[112] R. S. Hartshorne, C. L. Reardon, D. Ross, J. Nuester, T. A. Clarke, A. J. Gates, P. C. Mills, J. K. Fredrickson, J. M. Zachara, L. Shi, *Proceedings of the National Academy of Sciences* **2009**, *106*, 22169-22174.
[113] H. Hasegawa, *Japanese Journal of Applied Physics* **1999**, *38*, 1098.
[114] J. Li, G. Wang, H. Zhu, M. Zhang, X. Zheng, Z. Di, X. Liu, X. Wang, *Scientific reports* **2014**, *4*, 1-8.
[115] F. Perreault, A. F. De Faria, S. Nejati, M. Elimelech, *ACS nano* **2015**, *9*, 7226-7236.
[116] S. Liu, M. Hu, T. H. Zeng, R. Wu, R. Jiang, J. Wei, L. Wang, J. Kong, Y. Chen, *Langmuir* **2012**, *28*, 12364-12372.
[117] M.-Y. Xia, Y. Xie, C.-H. Yu, G.-Y. Chen, Y.-H. Li, T. Zhang, Q. Peng, *Journal of Controlled Release* **2019**, *307*, 16-31.
[118] L. A. Chernozatonskii, P. B. Sorokin, A. Artukh, *Russian Chemical Reviews* **2014**, *83*, 251.
[119] G. Deokar, J. Avila, I. Razado-Colambo, J.-L. Codron, C. Boyaval, E. Galopin, M.-C. Asensio, D. Vignaud, *Carbon* **2015**, *89*, 82-92.
[120] P. Feicht, S. Eigler, *ChemNanoMat* **2018**, *4*, 244-252.
[121] T. Kuila, S. Bose, A. K. Mishra, P. Khanra, N. H. Kim, J. H. Lee, *Progress in Materials Science* **2012**, *57*, 1061-1105.
[122] M. Maas, J. Wehling, *Surface-Functionalized Ceramics: For Biotechnological and Environmental Applications* **2023**, 337-368.
[123] V. D. Punetha, S. Rana, H. J. Yoo, A. Chaurasia, J. T. McLeskey Jr, M. S. Ramasamy, N. G. Sahoo, J. W. Cho, *Progress in Polymer Science* **2017**, *67*, 1-47.
[124] V. Georgakilas, M. Otyepka, A. B. Bourlinos, V. Chandra, N. Kim, K. C. Kemp, P. Hobza, R. Zboril, K. S. Kim, *Chemical reviews* **2012**, *112*, 6156-6214.
[125] V. Georgakilas, *Functionalization of Graphene*, Wiley, **2014**.
[126] P. Hobza, K. Müller-Dethlefs, *Non-covalent interactions: theory and experiment, Vol. 2*, Royal Society of Chemistry, **2010**.
[127] G. Yang, L. Li, W. B. Lee, M. C. Ng, *Science and technology of advanced materials* **2018**, *19*, 613-648.
[128] C. A. Hunter, J. K. Sanders, *Journal of the American Chemical Society* **1990**, *112*, 5525-5534.
[129] V. Georgakilas, J. N. Tiwari, K. C. Kemp, J. A. Perman, A. B. Bourlinos, K. S. Kim, R. Zboril, *Chemical reviews* **2016**, *116*, 5464-5519.
[130] Y. Zhang, C. Wu, S. Guo, J. Zhang, *Nanotechnology Reviews* **2013**, *2*, 27-45.
[131] H. Li, S. I. Song, G. Y. Song, I. Kim, *Journal of Nanoscience and Nanotechnology* **2014**, *14*, 1425-1440.
[132] K. Lum, D. Chandler, J. D. Weeks, ACS Publications, **1999**.
[133] M. Lotya, P. J. King, U. Khan, S. De, J. N. Coleman, *ACS nano* **2010**, *4*, 3155-3162.
[134] A. B. Bourlinos, V. Georgakilas, R. Zboril, T. A. Steriotis, A. K. Stubos, C. Trapalis, *Solid State Communications* **2009**, *149*, 2172-2176.
[135] Y. Liang, D. Wu, X. Feng, K. Müllen, *Advanced materials* **2009**, *21*, 1679-1683.
[136] V. Nanjundappa, T. Ramakrishnappa, S. Kempahanumakkagari, H. Prakash, B. Praveen, *Applied Surface Science Advances* **2023**, *14*, 100386.
[137] B. Ou, Z. Zhou, Q. Liu, B. Liao, S. Yi, Y. Ou, X. Zhang, D. Li, *Polymer Chemistry* **2012**, *3*, 2768-2775.
[138] M. Bagherzadeh, A. Farahbakhsh, *Graphene materials: Fundamentals and emerging applications* **2015**, 25-65.
[139] M. Quintana, K. Spyrou, M. Grzelczak, W. R. Browne, P. Rudolf, M. Prato, *ACS nano* **2010**, *4*, 3527-3533.

[140] S. Lai, Y. Jin, X. Sun, J. Pan, W. Du, L. Shi, *Research on Chemical Intermediates* **2018**, *44*, 3523-3536.
[141] R. Khan, K. Miyagawa, A. Bianco, Y. Nishina, *Applied Materials Today* **2021**, *24*, 101120.
[142] P. Laaksonen, M. Kainlauri, T. Laaksonen, A. Shchepetov, H. Jiang, J. Ahopelto, M. B. Linder, *Angewandte Chemie International Edition* **2010**, *49*, 4946-4949.
[143] A. B. Bourlinos, D. Gournis, D. Petridis, T. Szabó, A. Szeri, I. Dékány, *Langmuir* **2003**, *19*, 6050-6055.
[144] H. Yang, C. Shan, F. Li, D. Han, Q. Zhang, L. Niu, *Chemical Communications* **2009**, 3880-3882.
[145] Y. Cui, S. N. Kim, S. E. Jones, L. L. Wissler, R. R. Naik, M. C. McAlpine, *Nano letters* **2010**, *10*, 4559-4565.
[146] T. A. Pham, N. A. Kumar, Y. T. Jeong, *Synthetic Metals* **2010**, *160*, 2028-2036.
[147] M. Raji, N. Zari, A. El Kacem Qaiss, R. Bouhfid, Elsevier, **2019**.
[148] S. Lai, Y. Jin, X. Sun, J. Pan, W. Du, L. Shi, *Research on Chemical Intermediates* **2018**, *44*, 3523-3536.
[149] E. Bekyarova, M. E. Itkis, P. Ramesh, C. Berger, M. Sprinkle, W. A. de Heer, R. C. Haddon, *Journal of the American Chemical Society* **2009**, *131*, 1336-1337.
[150] D. Yu, Y. Yang, M. Durstock, J.-B. Baek, L. Dai, *ACS nano* **2010**, *4*, 5633-5640.
[151] H. J. Salavagione, M. A. Gomez, G. Martinez, *Macromolecules* **2009**, *42*, 6331-6334.
[152] Z. Liu, J. T. Robinson, X. Sun, H. Dai, *Journal of the American Chemical Society* **2008**, *130*, 10876-10877.
[153] H. Hu, X. Wang, J. Wang, F. Liu, M. Zhang, C. Xu, *Applied Surface Science* **2011**, *257*, 2637-2642.
[154] S. Stankovich, R. D. Piner, S. T. Nguyen, R. S. Ruoff, *Carbon* **2006**, *44*, 3342-3347.
[155] J. L. Delgado, P. de la Cruz, F. Langa, A. Urbina, J. Casado, J. T. L. Navarrete, *Chemical communications* **2004**, 1734-1735.
[156] C. Bingel, *Chemische Berichte* **1993**, *126*, 1957-1959.
[157] S. P. Economopoulos, G. Rotas, Y. Miyata, H. Shinohara, N. Tagmatarchis, *ACS nano* **2010**, *4*, 7499-7507.
[158] J. Choi, K.-j. Kim, B. Kim, H. Lee, S. Kim, *The Journal of Physical Chemistry C* **2009**, *113*, 9433-9435.
[159] A. Faghani, I. S. Donskyi, M. Fardin Gholami, B. Ziem, A. Lippitz, W. E. Unger, C. Böttcher, J. P. Rabe, R. Haag, M. Adeli, *Angewandte Chemie* **2017**, *129*, 2719-2723.
[160] A. Ferretti, S. Sinha, L. Sagresti, E. Araya-Hermosilla, M. Prato, V. Mattoli, A. Pucci, G. Brancato, *Physical Chemistry Chemical Physics* **2022**, *24*, 2491-2503.
[161] S. Munirasu, J. Albuerne, A. Boschetti-de-Fierro, V. Abetz, *Macromolecular rapid communications* **2010**, *31*, 574-579.
[162] J. Li, M. Li, L.-L. Zhou, S.-Y. Lang, H.-Y. Lu, D. Wang, C.-F. Chen, L.-J. Wan, *Journal of the American Chemical Society* **2016**, *138*, 7448-7451.
[163] X. Zhong, J. Jin, S. Li, Z. Niu, W. Hu, R. Li, J. Ma, *Chemical communications* **2010**, *46*, 7340-7342.
[164] M. Maggini, G. Scorrano, M. Prato, *Journal of the American Chemical Society* **1993**, *115*, 9798-9799.
[165] X. Zhang, L. Hou, A. Cnossen, A. C. Coleman, O. Ivashenko, P. Rudolf, B. J. van Wees, W. R. Browne, B. L. Feringa, *Chemistry-A European Journal* **2011**, *17*, 8957.
[166] J. L. Bahr, J. Yang, D. V. Kosynkin, M. J. Bronikowski, R. E. Smalley, J. M. Tour, *Journal of the American chemical society* **2001**, *123*, 6536-6542.
[167] L. Kan, Z. Xu, C. Gao, *Macromolecules* **2011**, *44*, 444-452.
[168] J. Shen, Y. Hu, C. Li, C. Qin, M. Ye, *small* **2009**, *5*, 82-85.

[169] H. Mohammed, A. Kumar, E. Bekyarova, Y. Al-Hadeethi, X. Zhang, M. Chen, M. S. Ansari, A. Cochis, L. Rimondini, *Frontiers in Bioengineering and Biotechnology* **2020**, *8*, 465.
[170] H. Ji, H. Sun, X. Qu, *Advanced drug delivery reviews* **2016**, *105*, 176-189.
[171] T. C. Dakal, A. Kumar, R. S. Majumdar, V. Yadav, *Frontiers in microbiology* **2016**, 1831.
[172] R. Moosavi, S. Ramanathan, Y. Y. Lee, K. C. S. Ling, A. Afkhami, G. Archunan, P. Padmanabhan, B. Gulyás, M. Kakran, S. T. Selvan, *RSC advances* **2015**, *5*, 76442-76450.
[173] A. Sirelkhatim, S. Mahmud, A. Seeni, N. H. M. Kaus, L. C. Ann, S. K. M. Bakhori, H. Hasan, D. Mohamad, *Nano-micro letters* **2015**, *7*, 219-242.
[174] Y.-W. Wang, A. Cao, Y. Jiang, X. Zhang, J.-H. Liu, Y. Liu, H. Wang, *ACS applied materials & interfaces* **2014**, *6*, 2791-2798.
[175] J. Liu, M. D. Rojas-Andrade, G. Chata, Y. Peng, G. Roseman, J.-E. Lu, G. L. Millhauser, C. Saltikov, S. Chen, *Nanoscale* **2018**, *10*, 158-166.
[176] K. Turcheniuk, C.-H. Hage, J. Spadavecchia, A. Y. Serrano, I. Larroulet, A. Pesquera, A. Zurutuza, M. G. Pisfil, L. Héliot, J. Boukaert, *Journal of Materials Chemistry B* **2015**, *3*, 375-386.
[177] F. Naseer, E. Zahir, E. Y. Danish, M. Gull, S. Noman, M. T. Soomro, *Journal of Environmental Chemical Engineering* **2020**, *8*, 104424.
[178] J. Venkatesan, R. Jayakumar, A. Mohandas, I. Bhatnagar, S.-K. Kim, *Materials* **2014**, *7*, 3946-3955.
[179] K. H. Tan, S. Sattari, I. S. Donskyi, J. L. Cuellar-Camacho, C. Cheng, K. Schwibbert, A. Lippitz, W. E. Unger, A. Gorbushina, M. Adeli, *Nanoscale* **2018**, *10*, 9525-9537.
[180] S. Aslan, C. Z. Loebick, S. Kang, M. Elimelech, L. D. Pfefferle, P. R. Van Tassel, *Nanoscale* **2010**, *2*, 1789-1794.
[181] S. Duri, A. L. Harkins, A. J. Frazier, C. D. Tran, *ACS Sustainable Chemistry & Engineering* **2017**, *5*, 5408-5417.
[182] V. K. Gupta, I. Ali, T. A. Saleh, A. Nayak, S. Agarwal, *Rsc Advances* **2012**, *2*, 6380-6388.
[183] Q. Li, *Water Res* **2008**, *42*, 4591-4602.
[184] C. T. Cleveland, *Journal-American Water Works Association* **1999**, *91*, 10-10.
[185] M. R. Esfahani, S. A. Aktij, Z. Dabaghian, M. D. Firouzjaei, A. Rahimpour, J. Eke, I. C. Escobar, M. Abolhassani, L. F. Greenlee, A. R. Esfahani, *Separation Purification Technology* **2019**, *213*, 465-499.
[186] S. Nagandran, P. S. Goh, A. F. Ismail, T.-W. Wong, W. R. Z. B. W. Dagang, *Symmetry* **2020**, *12*, 239.
[187] P. Bernardo, E. Drioli, G. J. I. Golemme, e. c. research, **2009**, *48*, 4638-4663.
[188] M. Ulbricht, *Polymer* **2006**, *47*, 2217-2262.
[189] S. J. Tesh, T. B. Scott, *Advanced Materials* **2014**, *26*, 6056-6068.
[190] T. Nguyen, F. A. Roddick, L. Fan, *Membranes* **2012**, *2*, 804-840.
[191] A. Lee, J. W. Elam, S. B. Darling, *Environmental Science: Water Research Technology* **2016**, *2*, 17-42.
[192] H. Z. Shafi, A. Matin, S. Akhtar, K. K. Gleason, S. M. Zubair, Z. Khan, *Journal of Membrane Science* **2017**, *527*, 152-163.
[193] S. Shirazi, C.-J. Lin, D. Chen, *Desalination* **2010**, *250*, 236-248.
[194] S. Kerdi, A. Qamar, A. Alpatova, N. Ghaffour, *Journal of Membrane Science* **2019**, *583*, 81-92.
[195] R. A. Al-Juboori, T. Yusaf, *Desalination* **2012**, *302*, 1-23.

[196] B. Bendinger, H. H. Rijnaarts, K. Altendorf, A. J. Zehnder, *Applied environmental microbiology* **1993**, *59*, 3973-3977.
[197] J. Wingender, H. Flemming, *Nature Rev Microbiol* **2010**, *8*, 623-633.
[198] J. Mansouri, S. Harrisson, V. Chen, *Journal of Materials Chemistry* **2010**, *20*, 4567-4586.
[199] Y. Xue, H. Xiao, Y. Zhang, *International journal of molecular sciences* **2015**, *16*, 3626-3655.
[200] M. R. Esfahani, S. A. Aktij, Z. Dabaghian, M. D. Firouzjaei, A. Rahimpour, J. Eke, I. C. Escobar, M. Abolhassani, L. F. Greenlee, A. R. Esfahani, *Separation and Purification Technology* **2019**, *213*, 465-499.
[201] M. A. A. Shahmirzadi, A. Kargari, in *Emerging technologies for sustainable desalination handbook*, Elsevier, **2018**, pp. 285-330.
[202] P. Aryanti, M. Sianipar, M. Zunita, I. Wenten, *Membrane Water Treatment* **2017**, *8*, 463-481.
[203] A. F. de Faria, A. C. M. de Moraes, P. D. Marcato, D. S. T. Martinez, N. Durán, A. G. Souza Filho, A. Brandelli, O. L. Alves, *Journal of nanoparticle research* **2014**, *16*, 1-16.
[204] H.-C. Yang, J. Hou, V. Chen, Z.-K. Xu, *Journal of Materials Chemistry A* **2016**, *4*, 9716-9729.
[205] G.-d. Kang, Y.-m. Cao, *Journal of membrane science* **2014**, *463*, 145-165.
[206] L. Y. Ng, A. W. Mohammad, C. P. Leo, N. Hilal, *Desalination* **2013**, *308*, 15-33.
[207] P. Aryanti, M. Sianipar, M. Zunita, I. Wenten, *Membrane Water Treatment* **2017**, *8*, 463-481.
[208] A. Behboudi, Y. Jafarzadeh, R. Yegani, *Journal of Environmental Chemical Engineering* **2018**, *6*, 1764-1773.
[209] D. Rana, Y. Kim, T. Matsuura, H. A. Arafat, *Journal of Membrane Science* **2011**, *367*, 110-118.
[210] M. E. Ali, L. Wang, X. Wang, X. Feng, *Desalination* **2016**, *386*, 67-76.
[211] N. Akther, S. Phuntsho, Y. Chen, N. Ghaffour, H. K. Shon, *Journal of Membrane Science* **2019**, *584*, 20-45.
[212] Z. Liu, L. Qi, X. An, C. Liu, Y. Hu, *ACS applied materials interfaces* **2017**, *9*, 40987-40997.
[213] L. He, L. F. Dumée, C. Feng, L. Velleman, R. Reis, F. She, W. Gao, L. Kong, *Desalination* **2015**, *365*, 126-135.
[214] H. Alhadrami, F. Al-Hazmi, *J. Bioelectron. Nanotechnol* **2017**, *2*.
[215] H. Saleem, S. J. Zaidi, *Nanomaterials* **2020**, *10*, 1764.
[216] B. Le Ouay, F. Stellacci, *Nano today* **2015**, *10*, 339-354.
[217] H. Shi, F. Liu, L. Xue, *Journal of Membrane Science* **2013**, *437*, 205-215.

7 Appendix

7.1 List of abbreviations

AFM	Atomic force microscopy
AgNPs	Silver nanoparticles
AIBN	azobisisobutyronitrile
CVD	Chemical vapor deposition
Cryo-TEM	Cryogenic transmission electron microscopy
E. coli	*Escherichia coli*
GMs	Graphenic materials
GO	Graphene oxide
GOX fibers	GO PTEMA immobilized cellulose fibers
MWNTs	Multi-walled carbon nanotubes
MDR	Multidrug-resistant
MRSA	Methicillin-resistant *Staphylococcus aureus*
NP	Nanoparticles
PEG	Polyethylene glycol
PEI	polyethyleneimine
PG	Hyperbranched polyglycerol
PDEMA	poly 2-(dimethylamino)ethyl methacrylate
PTEMA	poly 2-(dimethylamino)ethyl methacrylate
PVA	Polyvinyl alcohol
rGO	Reduced graphene oxide
ROS	Reactive oxygen species
TEM	Transmission electron microscopy
TFCs	thin-film composites
TRGO	Thermally reduced graphene oxide
TRGO-Trz	Dichlorotriazine-functionalized TRGO
UV	Ultraviolet
XPS	X-ray photoelectron spectroscopy

7.2 Publications and patent applications

- **Ahmed, R**., Vaishampayan, A., Cuellar-Camacho, J. L., Wight, D. J., Donskyi, I., Unger, W., Grohmann, E., Haag, R., Wagner, O. (2020). Multivalent bacteria binding by flexible polycationic microsheets matching their surface charge density. *Advanced Materials Interfaces*, 7(15), 1902066.
- Wischer, D., Schneider, D., Poehlein, A., Herrmann, F., Oruc, H., Meinhardt, J., Wagner, O., **Ahmed, R**., Kharin, S., Novikova, N. and Haag, R., Grohmann, E. (2020). Novel antimicrobial cellulose fleece inhibits growth of human-derived biofilm-forming staphylococci during the SIRIUS19 simulated space mission. *Frontiers in Microbiology*, 11, 1626.
- Vaishampayan, A., **Ahmed, R.**, Wagner, O., de Jong, A., Haag, R., Kok, J., Grohmann, E. (2021). Transcriptomic analysis of stress response to novel antimicrobial coatings in a clinical MRSA strain. *Materials Science and Engineering: C*, *119*, 111578.
- Donskyi, I.S., Nie, C., Ludwig, K., Trimpert, J., **Ahmed, R.**, Quaas, E., Achazi, K., Radnik, J., Adeli, M., Haag, R., Osterrieder, K., (2021). Graphene sheets with defined dual functionalities for the strong SARS-CoV-2 interactions. *Small*, 17(11), 2007091.
- **Ahmed, R.**, Vaishampayan, A., Achazi, K., Grohmann, E., Haag, R., Wagner, O. (2022). Graphene-Based Bacterial Filtration via Electrostatic Adsorption. *Advanced Materials Interfaces*, 9(6), 2101917.
- Donskyi, I.S., Huang, X., Wichmann, N., Bawadkji, O., **Ahmed, R**., Nickl, P., Herziger, S., Radnik, J., Achazi, K., Qiao, H., Adeli, M. (2022). Polylactide-Block-Polyglycerol-Functionalized Black Phosphorous Nanosheets for Tumor Therapy. *ACS Applied Nano Materials*, 5(9), 13417-13424.
- Landau, U., Wagner, O., Meyer, C., Haag, R., **Ahmed, R.** (2021). Device for depleting active microorganisms in fluids, WO/2022/008520.